NTNU
Norwegian University of
Science and Technology

Harmonic Propagation and Production in Offshore Wind Farms

Audun Matre Meinich

Master of Energy and Environmental Engineering
Submission date: July 2018
Supervisor: Elisabetta Tedeschi, IEL
Co-supervisor: Fernando Marafao, Univ Estadual Paulista
Lukasz Kocewiak, Ørsted

Norwegian University of Science and Technology
Department of Electric Power Engineering

Preface

This master thesis is written as a final project for the study program Energy and Environmental Engineering with a concentration in Electric Energy Conversion. It was carried out during the spring of 2018. The project is part of the international research project NBPOCCREI and is written in cooperation with São Paulo State University (UNESP), Campus of Sorocaba. The author spent three months in Sorocaba conducting research in conjunction with this master thesis. The reader of this report is assumed to have a good grasp of the field of power electronics, but no knowledge of voltage source converters or harmonic distortions is required.

Oslo, 2018-07-05

Audun Matre Meinich

Acknowledgments

I would like to thank my supervisors, Elisabetta Tedeschi and Fernando Marafao, for advising me and giving me insight into the world of power electronics. I would also like to thank Łukasz Kocewiak for proofreading the chapters about harmonics and giving me valuable insight.

As part of this master project, I spent three months in Brazil. I would like to thank the Tambaras for letting me stay in their home, Augusto and Eduardo for helping me with my research, and Schuma for showing me how a real Brazilian barbecue is done.

Last but not least, I would like to thank my smart and lovely girlfriend, Anna, for proofreading my master thesis and lifting my spirits.

A.M.M.

Abstract

Modern wind farms are increasing in size and complexity. As a result, increased power injected from large offshore wind farms is having a significant impact on the stability and power quality of the grid. Harmonics are a fundamental aspect to be evaluated during power quality assessment. Therefore, a thorough understanding of their behavior is needed to successfully plan an offshore wind farm.

In this master thesis, the production and propagation of harmonic components in offshore wind farms are investigated. All relevant theory required to fully understand harmonics and how they can be filtered is included. A guide for simulating the electrical components of an offshore wind farm, such as voltage source converters, cables, and transformers, is also provided.

A Simulink model of an offshore wind farm is built using data from Anholt Offshore Wind Farm in Denmark. The wind turbine in this model is simulated as a voltage source converter with an LCL-filter. A $d-q$ reference frame is used in the control system of the converter, with a pulse width modulator to control the switches and a phase locked loop to synchronize the converter with the grid. The turbine itself is connected to a simplified offshore grid with transformers and subsea cables. Nine different scenarios (running the turbines at half power, grid harmonics and adding a switch-on delay among others) are simulated on this model, each designed to mimic factors present in real offshore wind farms. In addition, active filtering is implemented to limit specific harmonic frequencies.

Results from all nine scenarios show that harmonics vary greatly in the presence of each simulated factor. There are two kinds of current harmonics produced by the wind turbine; high-order switching harmonics and low-order harmonics produced by the phase locked loop. While most of the scenarios had a constant harmonic output from the switches, the harmonics created in the phase locked loop varied as much as 120%, depending on the conditions under which the turbine is running.

While it is documented that the phase locked loop can cause harmonics and instability in the system, this thesis investigates specifically what amplifies harmonics by investigating several practical scenarios in offshore wind farms.

Contents

Acronyms

VSC Voltage Source Converter

PCC Point of Common Coupling

AC Alternating Current

DC Direct Current

RMS Root Mean Square

THD Total Harmonic Distortion

TDD Total Demand Distortion

DFIG Doubly Fed Induction Motor

LCL-filter Inductor-Capacitor-Inductor-filter

PWM Pulse Width Modulator

PLL Phase Locked Loop

WT Wind Turbine

Chapter 1: Introduction

With climate change becoming an important item on the agenda of most countries, the world is striving towards a carbon neutral society. To achieve this, renewable energy is becoming a more and more vital aspect of the energy mix. Oil companies are diverting their investments into renewable energy, and policy makers and climate activists across the globe are looking to newly emerging technology to guide us into a carbon neutral future. [1]

Wind energy is one of these rapidly growing renewable energy sources, with the offshore wind industry leading the charge. Offshore wind is an abundant and reliable source of energy. Offshore wind is also more stable and less prone to visual complaints than onshore wind energy [2]. As floating wind turbines become competitive, more and more wind resources become harvestable. Offshore wind energy is destined to continue this rapid growth. [2]

In addition to the growing number of offshore wind farms, the size of the wind farms themselves are increasing rapidly [3]. With wind turbines soon hitting the 10 MW mark [4], more energy will be injected from a single wind farm. The energy coming from these offshore wind farms will have a great impact on the power quality in the grid, and with the farms growing bigger, the power quality constraints become stricter [5]. It is therefore of utmost importance to investigate which aspects of the offshore wind farm are participating in reducing the produced power quality, with specific examination in voltage drops and swells, flicker, harmonics and frequency drop.

In this master thesis, the harmonics produced in offshore wind farms will be investigated. As offshore wind farms grow larger, the allowed harmonic pollution decreases, making it of major importance to know where the harmonics are produced and what mechanisms amplify them. An offshore wind farm will be simulated with parameter values taken from already existing offshore wind farms where possible, and assumed based on common practice where not possible.

1.1 Related work

While the current research on harmonics in offshore wind farms is rather limited, several articles discussing the topic exist. Ł. Kocewiak has written a PhD on the harmonics in offshore wind farms [6], in addition to papers discussing the harmonic impact from the passive elements [7]

and the converters [8].

Other sources document the fact that harmonics are indeed a problem in offshore wind farms. [9] is a case study of Bard Offshore Wind Farm, where over voltage and harmonic overload caused one of the transformers to catch fire, resulting in the wind farm being out of operation for most of 2014. [10] is a study of an unspecified Brazilian offshore wind farm, where it was found that reducing the power factor of the produced power increased the produced harmonics. This finding is highly relevant to growing wind farms since they will be required to produce and consume reactive power to balance out the grid. [11] studies the harmonic impact of expanding an offshore wind farm and concludes that additional filters are indeed required, while [12] studies the harmonics in Anholt Offshore Wind Farm and the ways in which active filtering can be used to limit these harmonics.

When it comes to harmonics, Anholt Offshore Wind Farm is the best documented offshore wind farm. There are also several papers discussing how to model Anholt, and the wind farm will be modeled according to these sources. They are mostly written by H. Brandtster [13], [14]. While the fact that harmonics in offshore wind farms exist and the tools to limit these harmonics using active or passive filters are fairly well documented, the source of these harmonics and the ways in which the layout and design of the wind farm impacts the harmonic level is poorly documented.

D. Dhua et al. experimented on the amplification of the harmonics in the offshore grid [15]. This master thesis will focus mainly on the harmonic impact from the converter using a similar method as D. Dhua et al used. However, this paper will focus on the converter while keeping the wind farm parameters constant, as opposed to D. Dhua et al., who changed the grid parameters and kept the wind turbine converter constant.

1.2 Objectives

The main objectives of this master thesis are:

1. Design and simulate the electrical components of a wind turbine, using data from already existing offshore wind farms.

2. Design and simulate the associated electrical offshore grid in the wind farm.

3. Examine how different scenarios, mainly with the control of the Voltage Source Converter (VSC) in the wind turbine, impact the harmonics in the offshore wind farm at Point of Common Coupling (PCC), point of grid connection and at the wind turbine.

4. Examine how the harmonics can be limited or shifted by using active filtering.

The two first two objectives include making a model that can be used for further analysis. All information required to make this model will be provided in the thesis so that it can be used by other students in their investigations into harmonics in offshore wind farms. The last two objectives simulate different scenarios using the aforementioned model.

1.3 Approach and limitations

This master thesis is following a specialization project, which was a literature review researching the harmonics in offshore wind farms. Since the specialization project is unpublished, the most important findings will be presented in the literature review and the theory section of this master thesis. The main focus will, however, be on creating and simulating a credible and realistic model of an offshore wind farm.

This model will be built using Matlab and Simulink. The computer running the simulations is a MacBook Pro from late 2013 with a 2.3 GHz Intel Core i7 processor, 16 GB of memory and a NVIDIA GeForce GT 750M Graphics card. This is the personal computer of the author of this master thesis, and sets limitations on the complexity of the model.

The model will be built from the bottom up, expanding gradually to keep track of the complexity and run time. It will start by simulating only one wind turbine before filters, cables and transformers are added. Eventually, more wind turbines will be added. Due to the run time of the simulations, different approaches to adding turbines will be used, either as current sources or VSC. Simplifications and assumptions are made throughout the modelling and will be explained. Some simplifications are made to make the run time of the model shorter, and their impact will be discussed. Other simplifications due to practical reasons and having a small impact on the harmonics in the simulations will be justified throughout the thesis.

1.4 Outline

This thesis starts by introducing the project, giving a short literature review and stating the objectives, approach and limitations.

- Chapter 2 introduces the relevant theory, including a brief background in harmonics, resonance and harmonic filtering.
- Chapter 3 discusses the design of an offshore wind turbine and how to model a VSC. The last part of this chapter shows the results from modeling the wind turbine as a VSC, and the impact of tuning the control system.
- Chapter 4 discusses the modelling of the passive components in the full wind farm, including the grid, cables and transformers.

- Chapter 5 presents the different scenarios that are simulated in this thesis, and shows the results of these simulations. In addition, a frequency sweep of the system is performed to determine the frequency-dependant impedance of the offshore wind farm.
- Chapter 6 introduces active filtering by adding a notch filter to the control system. The results from the active filtering are also presented.
- Chapter 7 discusses the results found in the earlier chapters, confirming already tested hypotheses and presenting new knowledge found in the simulations.
- Chapter 8 summarizes the most important findings in this master thesis.
- Chapter 9 suggests what can be done as further work in conjunction with this master thesis.

Chapter 2: Theory

In this chapter, the relevant theory for this master thesis will be explained. The reader is assumed to have a good grasp of the field of power electronics, but no extensive knowledge of harmonics and resonance. Both will be explained in this section, in addition to passive and active filtering. The last section will present the IEEE harmonic standards.

2.1 Harmonic distortion

Current and voltage are expressed as either Alternating Current (AC) or Direct Current (DC) with AC current or voltage defined as:

$$V(t) = \bar{V} sin(\omega t + \phi) \tag{2.1}$$

An AC current or voltage is referred to as having a frequency $f = \frac{\omega}{2\pi}$ and a Root Mean Square (RMS) value $V_{RMS} = \frac{\bar{V}}{\sqrt{2}}$. However, current coming from a converter or a water turbine will not be perfectly sinusoidal and harmonic distortion is used to describe the aspects of the current or voltage that do not fit in Eq. 2.1. By using Fourier analysis of repetitive wave forms, any current or voltage can be described as the superposition of a sinusoidal wave with a fundamental frequency and harmonic distortions [16].

In general, a non-sinusoidal waveform $f(t)$ periodically repeating with an angular frequency w can be expressed as

$$f(t) = F_0 + \sum_{h=1}^{\infty} f_h(t) = \frac{1}{2} a_0 + \sum_{h=1}^{\infty} \{a_h cos(h\omega t) + b_h sin(h\omega t)\} \tag{2.2}$$

where $F_0 = \frac{1}{2} a_0$ is the average value,

$$a_h = \frac{1}{\pi} \int_0^{2\pi} f(t) cos(h\omega t) d(\omega t) \qquad h = 0, 1, \cdot\cdot, \infty \tag{2.3}$$

and

$$b_h = \frac{1}{\pi}\int_0^{2\pi} f(t)sin(h\omega t)d(\omega t) \qquad h = 1,\cdots,\infty \tag{2.4}$$

Table 2.1 summarizes the most common symmetries associated with Fourier transformations.

Table 2.1: Use of symmetry in Fourier analysis

Symmetry	Condition required	a_h and b_h
Even	$f(-t) = f(t)$	$b_h = 0 \quad a_h = \frac{2}{\pi}\int_0^{\pi} f(t)cos(h\omega t)d(\omega t)$
Odd	$f(-t) = -f(t)$	$a_h = 0 \quad b_h = \frac{2}{\pi}\int_0^{\pi} f(t)sin(h\omega t)d(\omega t)$
Half-wave	$f(t) = -f(t+\frac{1}{1}T)$	$a_h = b_h = 0$ for even h $a_h = \frac{2}{\pi}\int_0^{\pi} f(t)cos(h\omega t)d(\omega t)$ for odd h $b_h = \frac{2}{\pi}\int_0^{\pi} f(t)sin(h\omega t)d(\omega t)$ for odd h
Even quarter-wave	Even and half-wave	$b_h = 0$ for all h $a_h = \begin{cases} \frac{4}{\pi}\int_0^{\frac{\pi}{2}} f(t)cos(h\omega t)d(\omega t) & \text{for odd } h \\ 0 & \text{for even } h \end{cases}$
Odd quarter-wave	Even and half-wave	$a_h = 0$ for all h $b_h = \begin{cases} \frac{4}{\pi}\int_0^{\frac{\pi}{2}} f(t)sin(h\omega t)d(\omega t) & \text{for odd } h \\ 0 & \text{for even } h \end{cases}$

A current or voltage in steady state will always be odd, meaning that $a_h = 0$. A harmonic component is referred to by the value of h, meaning the h^{th} harmonic will have a frequency of $f_h = hf_1$. The amplitude of the harmonic is expressed as a percentage value of the fundamental amplitude. If this is calculated in steady state, the percentage value of a single harmonic component will be:

$$H_h = \frac{b_h}{b_1}\cdot 100\% \tag{2.5}$$

where b_1 is the peak value of the fundamental frequency and b_h is the peak of the h^{th} harmonic component, as defined in Eq. 2.4.

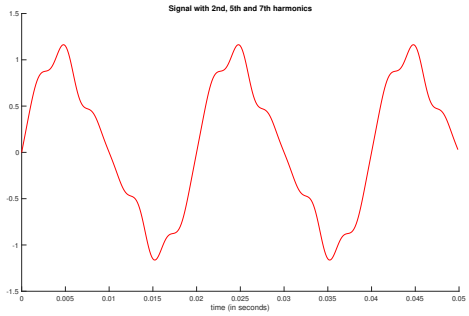

(a) Signal with harmonic components

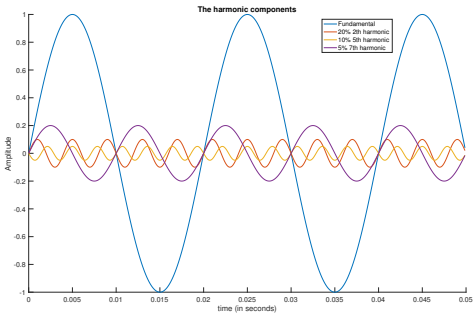

(b) All the harmonic components plotted individually

Figure 2.1: Harmonic plot with the superposition of the harmonics and the individual harmonic components

Figure 2.1 shows an example of what a signal with harmonic components looks like. Figure 2.1a is a signal with 20% 2^{nd}, 10% 5^{th} and 5% 7^{th} harmonic components. Figure 2.1b shows all these harmonic components plotted individually in addition to the fundamental component.

The Total Harmonic Distortion (THD) is a measurement to specify the total amount of harmonics in a signal. It is measured as a percentage of the fundamental component and can be seen in Eq. 2.6

$$THD = 100 \cdot \sqrt{\sum_{h=2}^{\infty} H_h^2} \tag{2.6}$$

2.2 Resonance

Resonance is a phenomena that causes specific electric frequencies to be amplified. Resonance is caused by the reactance of an electric circuit being frequency dependant, meaning that at a specific frequency there can be zero or infinite reactance. There are two different types of electric resonance: series resonance and parallel resonance.

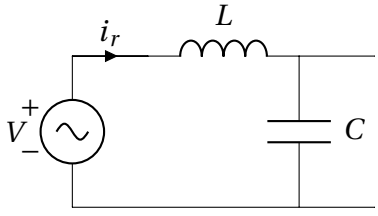

Figure 2.2: Voltage source with an inductive and conductive load in series

Figure 2.2 shows a circuit with a voltage source in series with an inductor and capacitor. This could, for example, be an underground cable or an overhead cable with an installed capacitor

bank. The current i_r from the voltage source is:

$$i_r = \frac{V}{j\omega L + \frac{1}{j\omega C}} \tag{2.7}$$

It is evident that as the denominator approaches 0, i_r will approach infinity. The frequency $f_{r,s}$ that makes the reactance in series with a voltage source equal to zero is called the series resonance frequency. In figure 2.2 this frequency would be:

$$f_{r,s} = \frac{1}{2\pi\sqrt{CL}} \tag{2.8}$$

The resonance can be dampened by putting a resistance in series with the inductance or capacitance. This would lessen the resonance current, but would also cause losses in the system.

Parallel resonance is caused by a current source connected to an inductor and capacitor in parallel, as seen in figure 2.3. The voltage v_c would then be equal to:

$$v_c = I\frac{-\omega^2 LC}{j\omega L + \frac{1}{j\omega C}} \tag{2.9}$$

When the denominator in the reactance approaches zero, the total reactance approaches infinity, making an infinite induced voltage. This happens when the frequency is equal to:

$$f_{r,p} = \frac{1}{2\pi\sqrt{CL}} \tag{2.10}$$

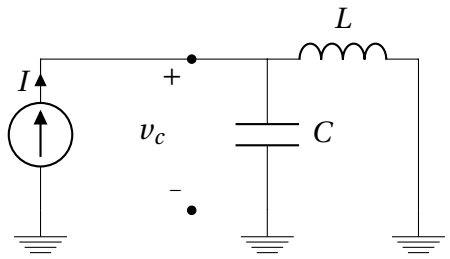

Figure 2.3: Current source with a inductive and conductive load in parallel

While the term resonance often refers to the specific frequency that has either zero or infinite reactance, the term can also be used to describe frequencies that have a relatively high or low reactance compared to the fundamental frequency. This is essential when investigating harmonic distortion in offshore grids as different harmonics spread differently through the grid due to the frequency dependant impedance.

2.3 Passive filtering

The previous section explained how currents and voltages will experience a frequency dependant reactance. While this may cause resonance in the system, it is also used for passive filtering.

If a current or voltage has harmonic components, each component will experience a different reactance. An overhead cable simplified to an RL circuit will have a significantly higher impedance for the high frequency harmonic components than it will for the low frequency harmonic components. Figure 2.4 shows an overhead line or an RL filter. The frequency dependent current will then be:

$$i_f = \frac{V_{inn,f} - V_{out,f}}{j\omega L + R} \tag{2.11}$$

Eq. 2.11 shows that the current will be higher at the lower frequencies, even if the higher order harmonics in the voltage are the same as the lower order harmonics. An RL filter is efficient in filtering high order voltage harmonics, and is used in connection with converters and other electrical equipment where there is a DC-voltage connected to the grid.

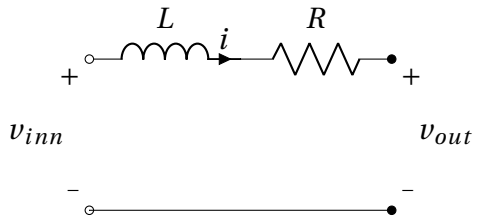

Figure 2.4: Overhead cable modeled as an RL-section

While overhead cables, transformers and other inductive components naturally filter out the higher order harmonics, current harmonics already existing can be filtered out by using a designated passive filter. These filters are designed to sink the harmonic current into the ground, which it does by having an inductor and a capacitor connected in series between the ground and the cable. By adjusting the inductance and the capacitance, the filter can be tuned to have zero reactance at one specific harmonic frequency, while having a relatively high reactance at the fundamental frequency.

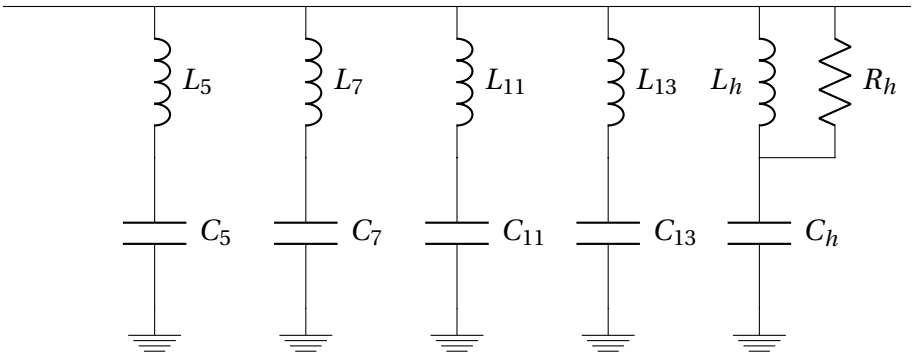

Figure 2.5: Passive filters tuned for each harmonic frequency with a high-pass filter at the end

Figure 2.5 shows four single-tuned passive filters connected in parallel, with a high-pass filter at the end. Passive filters are normally single-tuned at the lower harmonic frequencies to make sure the impedance at the fundamental frequency is as high as possible. The impedance of each individual filter will be:

$$Z_f = j\omega L + \frac{1}{j\omega C} \tag{2.12}$$

The filter frequency will then be the frequency where the impedance is at its minimum:

$$f_f = \frac{1}{2\pi\sqrt{CL}} \tag{2.13}$$

From Eq. 2.13, it is evident that there are two orders of freedom when designing a passive filter; the capacitance and the inductance. The relation between these two values will determine the impedance at the fundamental frequency, and thus the quality of the filter. Figure 2.6 shows the frequency dependent impedance of four different passive filters, two tuned to the 2^{nd} harmonic and two tuned to the 5^{th} harmonic. The four filters have a different quality factor Q, which is a measurement of the width of the low impedance band. From the plot, it is evident that the filter for the 2^{nd} harmonic needs a higher Q to have the same impedance at the fundamental frequency than the Q needed for the 5^{th} harmonic. The quality factor Q is given as [17]:

$$Q = \frac{2\pi f_f L}{R} \tag{2.14}$$

A higher quality factor requires a higher inductance, or a smaller resistance, both of which make the filter bigger and more expensive. This is the reason why lower order current harmonics are harder and more expensive to filter than higher order current harmonics.

In addition to the simple shunt *LC* filter shown in this section, there is a wide range of set ups for passive filters with different performance and complexity [18], [19], [14].

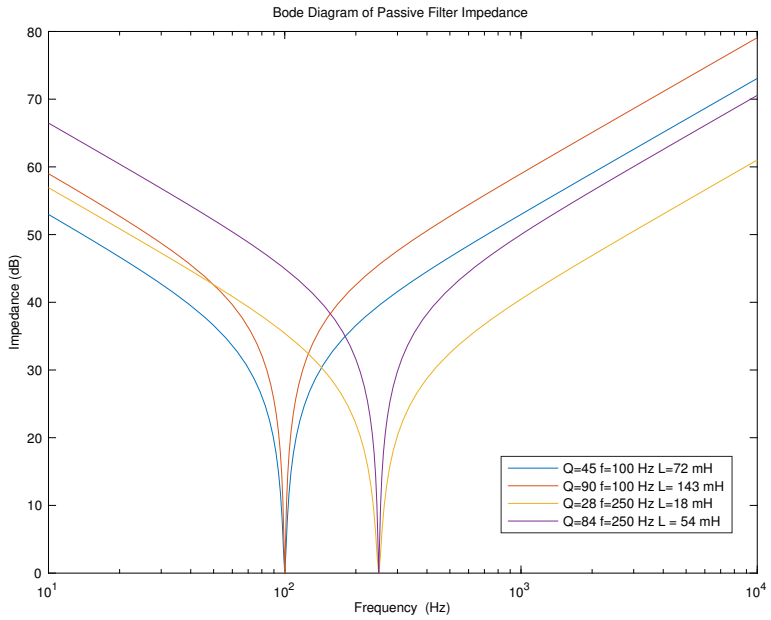

Figure 2.6: Impedance plot of four different passive filters

2.4 Active filtering

While passive filters consist of only passive elements like inductors and capacitors, active filters consist of active elements, like switches, which have to be controlled. Active filtering can be done in any component that is actively controlled, independent of whether filtering is the designated task of the component or not. The active filtering capability of a component is, among other things, dependant on the layout of the component, the control system and the switching frequency [20].

Active filtering can also be done by installing a designated active filter as seen in Figure 2.7. An active filter can be installed either in shunt or in series. A series active filter is more suitable to filter out voltage harmonics, while a shunt active filter is used to filter out current harmonics. The drawback with a series active filter is that all the current has to go through the filter, making it expensive to scale and hard to retrofit [21]. Therefore, the shunt active filter is the most common set up [18].

While installing a designated active filter normally has the best harmonic performance, retuning already existing active components is the cheaper option.

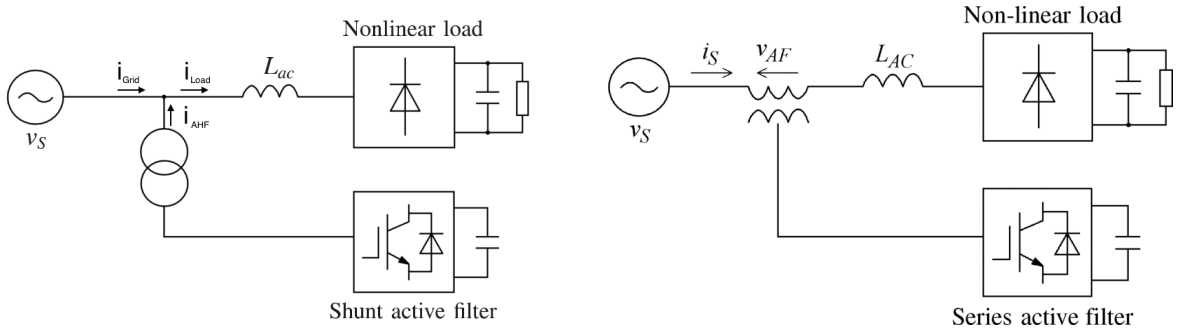

(a) Single-phase or three-phase shunt active filter (b) single-phase or three-phase series active filter

Figure 2.7: Shunt and series active filters [18]

2.5 Harmonic standards

Harmonic standards are created to make sure the harmonic level in the grid does not exceed levels that will put fragile electronic equipment at risk. These standards vary from country to country and are regularly republished.

IEEE has published a standard that provides guidance for operators installing electrical equipment to the grid [5]. The IEEE's regulations have been criticized for not being precise enough for big wind farms. This follows since different models for calculating the harmonics yield different results [8], and the specified method in the standards is not always the most precise [22].

The standard gives the recommended voltage and current harmonics at PCC. The responsibility of keeping the harmonics within the given limits is shared between the customer, the system owner and the operator.

Bus voltage V at PCC	Indivdual harmonic (%)	Total harmonic distortion THD (%)
$V \leq 1.0kV$	5.0	8.0
$1kV < V \leq 69kV$	3.0	5.0
$69KV < V \leq 161kV$	1.5	2.5
$161kV < V$	1.0	1.5

Table 2.2: Voltage distortion limits [5]

Table 2.2 shows the voltage distortion limits at PCC for buses at different voltages. The table shows that the lower the voltage, the more harmonics are allowed to be injected into the grid.

Table 2.3: Maximum harmonic current distortion in (%) of I_L for a system rated 120 V < V < 69 kV [5]

I_sc/I_L	$3 \leq h < 11$	$11 \leq h < 17$	$17 \leq h < 23$	$23 \leq h < 35$	$35 \leq h \leq 50$	TDD
< 20	4.0	2.0	1.5	0.6	0.3	5
20 < 50	7	3.5	2.5	1	0.5	8
50 < 100	10.0	4.5	4.0	1.5	0.7	12.0
100 < 1000	12.0	5.5	5.0	2.0	1.0	15.0
> 1000	15.0	7.0	6.0	2.5	1.4	20.0

The values given in this table are for odd harmonics. Even harmonics are limited to 25% of the values in this table.

Table 2.4: Maximum harmonic current distortion in (%) of I_L for a system rated > 161 kV [5]

I_{SC}/I_L	$3 \leq h < 11$	$11 \leq h < 17$	$17 \leq h < 23$	$23 \leq h < 35$	$35 \leq h \leq 50$	TDD
< 25	1.0	0.5	0.38	0.15	0.1	1.5
25 < 50	2.0	1.0	0.75	0.3	0.15	2.5
≥ 50	3.0	1.5	1.15	0.45	0.22	3.75

The values given in this table are for odd harmonics. Even harmonics are limited to 25% of the values in this table.

Table 2.3 and 2.4 show the maximum current distortion for low voltage and high voltage systems, respectively. h is the specific harmonic, I_L is the load current and I_{SC} is the maximum short circuit current at PCC. The short circuit current is a measure of the quality of the grid. A higher short circuit current means less impedance in the grid, which is a sign of a higher quality grid. Total Demand Distortion (TDD) is the THD of the maximum demand current.

Chapter 3: Designing the wind turbine

In this chapter, the wind turbine converter will be designed. The goal of these simulations is to investigate the harmonics produced in offshore wind turbines by the converters, with the main focus on the lower order harmonics having a frequency lower than 1000 Hz. The lower order harmonics are more troublesome to deal with, as described in section 2.3.

Modern wind turbines are connected to the grid with a VSC [23]. The two most dominant types of wind turbines today are the full scale back to back converter (Figure 3.1b) set up, and the doubly fed induction generator (DFIG) (Figure 3.1a). While the DFIG is the dominant wind turbine set up in the market at the moment, it is expected that the Type 4 full scale back to back converter set up will take over [23].

Anholt Offshore Wind Farm will be the basis for the simulations performed in this thesis, and data from the offshore wind farm will be used where available. Through several studies already conducted, namely [6], [13] and [14], a lot of data is available. In the cases where no data is available, assumptions will be made based on common practice.

Figure 3.1b shows what a wind turbine with a full scale back to back VSC looks like. Since this thesis is simulating the grid side harmonics, the generator side of the model is not required in the simulations. Only the grid side converter will be simulated. The capacitor between the converters will be replaced with a DC voltage source to further simplify the simulations. Another option would be to simulate the generator side of the turbine as a current source in parallel with a capacitor. The two different ways of simulating the generator side give slightly different results.

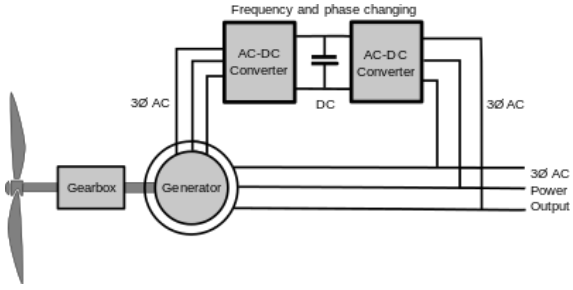

(a) Doubly fed induction generator for wind turbine [24]

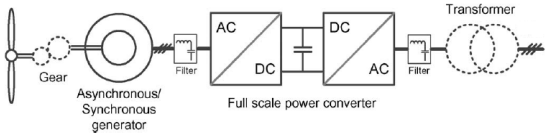

(b) Full scale converter wind turbine[25]

Figure 3.1: Doubly fed induction generator and full scale converter wind turbines

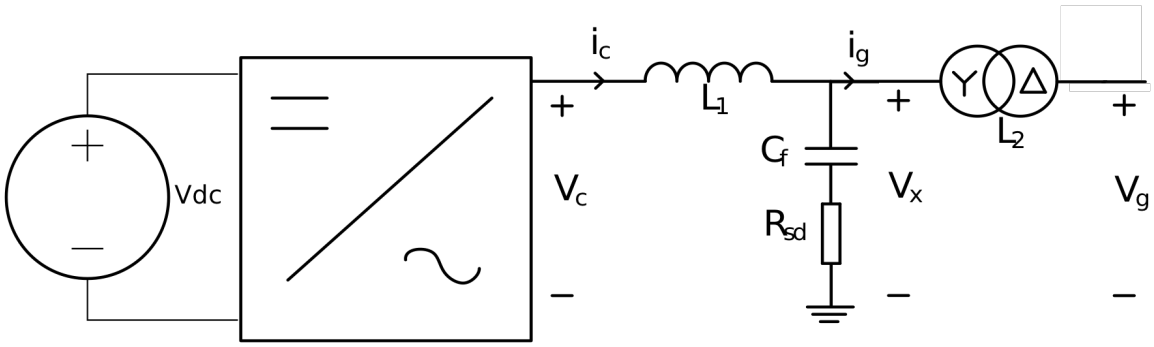

Figure 3.2: Model of the wind turbine

Ł. Kocewiak has shown that the real measurement results will lay somewhere in between these simulation methods [8]. Figure 3.2 shows how the turbine will be simulated.

3.1 LCL-filter

The grid side filter of the VSC will be simulated as a inductor-capacitor-inductor filter (LCL-filter) The last inductor L_2 will be the transformer. The first inductor L_1 is called the converter side inductor.

The inductance and capacitance of the filter will be based on real values from Anholt Offshore Wind Farm [14]. The voltage and currents used in the control system will be V_x and I_g as seen in Figure 3.2, measured before the transformer.

Normally the converter side inductor will be chosen so that the output current ripple from the converter is less than 10% [26]. The output value of the current from the converter can be seen in Eq 3.1. From the equation, it is evident that the highest amount of ripple will occur when the duty cycle D is 0.5. The duty cycle is a measure of the average fraction of the switching cycle in which the upper switch in the complementary pair of switches at each phase is open. The higher the duty cycle, the higher the output power of the converter. f_{sw} is the switching frequency, V_{dc} is the DC-voltage and I_{base} is the base value of the injected grid current from the converter. Figure 3.3 shows an overview of the switches, currents and voltages.

$$L_1 = \frac{(V_{dc} - DV_{dc})D}{2\Delta i_{imax,p-p} f_{sw}} = \frac{V_{dc}}{8\Delta i_{imax,p-p} f_{sw}} \tag{3.1}$$

$$where, \qquad \Delta i_{imax,p-p} = 0.1\sqrt{2} I_{base}$$

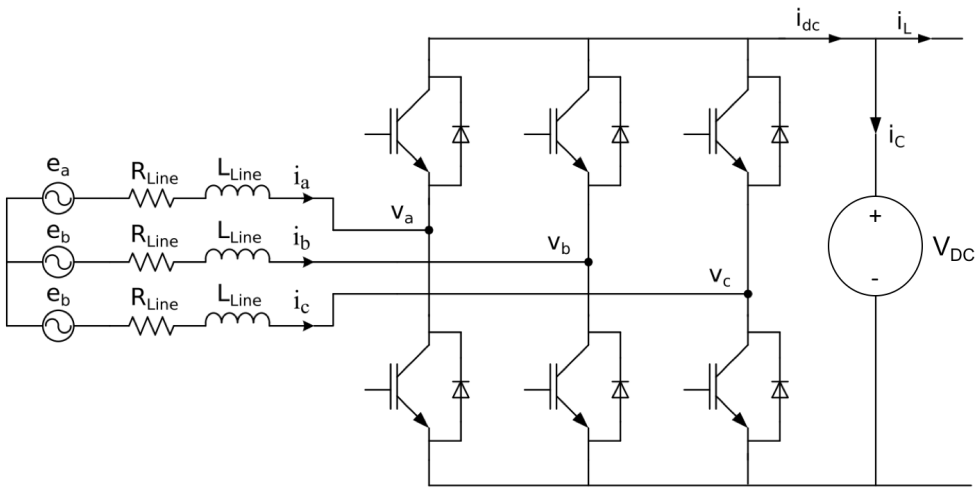

Figure 3.3: VSC consisting of switches, an RL-filter and a voltage source

Since the grid side inductor of the LCL-filter is a transformer, there are certain restrictions in deciding the inductance. When scaling the converter, there are a lot of important aspects that need to be taken into consideration, such as the winding ratio and the size and saturation of the transformer. The inductance of the transformer, therefore, can not be chosen arbitrarily, but is a result of these restrictions. This impacts the design of the converter side inductor as well as the capacitor.

Since this is an LCL-filter, there will be an associated resonance frequency. The resonance frequency of the LCL-filter can be seen in Eq. 3.2, where f_1 is the grid frequency. To dampen the resonance in the system, a resistance is added to the shunt branch of the LCL-filter. It is important that the resonance in the filter does not amplify the most common harmonic frequencies coming from the converter, and the LCL-filter is therefore tuned so that the resonance frequency is within the limits seen in Eq. 3.2.

$$f_{res} = \frac{1}{2\pi}\sqrt{\frac{L_1 + L_2}{L_1 L_2 C_f}} \qquad 10 f_1 < f_{res} < 0.5 f_{sw} \tag{3.2}$$

3.2 The control system

After the layout and the filtering of the converter is decided, a control system must be designed. The control system consists of three parts [27]:

1. Obtaining the applied current and voltage of the converter. The output current and voltage of the converter have to be measured.

2. Generating the reference signal. The control system has to be designed so that the converter will produce the desired current. In a wind turbine converter, this is done by controlling the reference current.

3. Generate a gate signal. The switches have to be controlled so that the desired current will be generated.

Figure 3.4 shows an overview of the control system for the converter. To control the switches, a Pulse Width Modulator (PWM) is used and a $d-q$ reference frame is used in the current controller.

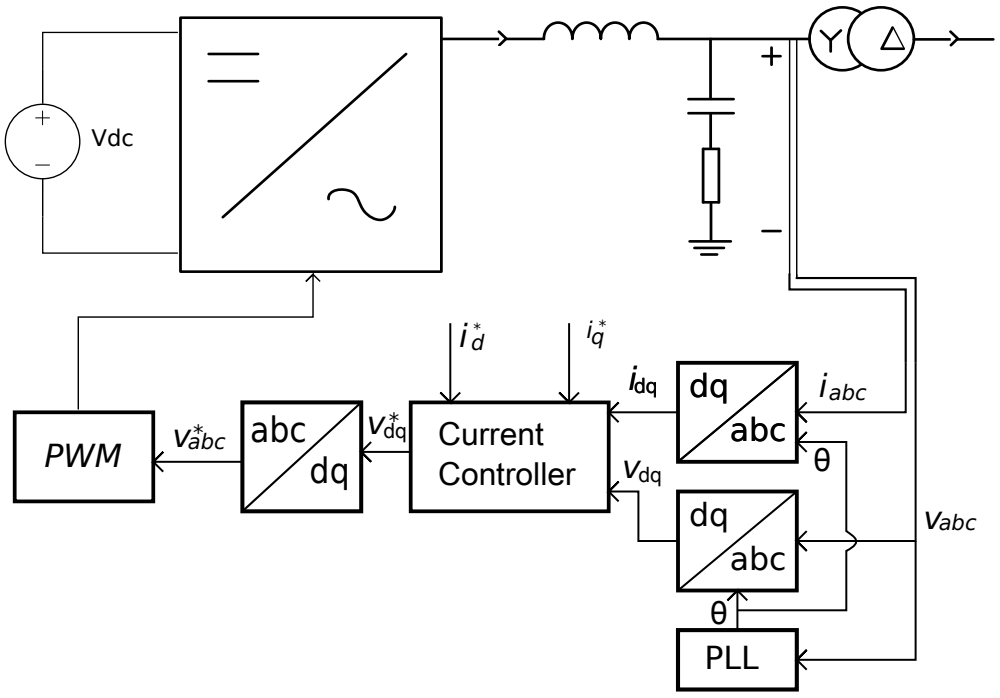

Figure 3.4: Overview of the control system of the converter

3.2.1 Pulse width modulator

There are several ways to generate a gate signal for the converter, which has an impact on the response speed and the generated harmonics around the switching frequency. In this master thesis, a PWM will be used due to the fact that it is rather common and because of the simplicity of its implementation.

The PWM takes the reference voltage as an input and returns the control signal to the switches as the output. The reference voltage given as input is the same voltage that is needed to generate the desired output current from the VSC and is calculated in the current controller. The goal of

the PWM is to make the converter generate the closest possible resemblance of the reference voltage [16].

In these simulations, a bipolar PWM is used. It compares a triangular signal with a frequency equal to the switching frequency, and an amplitude of $\pm V_{DC}$ to the reference voltage given as input. When the triangular signal is larger than the reference signal, the gate signal to the top switch will be 1 and the bottom switch 0, as seen in Figure 3.3. This will give an output voltage of V_{DC}. When the triangular signal is smaller than the reference signal, the gate signal to the top switch will be 0, and the bottom switch will be 1. This will generate a voltage of 0.

3.2.2 Current controller

The $d-q$ reference frame is chosen in the current controller due to how common it is in full scale converters, and because it is the same reference frame used in Anholt Offshore Wind Farm [12].

The $d-q$ reference frame is rotating with the same frequency as the fundamental component of the voltage, meaning the fundamental component of the voltage and current will be DC-components. In the control system of the VSC, the reference is set so that the reference frame is in phase with the voltage. This means that the current contributing to the active power will be set as i_d, while the current contributing to the reactive power will be set as i_q. The relation between the abc-reference frame and the $d-q$ reference frame can be seen in Eq. 3.3. As long as the system is balanced, the zero sequence component will be constant and equal to 0.

$$\begin{bmatrix} v_d \\ v_q \\ v_0 \end{bmatrix} = \frac{2}{3} \begin{bmatrix} cos(\omega t) & cos(\omega t - \frac{2\pi}{3}) & cos(\omega t + \frac{2\pi}{3}) \\ -sin(\omega t) & -sin(\omega t - \frac{2\pi}{3}) & -sin(\omega t + \frac{2\pi}{3}) \\ \frac{1}{2} & \frac{1}{2} & \frac{1}{2} \end{bmatrix} \begin{bmatrix} v_a \\ v_b \\ v_c \end{bmatrix} \tag{3.3}$$

Since the DC-side of the converter is represented as an ideal voltage source, the produced power will be decided by the reference current. This means that i_d^* and i_q^* can be set as desired, and will be used to represent the power output of the converter. The aim of the current controller is to provide a sinusoidal current with as few harmonic components as possible.

The influence of the capacitor in the LCL-filter will be neglected in the modeling of the current controller. In fact, it is only there to deal with the switching ripples, and for frequencies lower than half the resonance frequency, the converters with LCL-filters will behave the same way as converters with an RL-filter [20].

Figure 3.3 shows a schematic overview of the converter where the filter is modeled as an RL filter instead of an LCL filter. From the figure, Eq. 3.4 can be derived:

$$e_{abc} = R_{line} i_{abc} + L_{line} \frac{d i_{abc}}{dt} + v_{abc} \tag{3.4}$$

e_{abc} is the grid voltage at the point of connection for the converter. Since this is a simplification of the LCL filter, L_{line}, denoted as L from now on, will be the sum of the inductance in the LCL filter. R_{line}, denoted as R from now on, represents the losses in the switches and conduction losses. v_{abc} is the terminal voltage at the switches.

Since the current controller uses the $d-q$ reference frame, Eq. 3.4 has to be transformed from the abc to the $d-q$ reference frame [28]:

$$\begin{bmatrix} e_d \\ e_q \end{bmatrix} = R \begin{bmatrix} i_d \\ i_q \end{bmatrix} + L \frac{d}{dt} \begin{bmatrix} i_d \\ i_q \end{bmatrix} + \omega L \begin{bmatrix} 0 & -1 \\ 1 & 0 \end{bmatrix} \begin{bmatrix} i_d \\ i_q \end{bmatrix} + \begin{bmatrix} v_d \\ v_q \end{bmatrix} \tag{3.5}$$

Eq. 3.5 shows that there is a cross coupling between d and q axis, in the part with ωL. The cross coupling means that the current i_d is part of the voltage v_q, and also that i_q is part of v_d. The control system has to decouple this coupling to be able to control the reactive and active power independently of each other. In addition, a PI controller is used to stabilize the system due to its ability to eliminate offsets [29].

Taking this into account, a reference voltage can be designed so that the d and q components will be decoupled while at the same time generating the desired current [28]:

$$\begin{aligned} v_d^* &= -\left(K_{p,d} + \frac{K_{I,d}}{s}\right)(I_d^* - i_d) + \omega L i_q + e_d \\ v_q^* &= -\left(K_{p,q} + \frac{K_{I,q}}{s}\right)(i_q^* - i_q) - \omega L i_d + e_q \end{aligned} \tag{3.6}$$

Figure 3.5 shows a schematic model of Eq. 3.6, which is the implemented control system. K_p and K_I are the proportional and integral components of the PI-controller, with subscript d and q representing the two different PI-controllers.

With the control system established, the full system can be seen in Figure 3.6.

To tune the PI-controller, the transfer functions of the system and the PWM have to be derived. The PWM will cause a delay to the system dependent on the switching frequency f_s. The control signal will pass the reference signal twice in one cycle of the control signal, meaning this delay will be half the switching period [31].

$$H_{PWM}(s) = \frac{1}{1 + T_a s} \qquad T_a = \frac{1}{2 f_s} \tag{3.7}$$

So far the system has been modelled as an L-filter. This is a valid simplification when modeling the control system. However, the author experienced instabilities in the system when this simplification was kept to tune the PI-controllers, and the full transfer function of the LCL-filter

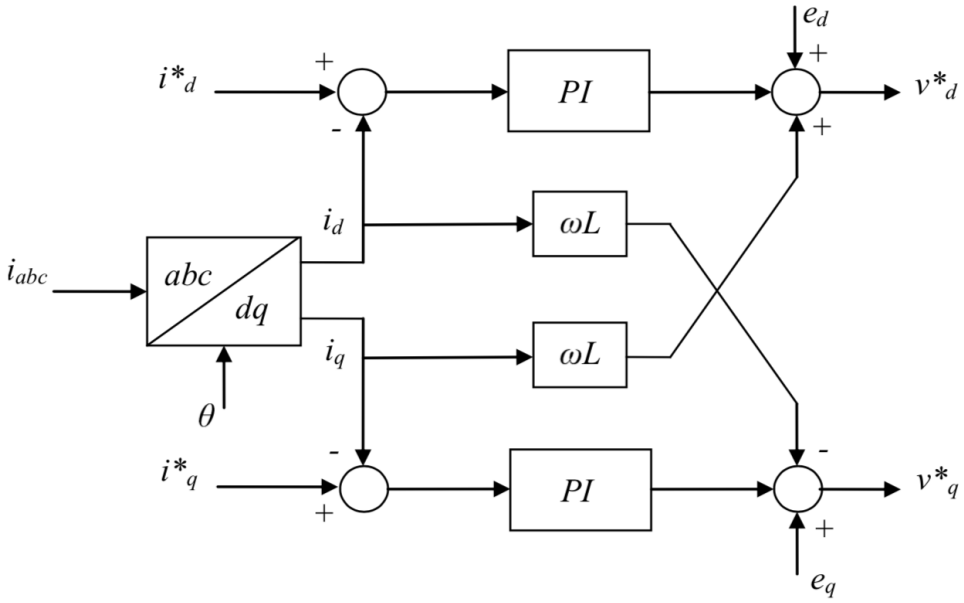

Figure 3.5: Control system with the $d-q$ reference frame [30]

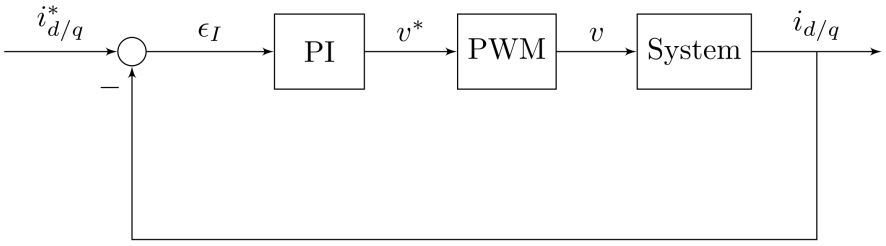

Figure 3.6: Schematic overview of the full system

was therefore used. The transfer function of an LCL-filter can be seen in Eq 3.8 [32].

$$H_{System} = \frac{R_{sd}C_f s + 1}{L_1 L_2 C_f s^3 + (L_1 + L_2)R_{sd}C_f s^2 + (L_1 + L_2)s} \tag{3.8}$$

The variables in Eq. 3.8 are the same as in Figure 3.2. The transfer function for the PI-controller is:

$$H_{PI} = Kp + \frac{K_I}{s} \tag{3.9}$$

3.2.3 Phase locked loop

The current controller uses a rotating $d-q$ reference frame synchronized with the grid voltage at the converter side of the transformer. A Phase Locked Loop (PLL) is required to synchronize the reference frame with the voltage angle. The PLL is analyzing the three phase voltage, and

then finding the angle θ or ωt of the voltage in an exact moment. The signal coming out of the PLL should be a triangular signal going from 0 to 2π with a period $T = 1/f_g$, where f_g is the grid frequency

There are different methods for modelling the PLL, like using the orthogonal voltages and comparing the error [33], or doing a closed loop $d-q$ transformation [34]. Since the current controller already use a $d-q$ reference frame, the PLL is modelled using the $d-q$ transformation [34]:

$$\frac{d\theta}{dt} = \omega_{ref} + \Delta\omega = \omega_{ref} + K_p(x_q - x_{q,ref}) + K_I \int (x_q - x_{q,ref})\,dt \tag{3.10}$$

K_I and K_p are the integral and proportional parts of the PI-controller, and θ is the phase angle of the a-phase of the voltage, also known as ωt. ω_{ref} is the reference frequency speed of the grid. x is the voltage at PCC in the $d-q$ reference frame, meaning that x_q is the q component of the voltage and $x_{q,ref}$ is the reference q component of the voltage. Since the production of reactive energy will be controlled in the current controller, $x_{q,ref}$ will be set to 0.

From Eq. 3.10, the control system of the PLL can be modelled as seen in Figure 3.7. Normally, there would be a delay block in this function [33], but in these simulations the delay is not included.

The transfer function of this system can be seen in Eq 3.11:

$$H_{cl}(s) = \frac{K_p s + K_I}{s^2 + K_p s + K_I} \tag{3.11}$$

This is a second order transfer functions, and can be tuned as seen in Eq: 3.12:

$$K_p = 2\zeta\omega_n \qquad K_I = \omega_n^2 \tag{3.12}$$

where ζ impacts the shape of the response signal and is called the damping factor. ζ is normally set between 0.5 and 1 [33]. ω_n is the crossover frequency where the gain is equal to 1.

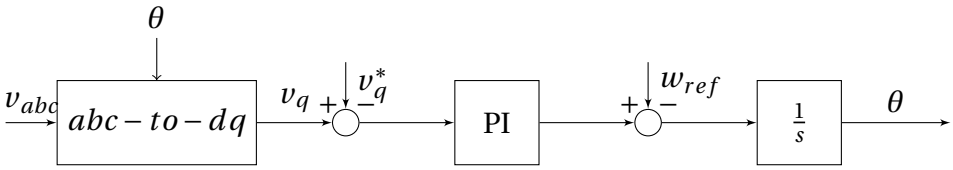

Figure 3.7: Control system of the PLL

3.3 Wind turbine parameters

The set up of the converter described so far can be used in a wide range of appliances, and the performance of the converter is dependant on the tuning of the control system and filters. For example, a higher switching frequency will lead to a lower THD, but also higher switching losses. Deciding the inductance and capacitance of the LCL-filter is another example of properties that will impact the losses and harmonics from the converter. Since there are sources on the values of both the switching frequency and the LCL-filter for Anholt Offshore Wind Farm [14] [15], the harmonic impact on tuning these components will not be discussed further in this master thesis. Instead, this thesis will look into the PLL and the PI-controllers in the current controller.

In this section, a base case will be established, so that different tuning scenarios can be compared to the base case. The control system will be designed as a per unit system. The base values of this system will be based on the RMS line to line voltage on the converter side of the transformer ($V_{LL,rms}$) and the rated power of the converter (S_n). These values are from Anholt, while the rest of the base values are calculated using the equations in Eq 3.13.

$$S_{base} = S_n; \quad V_{base} = V_{LL,rms}; \quad Z_{base} = \frac{V_{base}^2}{S_{base}}; \quad L_{base} = \frac{Z_{base}}{\omega_n};$$
$$C_{base} = \frac{1}{\omega_n Z_{base}}; \quad I_{base} = \frac{S_{base}}{\sqrt{3}V_{base}}; \quad \omega_n = 2\pi f_n \tag{3.13}$$

Table 3.1: Per unit bases

S_b	$5MVA$
V_b	$690V$
Z_b	$95.22m\Omega$
L_b	$303.1\mu H$
C_b	$33.43mF$
I_b	$4.184kA$

Both the transformer and the LCL-filter are described in [14], and their parameters can be seen in Tables 3.2 and 3.3.

Table 3.2: Parameters found in the Literature [14]

Parameter	Pu value	Absolute value
Grid frequency f_n	-	50 Hz
Converter side inductance L_1	0.10	$30.21\mu H$
Filter capacitor C_f	10.15	$3.293mF$
Grid side inductance L_2	0.075	$22.73\mu H$
Damping resistor R_{sd}	0.2198	$20.93m\Omega$

Table 3.3: Transformer Data for a 5 MVA $\Delta - Y$ WTG Transformer [14]

Rated voltage	33 kV/690 V
Primary side inductance	0.0375 pu
Primary side resistance	$2.675 * 10^{-3}$ pu
Secondary side inductance	0.0375 pu
Secondary side resistance	$2.675 * 10^{-3}$ pu
Shunt inductance	50 pu
Shunt resistance	870 pu

Since the grid side inductor is a transformer, L_2 is the Thevenin equvalent of the transformer. The full data for the transformer can be seen in Table 3.3. In the simulations, the simulink transformer block is used to simualte the transformer.

As discussed earlier, there was no data on the control system of the converters. The design of the control system is already discussed, but the PI-controllers in the current controller and the PLL have to be tuned.

The value of the PI-controllers can be seen in Table 3.4. The PLL is tuned by using Eq. 3.12 with a crossover frequency of $\omega_n = 10Hz$ and a damping factor of $\zeta = 1$, which is the same crossover frequency and damping factor used by S. Sanchez in [34].

The current controller is tuned by using the Matlab tool *Sisotool*. By entering the transfer function from Eq. 3.7 and Eq. 3.8, the PI-controller values are found by using the Ziegler-Nichols frequency response [35]. *Sisotool* was used for tuning the converters because of the complexity of the LCL transfer function.

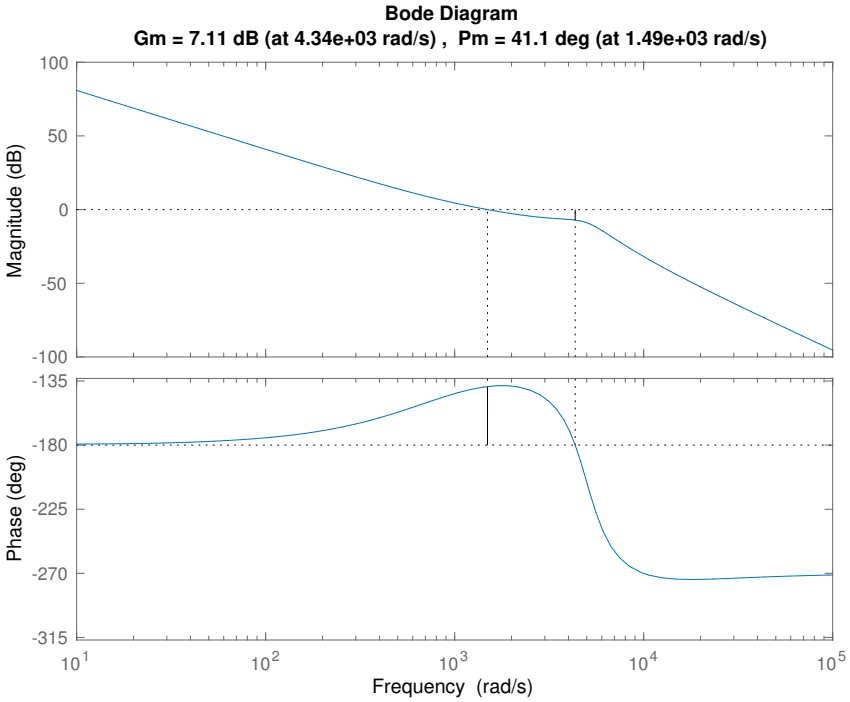

Figure 3.8: Bode plot of $\frac{i^*_{d/q}(s)}{i_{d/q}(s)}$ in base case

Table 3.4: PI-controller values

Current controller		PLL controller	
K_p	0.0644	K_p	20
K_I	58.558	K_I	100

K_p and K_I are the same for both PI controllers in the current controller

Figure 3.8 shows the Bode plot of the full open loop system as seen in Eq. 3.14

$$\frac{i^*_{d/q}(s)}{i_{d/q}(s)} = H_{PI}(s)H_{PWM}(s)H_{system}(s)$$

$$\frac{i^*_{d/q}(s)}{i_{d/q}(s)} = K_p + \frac{K_I}{s}\frac{1}{T_a s} \cdot \frac{R_{sd}C_f s + 1}{L_1 L_2 C_f s^3 + (L_1 + L_2)R_{sd}C_f s^2 + (L_1 + L_2)s} \tag{3.14}$$

The Bode plot shows that the system is stable, with a phase margin of 41.1° and a gain margin of 7.11 dB. While there is some room for maneuvering within the phase margin, a small change in the gain will make the system unstable.

3.4 Results from turbine simulation

The scope of these simulations is to compare the current and voltage harmonics coming from the converter. In this section, the harmonic impact on the feedback loop in the control system will be investigated, and the different components in the control system will be experimented with to find the sources of the harmonics. A base case is established to make it easier to compare the different cases against each other.

3.4.1 Results from base case

The simulations are started from zero state, with the capacitors and inductors not energized. Figure 3.9 shows the current and voltage at the point of connection for the converter (V_x and i_g from Figure 3.2), which is the same current and voltage that is used in the control system of the converter. It is evident from the plot that it takes about 0.1 second for the system to stabilize. Figure 3.10 takes a closer look at the voltage and current plots, and while the signals are sinusoidal, it is obvious that there is some harmonic distortion in both the current and the voltage. From the harmonic plots (Figure 3.11 and 3.12), it is evident that there are harmonics around the switching frequency, at 2400 Hz (48^{th}) and 2600 Hz (52^{nd}), for both the current and the voltage. This is as expected, as the switches will generate some harmonics [16]. It should be noted that there are more switching harmonics in the voltage than the current. This is caused by the voltage being measured before the final inductor in the LCL-filter. Since there is no saturation in the transformer, only the magnitude of the current will change while going through the transformer, meaning the current harmonics are the same before and after the transformer.

Figure 3.11 shows that there is a significant amount of 5^{th} order harmonics in the current, almost 2.5%. There is also more than 0.5% 7^{th} order harmonic. An ideal perfectly tuned converter should only have harmonics around the multiples of the switching frequency [16], and all the components of this converter are ideal. It should be noted however that the voltage at the converter side of the transformer has a non-trivial amount of high order harmonics, which will impact the control system. This will be further discussed in the next section.

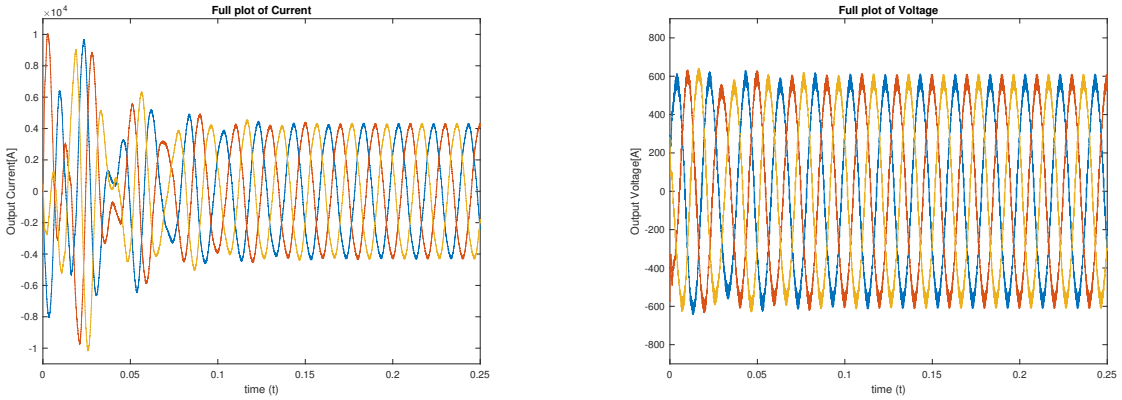

(a) Output current (b) Output voltage

Figure 3.9: Transient response from the current and voltage in base case

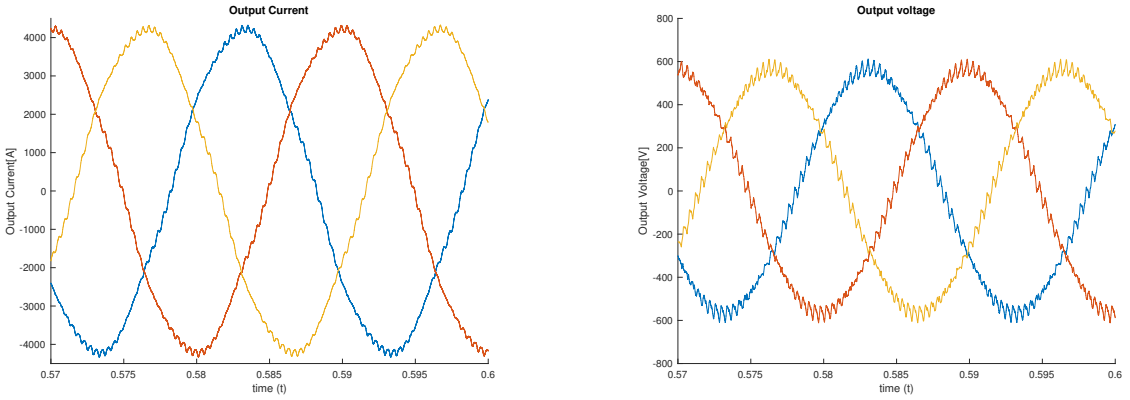

(a) Output current (b) Output voltage

Figure 3.10: Output current and voltage at converter side of transformer in base case

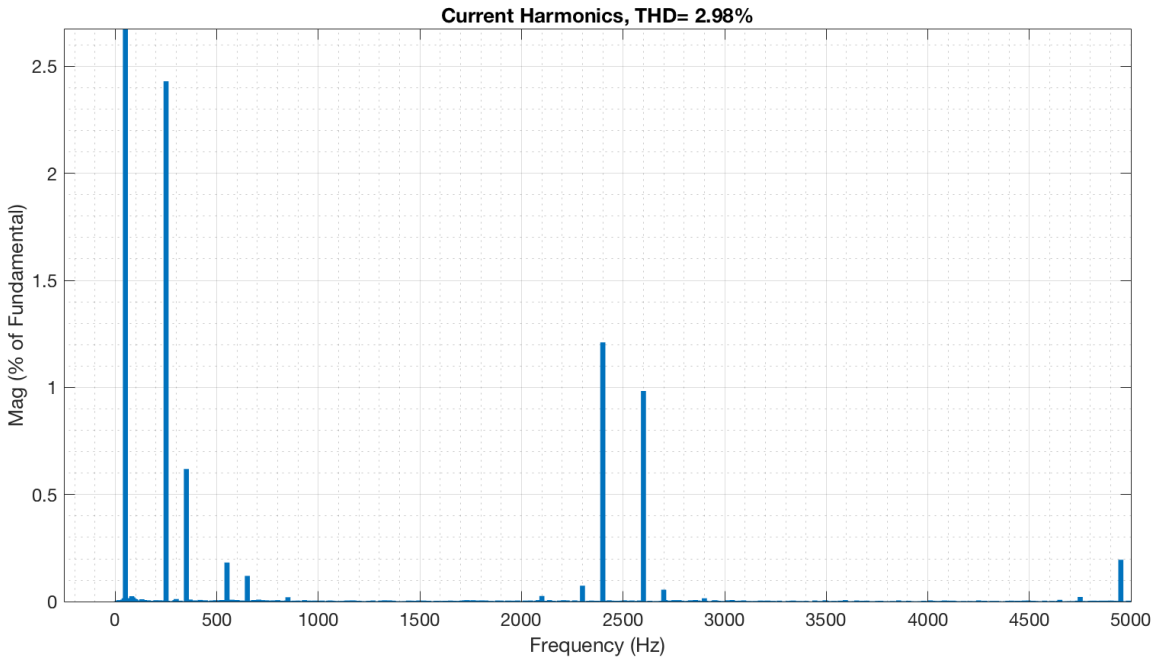

Figure 3.11: Current harmonics from the converter in base case

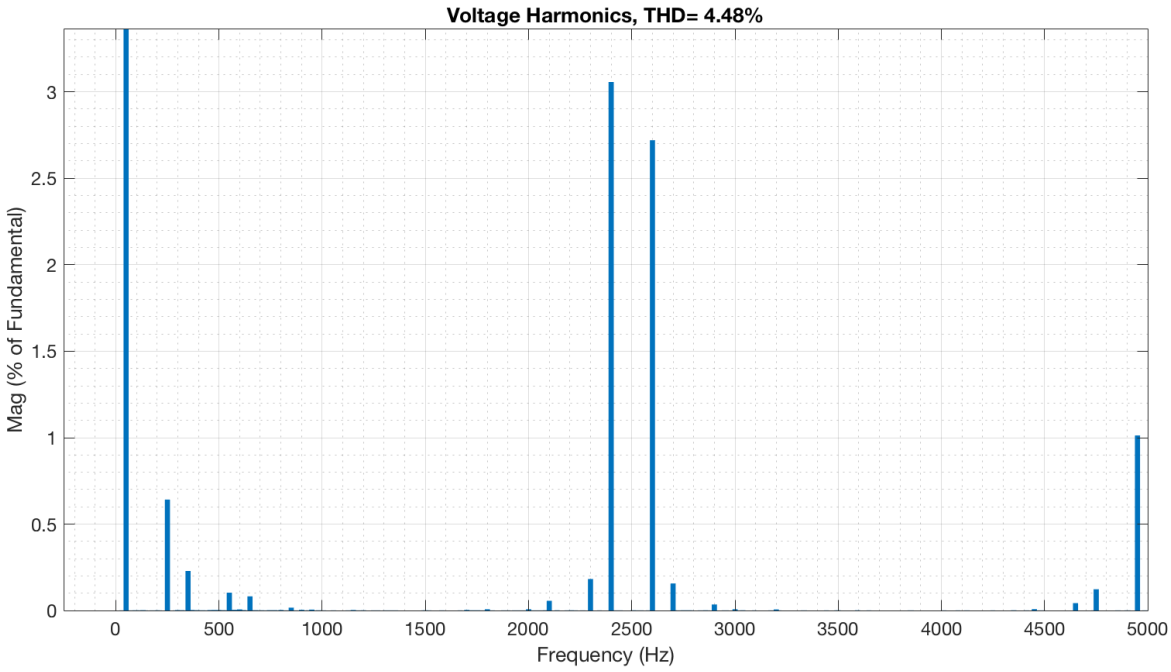

Figure 3.12: Voltage harmonics from the converter in base case

3.4.2 Harmonic impact from PLL

This subsection will look into the harmonic impact from the PLL. An ideal PLL will, in steady state, be a sawtooth signal without any oscillations. The PLL has to be able to adjust rapidly to transient changes in the reference voltage, and at the same time have good steady-state performance, even with a high amount of harmonics in the reference voltage. Figure 3.13 shows the sawtooth signal from the PLL in the base case (orange line) compared to an ideal sawtooth signal (blue line). It is evident that there are some high frequency oscillations in the PLL signal, originating from the high order harmonics in the measured voltage.

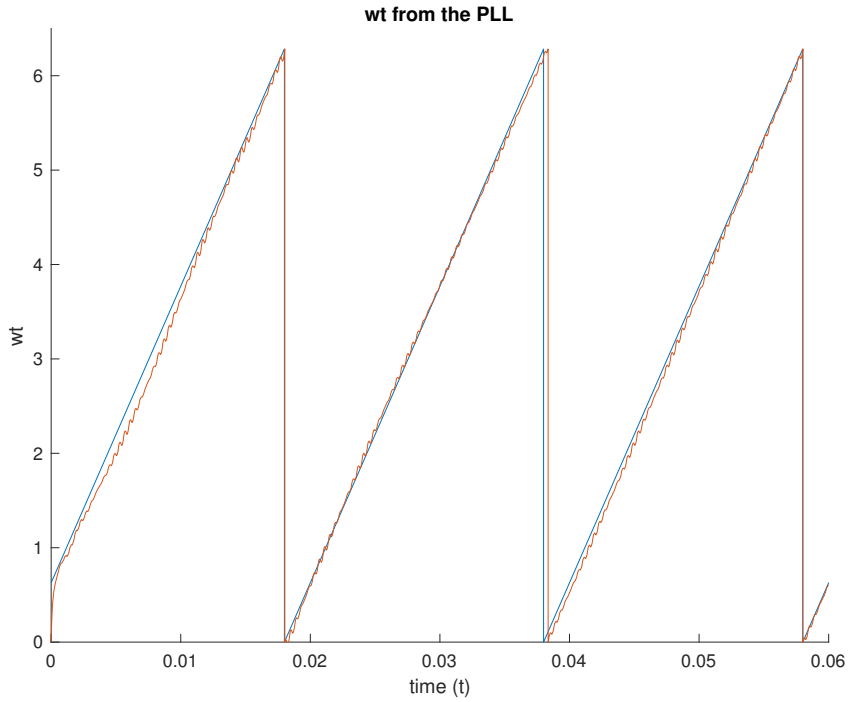

Figure 3.13: ωt from the PLL compared to an ideal sawtooth signal

Since the signal from the PLL is directly connected to the reference frame of the $d-q$ system, these oscillations are not desired. Figure 3.15 shows the results from the simulations when the PLL is switched out with an ideal sawtooth signal generator, which means the PLL will generate the blue signal from Figure 3.13. Figure 3.15 shows that the current and voltage plots looks very similar to the base case, and Figure 3.14 shows that the same holds true for the transient response. Figure 3.16 shows that there is a significant difference in the 5^{th} order current harmonic, however. That harmonic was more than 2.5% in the base case, and is now limited to a little over 0.2%. The 7^{th} order harmonic is also greatly reduced, and the total current harmonic distortion has decreased from 2.97% to 1.59%, with the only significant harmonic distortions being around the switching frequency. This shows the importance of tuning the PLL properly. The

voltage harmonics are also slightly reduced, but since the dominant harmonics in the voltage are those of multiples of the switching frequency, the effect is not as great.

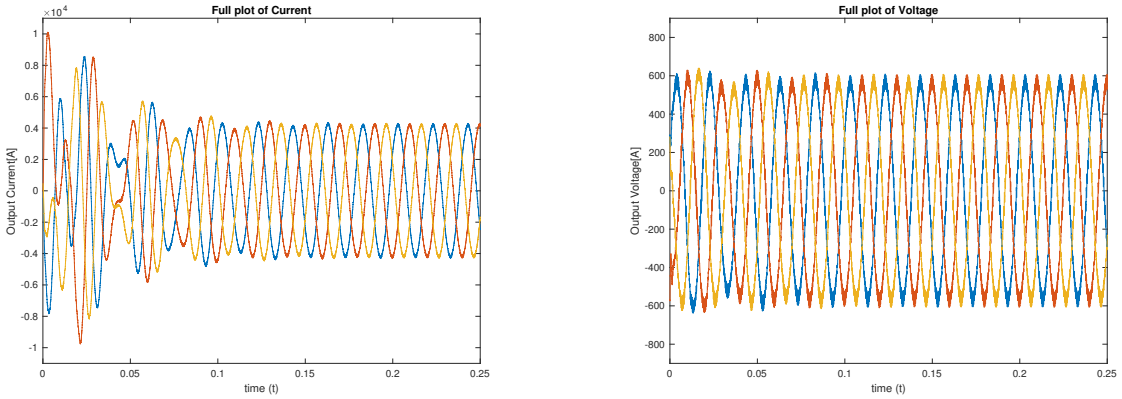

(a) Output current (b) Output voltage

Figure 3.14: Transient response from the current and voltage with ideal PLL

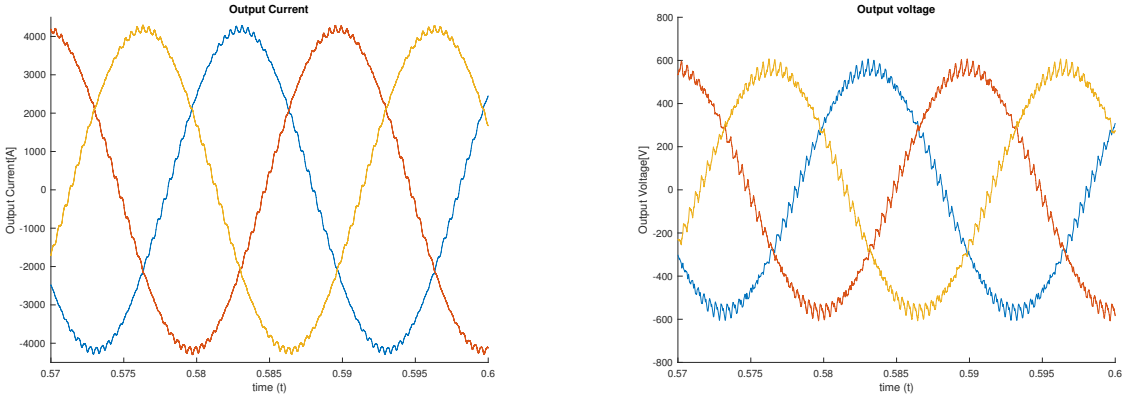

(a) Output current (b) Output voltage

Figure 3.15: Output current and voltage at converter side of transformer with ideal PLL

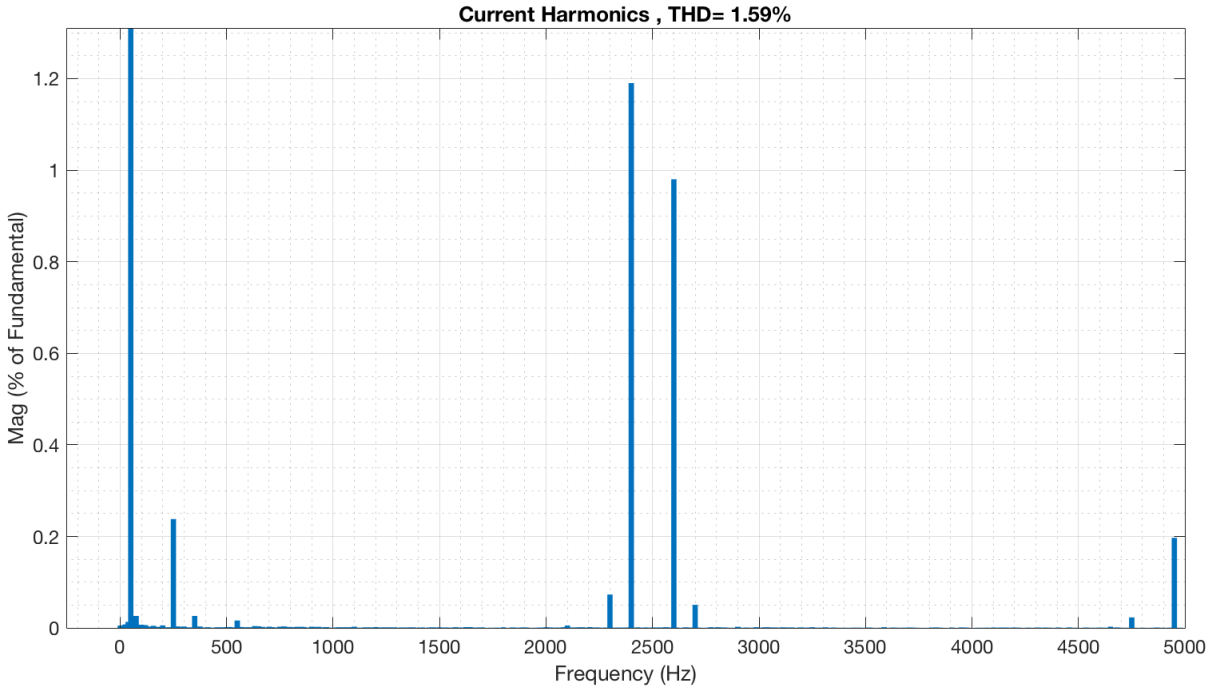

Figure 3.16: Current harmonics from the converter with ideal PLL

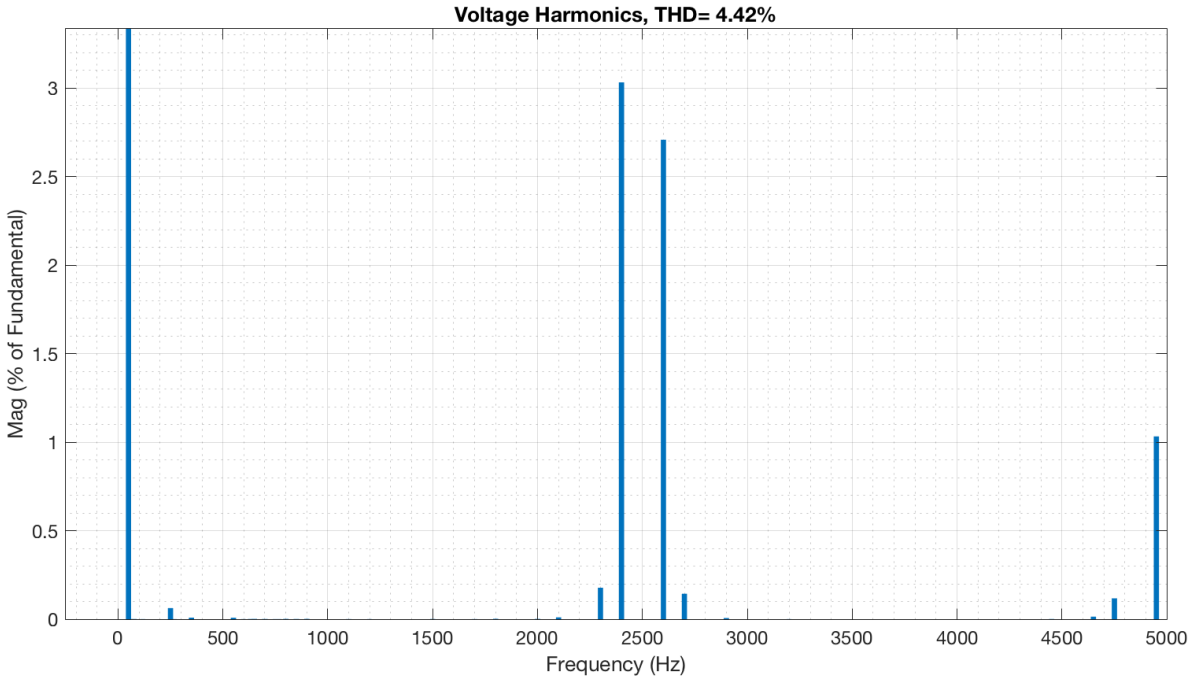

Figure 3.17: Voltage harmonics from the converter with ideal PLL

3.4.3 Harmonic impact from de-tuning the current controller

The PI-controller in the current loop is there to stabilize the system. The tuning of this controller determines the response time of the system when exposed to a transient, as well as the stability of the system. In the previous section, it was proved that by using an ideal PLL, the 5^{th} and 7^{th} harmonics were greatly reduced. There is no way to remove the harmonics around the switching frequency, so further tuning of the PI-controller in the current controller will not remove any more harmonics. However, if the current controller is not tuned carefully, the system will become unstable.

To prove this, a simulation was run with a de-tuned PI-controller. In section 3.3, the bode plot of the full system showed that while there was some room for change within the phase margin, there was barely any gain margin. The gain and phase of a PI-controller can be seen in Eq. 3.15 and shows that by increasing K_I and reducing K_p by the same factor, the impact on the phase will be relatively high compared to the impact on the gain.

$$|H(j\omega)| = \sqrt{K_I^2 + K_p^2} \qquad \angle H(jw)) = tan^{-1}\left(\frac{-K_I}{K_p}\right) \tag{3.15}$$

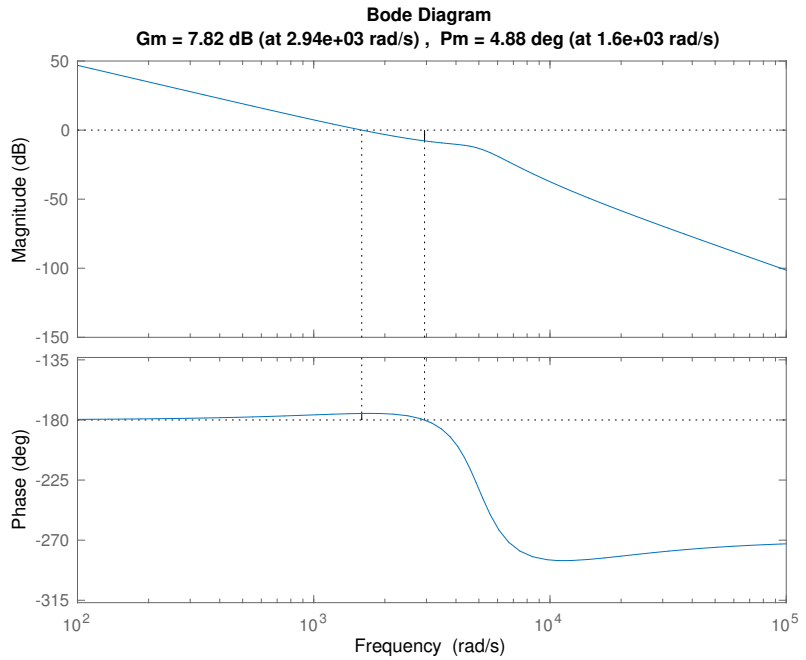

Figure 3.18: Bode plot of $\frac{i^*_{d/q}(s)}{i_{d/q}(s)}$ with de-tuned current controller

Figure 3.18 shows the bode plot of the system with a 100% increase in K_I and a 50% reduction of K_p compared to base case. It is evident that the system is at the brink of instability, with a

phase margin of only 4.88°. The phase is within 6° of the -180° mark in all frequencies, meaning that a small change in the model or a non-precise simplification will make the system unstable.

Figure 3.19 shows the harmonic plot when the system is stabilized, and the harmonics are almost exactly the same as in base case. However, it is evident from Figure 3.20 that it takes more than 0.2 seconds, more than twice as long as in base case, for the converter to stabilize when the PI-controller is de-tuned. This shows how the tuning of the PI-Controller does not impact the harmonic production, but rather the stability and the response time of the system.

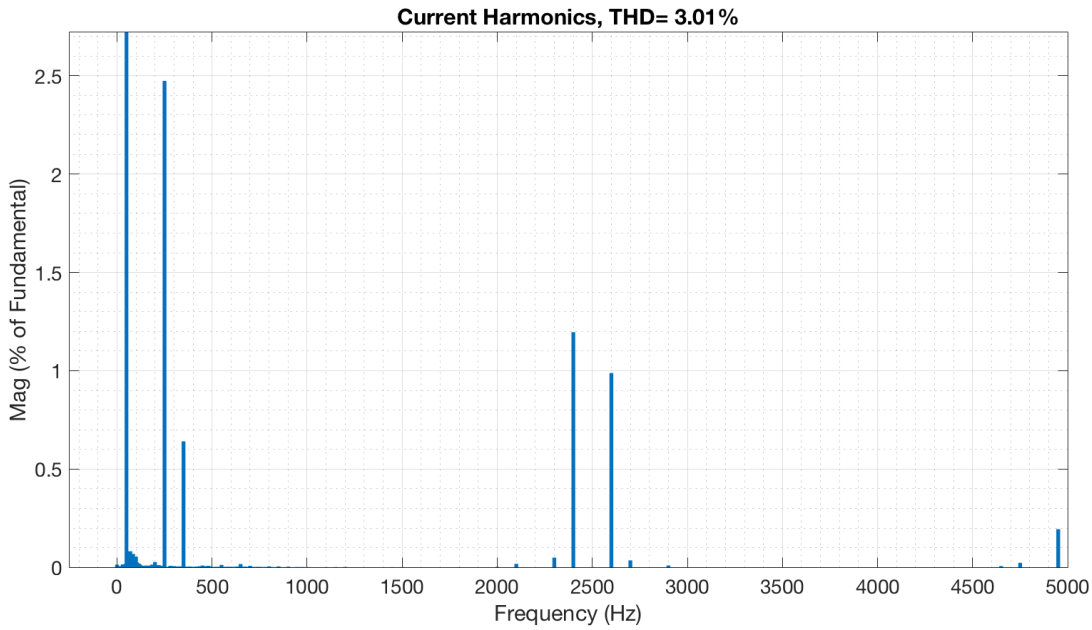

Figure 3.19: Current harmonics with poorly tuned current controller

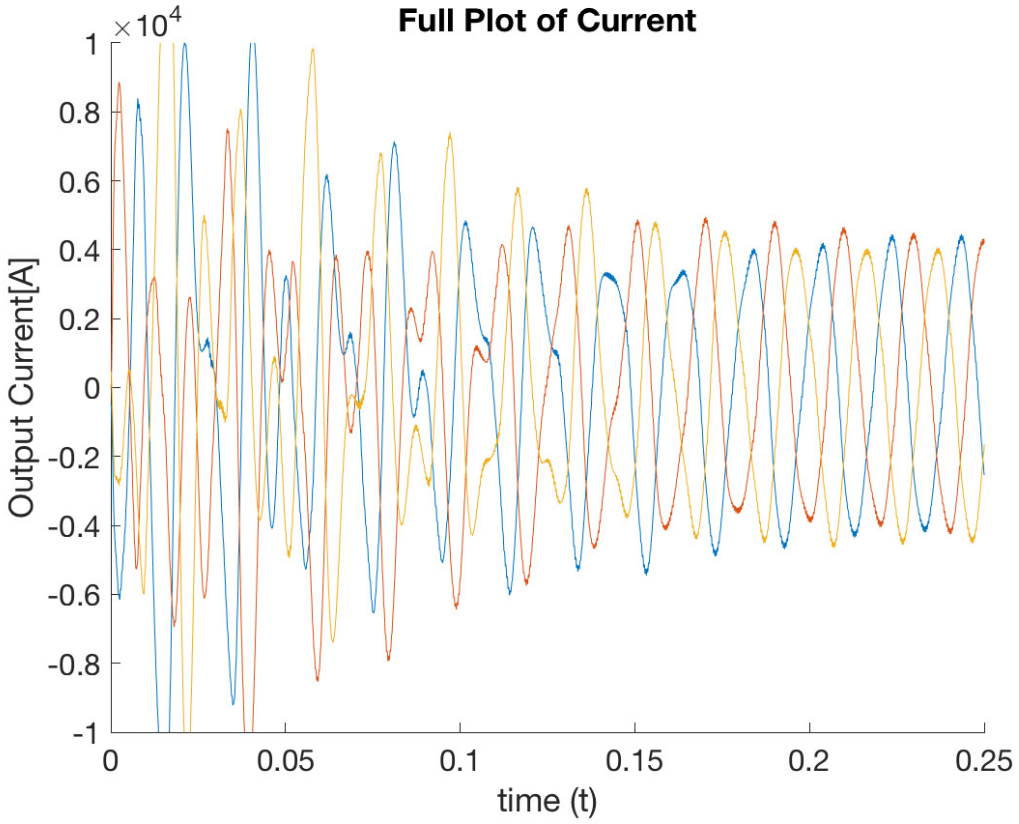

Figure 3.20: Output current with poorly tuned current controller

Chapter 4: Modeling the full wind farm

Anholt Offshore Wind Farm has 111 wind turbines spread into 12 radials with 9 or 10 wind turbines in each radial. Figure 4.1 shows an overview of all 111 wind turbines in Anholt Offshore Wind Farm. The turbines are connected in parallel by subsea copper cables, with a cross-section of either 150, 240 or 500 mm^2. The wind turbines are spread unevenly throughout the wind farm, which means that each radial has a different equivalent Thévenin impedance. There are three substations in the farm, each consisting of one transformer connected to four radials. The three substations are then connected to one single subsea cable, which transfers the power from the offshore wind farm to the main grid. This is an aluminum cable with a cross section of 1600 mm^2 [13]. A single line diagram of Anholt offshore WPP and export system can be seen in Figure 4.2.

The modeling of the turbine has been discussed in the previous chapter. In the simulation of the wind turbine, only minor simplifications have been made, allowing the model to represent a real wind turbine rather well. However, in the simulations of the full farm, major simplifications had to be done. Massive computational power is required just to simulate one turbine, and simulating a full wind farm would be impossible with the resources available to the author of this master thesis.

The shunt compensation and the onshore station will not be included in this simulation. The grid will be placed where the shunt compensation is in Figure 4.2. Only two wind turbines will be simulated to keep a reasonable run-time for the simulations. These two turbines will be in the same radial. The cables and transformers required between the defined grid placement and the turbines will be included in the simulation. The single line diagram of the simulations can be seen in Figure 5.1, and the values of the cables and the transformers are shown in the appendix.

4.1 Modelling the cables

There are several ways to simulate cables depending on the parameters of the cable and the goal of the simulations. An effective and precise simulation of a cable is not easy, and simplifications in the simulations must be made.

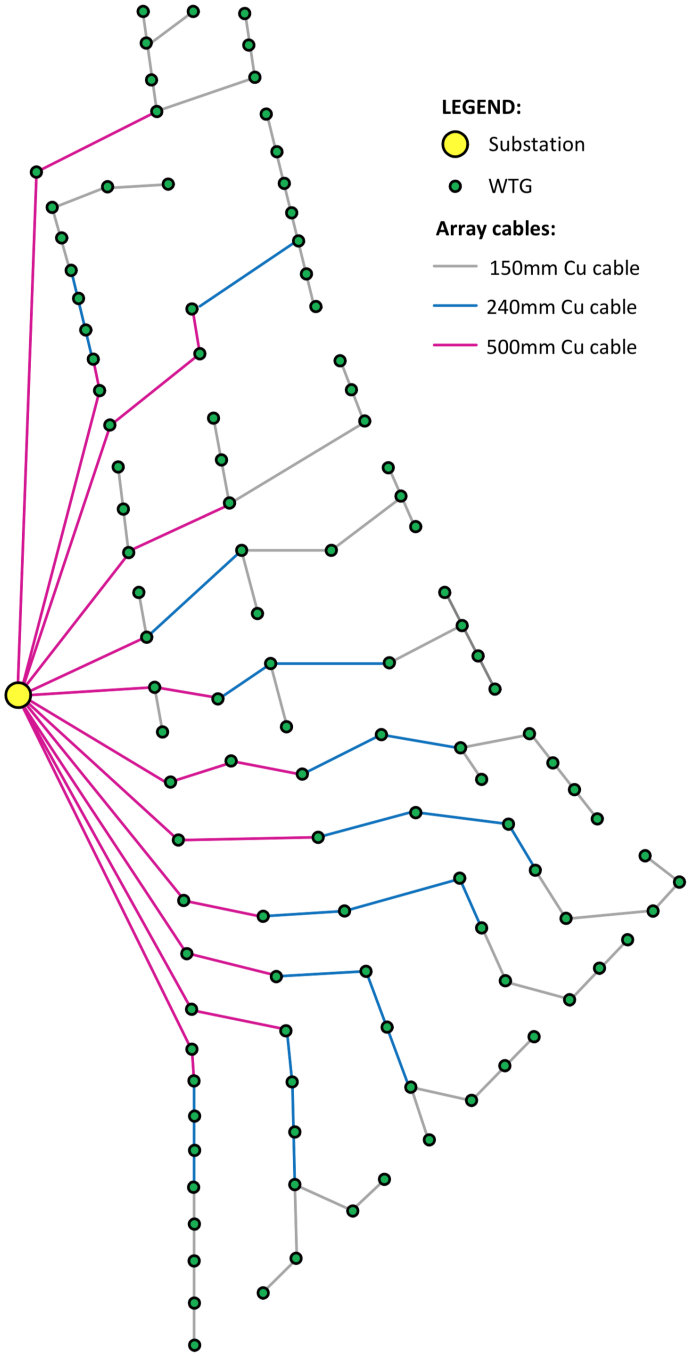

Figure 4.1: Single line overview of Anholt Offshore Wind Farm including cables and turbines [12]

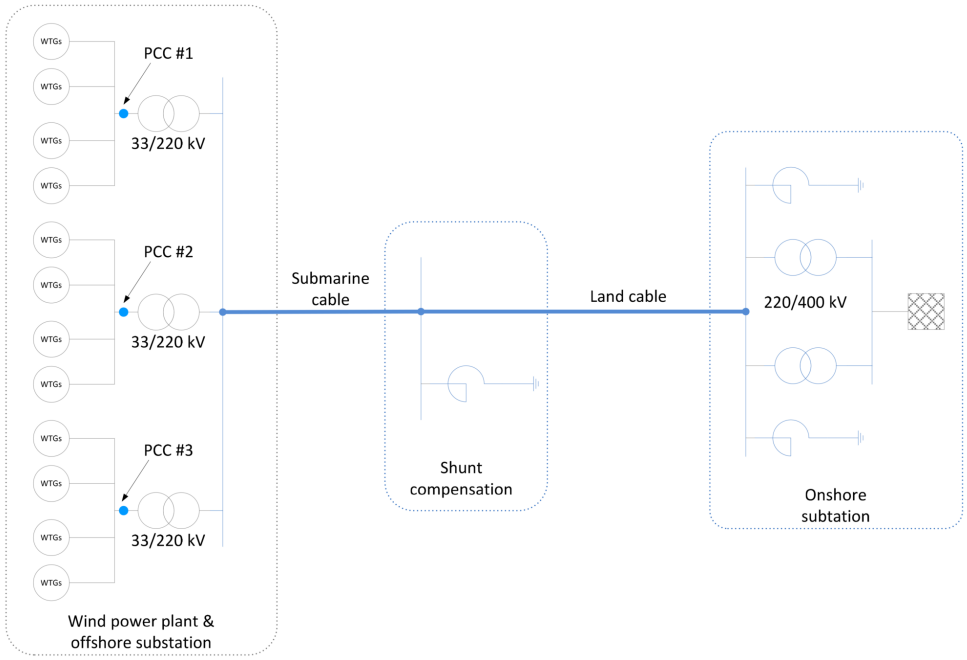

Figure 4.2: Single line diagram of Anholt Offshore Wind Farm and export system table [12]

A cable will have an inductance, capacitance and resistance. The capacitance is the capacitance between the inner conductor and the ground. In short overhead transmission lines, this can normally be ignored, but in cables, the ground is very close to the conductor and the capacitance is significant. The capacitance of a cable is a distributed capacitance, meaning that it should ideally be simulated as an infinite amount of small capacitors along the cable. This, however, is not possible, and the capacitance is therefore lumped together and represented with half of its value at the beginning of the cable and half at the end.

The resistance of the cable is mainly dependant on two things; the resistivity of the material in the conductor and the skin effect. The skin effect is caused by the electrons in the current pushing away from each other, and a higher frequency will cause more skin effect and, as a result, a higher resistance in the cable. This means that a cable will naturally increase the damping of the harmonics as the harmonic order grows. The skin effect will also impact the inductance of the cable [36]. Due to limitations in the simulation tool, the skin effect will not be included in the simulation.

The cables in this master thesis will be simulated as seen in Figure 4.3. This is called a π-section. Several π-sections can be put next to each other to make the simulations more precise. The required amount of π-sections depend on the length of the cable and the amount of harmonics that are analyzed. The more harmonics, and the longer the cable, the more π-sections are required [37].

In the Simulink simulation, the cables will be modelled as the three phase π-section block

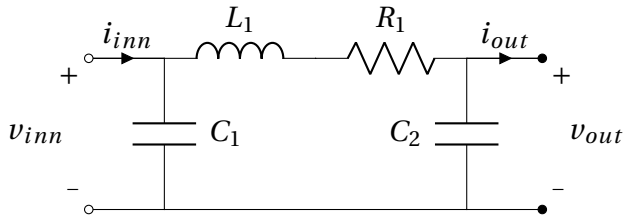

Figure 4.3: Subsea cable modeled as a π-section

from the Specialized Technology library [37]. The positive sequence values will be modelled using data from the ABB user guides [38] [39], while the zero-sequence data will be left as default. Since the analysis in this thesis is done in a balanced grid in steady state, the zero sequence parameters have no impact. The submarine cable will be split into three π-sections with equal parameters that are connected in series, so that the length of all the π-sections in the simulations will be similar.

4.2 Modeling the transformers

The transformers are modeled using the three phase transformer block in Simulink. The block models the three phase transformer by using three single phase transformers with two windings. The primary and secondary resistance and inductance are found from articles describing Anholt [14] [15], while the magnetization parameters are left at default again due to the fact that the studies are done in steady state.

4.3 Modeling the grid

The grid will be modeled as an ideal voltage source. Between the ideal voltage source and the cables, a small resistance of 1 Ω will be included because Simulink does not allow an ideal voltage source and a capacitor to be connected in parallel. This is equivalent to modelling the grid as a Thevenin equivalent with a very small series impedance.

Chapter 5: Full wind farm simulations

In this chapter, the full wind farm as defined in Chapter 4 will be simulated. The wind farm will be simulated using different scenarios in order to identify what causes the most harmonics, and how these harmonics propagate through the offshore grid. Each scenario will be discussed briefly, and the results from each simulation will be shown. In Chapter 7, the results will be discussed more thoroughly, and the most important results will be summarized and compared.

Figure 5.1 shows a single line diagram of the system simulated in this thesis. The harmonic measurements will be made at the wind turbine, the PCC and the grid, as highlighted in the figure.

The first section in this chapter will display the results from a frequency sweep. A frequency sweep is done to determine the frequency dependant impedance of the system.

There are nine different scenarios that will be simulated. The first scenario is the base case established in the previous chapter. The second and third scenarios are the same cases as in the previous chapter, with an ideal PLL and a de-tuned PI-controller in the current control loop.

The fourth and fifth scenarios are introduced to investigate the impact of turbines running at less than full speed, and the harmonic impact of forcing a big offshore wind farm to produce reactive energy. According to B. Block et al [10], there are significant differences in the harmonic level of a wind turbine producing at unity power factor and of one producing with a power factor

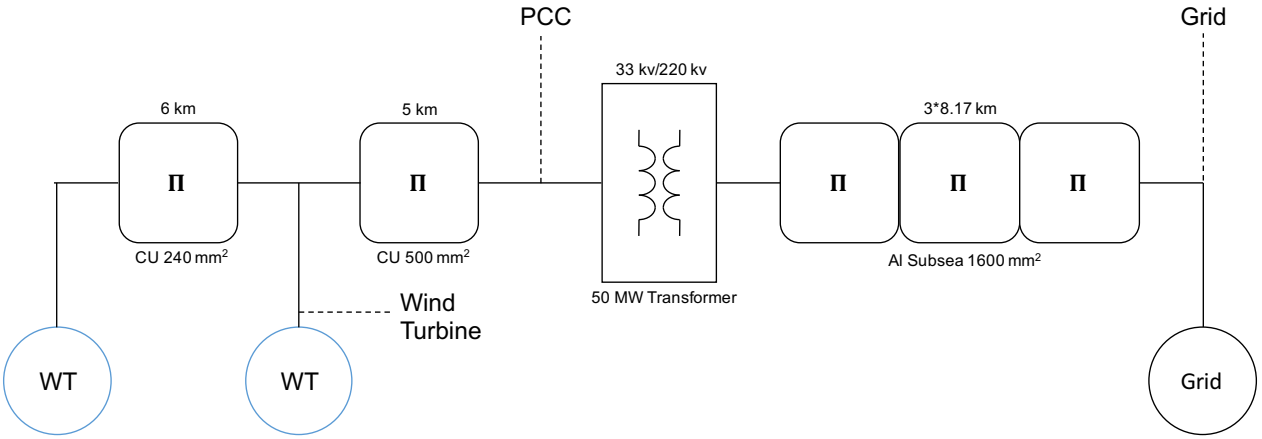

Figure 5.1: Single line diagram of the system

of 0.9.

Scenario 6 will have a delay in the switches of the converter and scenario 7 will have a non-ideal grid. Due to some unexpected results in scenario 6, the scenario was run several times with varying amounts of switch-on delay. The switch-on delay is chosen based on similar experiments done by D. Dhua et al. [15].

The last two scenarios are added to prove the scalability of the system. Since the author's computer is not powerful enough to run simulations of 18 wind turbines at the same time, there is one VSC working as normal, and 17 turbines modeled as current sources using the same signal generated by the VSC. This method is not suitable to investigate the harmonic generation in the different scenarios, but will show how the harmonic propagation is impacted by the amount of current in the cables and transformers. The different scenarios can be seen in Table 5.1.

Table 5.1: Overview of the different scenarios

Case	Description
Scenario 1	Base case
Scenario 2	Ideal PLL
Scenario 3	De-tuned PI-controller
Scenario 4	Pf = 0.9 ($i_d^* = 0.9,\ i_q^* = 0.436$)
Scenario 5	Half power ($i_d = 0.5,\ i_q = 0$)
Scenario 6	Switch-on delay of 0.5 μs
Scenario 7	Non-ideal grid
Scenario 8	Base case with 18 turbines
Scenario 9	18 turbines an non-ideal grid

The base case will be discussed thoroughly, and each harmonic plot will be examined at the different measuring points in the offshore wind farm. The rest of the scenarios will be compared to the base case, and each scenario will show only the harmonic plots that are relevant for the comparison. Note that the voltage harmonics of the turbine are measured on the grid side of the transformer while the voltage harmonics in Chapter 3 were measured on the converter side of the transformer. These two plots are therefore not comparable. This is done in order to compare the harmonics at the turbine and the PCC in this chapter. Since the transformer is part of the LCL-filter, it is natural that the measurements are made after the whole filter. In the previous section, the voltage harmonics were measured on the converter side to show the signal used in the control system of the converter.

5.1 Frequency sweep

In this section, the results from the frequency sweep of the system will be presented. A frequency sweep is done by sending a current of a specific frequency and peak value of 1A and measuring the induced voltage over the components. By performing this simulation with a wide range of frequencies, a frequency-dependant impedance plot can be created. Three different voltage measurements were made; the voltage from the first wind turbine to the PCC, the voltage from the second wind turbine to the PCC and the voltage from the PCC to the grid. Since the peak current is 1A, the peak voltage will be the same as the impedance at the simulated frequency.

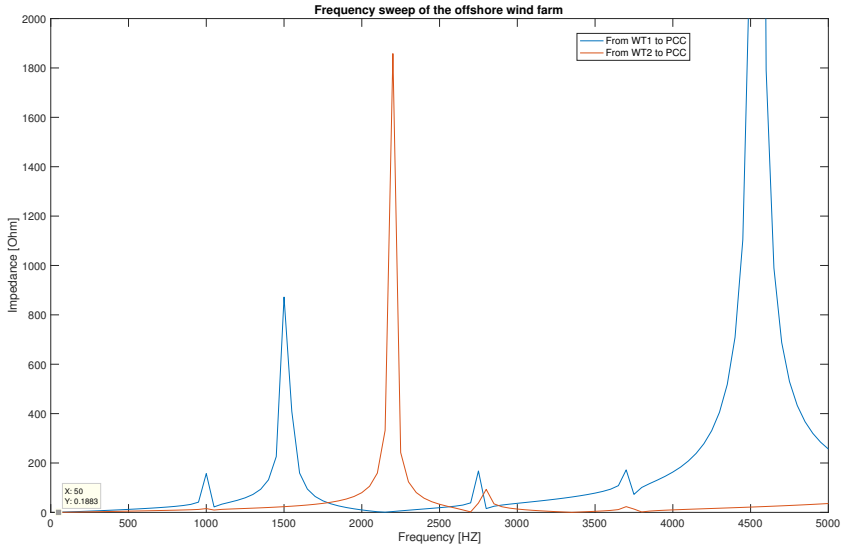

Figure 5.2: Frequency sweep from the wind turbines to the PCC

Figure 5.2 shows the frequency dependant impedance from the two wind turbines to the PCC. At the fundamental frequency, the impedance is only 0.1883Ω between the first wind turbine and the PCC, and 0.6207Ω between the second wind turbine and the PCC. However, there are some frequencies with a much higher impedance, like 1000 Hz, 1500 Hz and 4500 Hz for the wind turbine closest to the grid and 2200 Hz for the wind turbine furthest from the grid. While the resistance peak at 2200 Hz is very close to the switching harmonics, the inductance at the 48^{th} harmonic is only 58Ω and 14Ω between the first wind turbine and PCC and the second wind turbine and PCC, respectively. Having series resonance in the grid at or near the switching frequency is not ideal as it may cause instability and large amounts of voltage harmonics. Since the harmonic plots from the previous chapter (Figure 3.11 and 3.12) show that there are no harmonics at 2200 Hz, this peak will likely not cause resonance in these simulations.

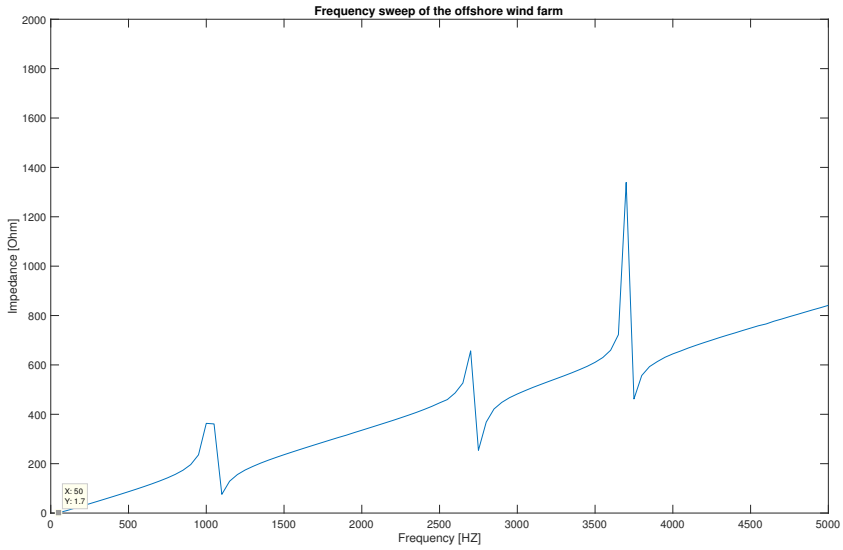

Figure 5.3: Frequency sweep from the PCC to the grid connection point

Figure 5.3 shows the frequency dependant impedance from the PCC to the grid connection point. From the shape of this plot, it is evident that the impedance is dominated by the inductance in the transformer due to its linear increase with the frequency. There are some local peaks and dips in the plot, but none are at the frequencies seen in the base case simulations in Figure 3.11. While the local peak at 2700 Hz is relatively close to the switching harmonics, the highest order harmonic from Figure 3.11 is at 2600 Hz, and should not be impacted. The lowest inductance is again at the fundamental frequency, being just 1.7 Ω.

5.2 Scenario 1: base case

From Figure 5.4, it is evident that the harmonics at the output of the turbine are similar to those in Figure 3.11, which shows the base case harmonics without the offshore wind farm grid. There is a slightly higher THD at the output of the turbine when it is connected to the grid compared to when it is connected to an ideal voltage source (3.16% in full grid scenario and 2.98% with only the turbine). This slight increase in current harmonics at the turbine is caused by a slight increase of voltage harmonics at the turbine. In the previous section, the turbine was connected to an ideal grid. In this chapter, the ideal grid is moved further away from the turbine, which results in a 0.44% voltage THD at the turbine.

With respect to the specific harmonics, the same trend can be seen as in the previous section. The current has a significant amount of 5^{th} harmonics and some 7^{th}, in addition to the harmonics around the multiples of the switching frequency. In the voltage, on the other hand, most of the harmonics are situated around the switching frequency. With a THD of 0.5%, there are much less voltage harmonics than current harmonics.

While the current THD is slightly less at PCC than at the wind turbine, this reduction is caused only by the harmonics around the switching frequency being smaller. This shows that the inductance in the cables works as a filter around the higher frequencies, but is not able to filter out the lower frequencies. The 5^{th} and 7^{th} current harmonics are in fact slightly higher at PCC than at the wind turbine. Figure 5.5 shows that the current at the second turbine is almost exactly the same as at the first turbine, and that at both turbines, the 5^{th} and 7^{th} harmonics are less than at PCC. This proves that while the copper cables between the turbines and PCC reduce the high order current harmonics, they actually increases the low order harmonics.

The voltage THD also decreases the closer it gets to the grid. Since the grid is ideal, the voltage harmonics are caused by the voltage drop over the passive elements in the offshore grid. There will therefore be more voltage harmonics the further away from the grid measurements are made.

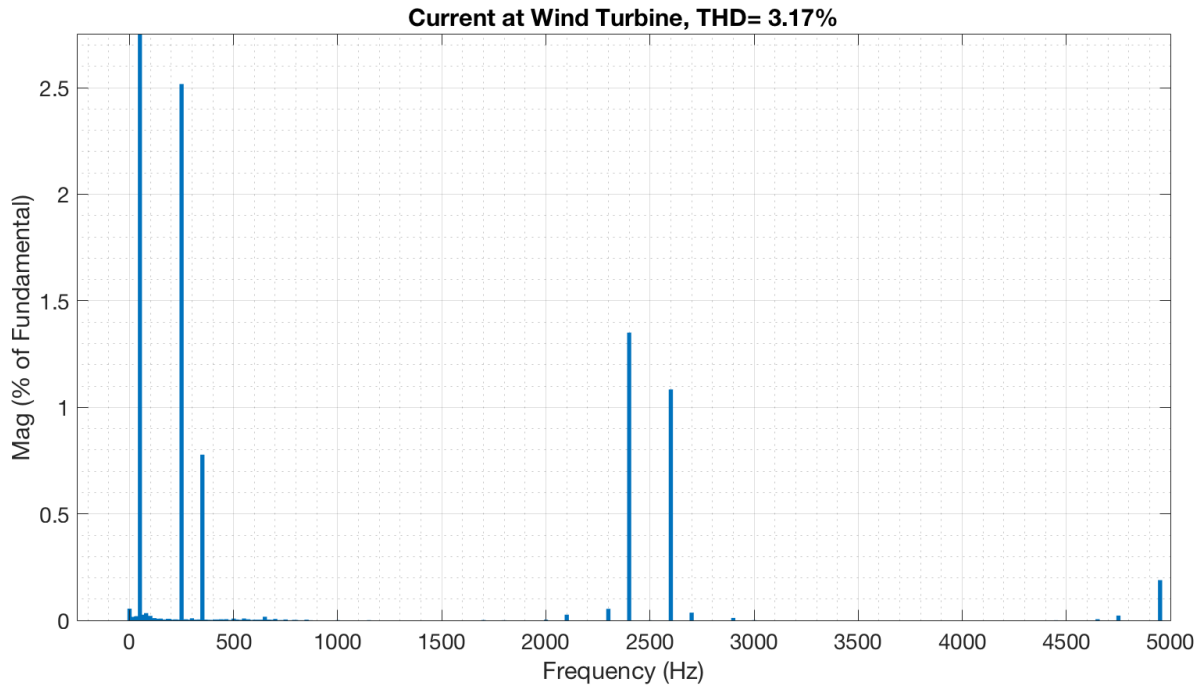

Figure 5.4: Current harmonics at the turbine in *Scenario 1: base case*

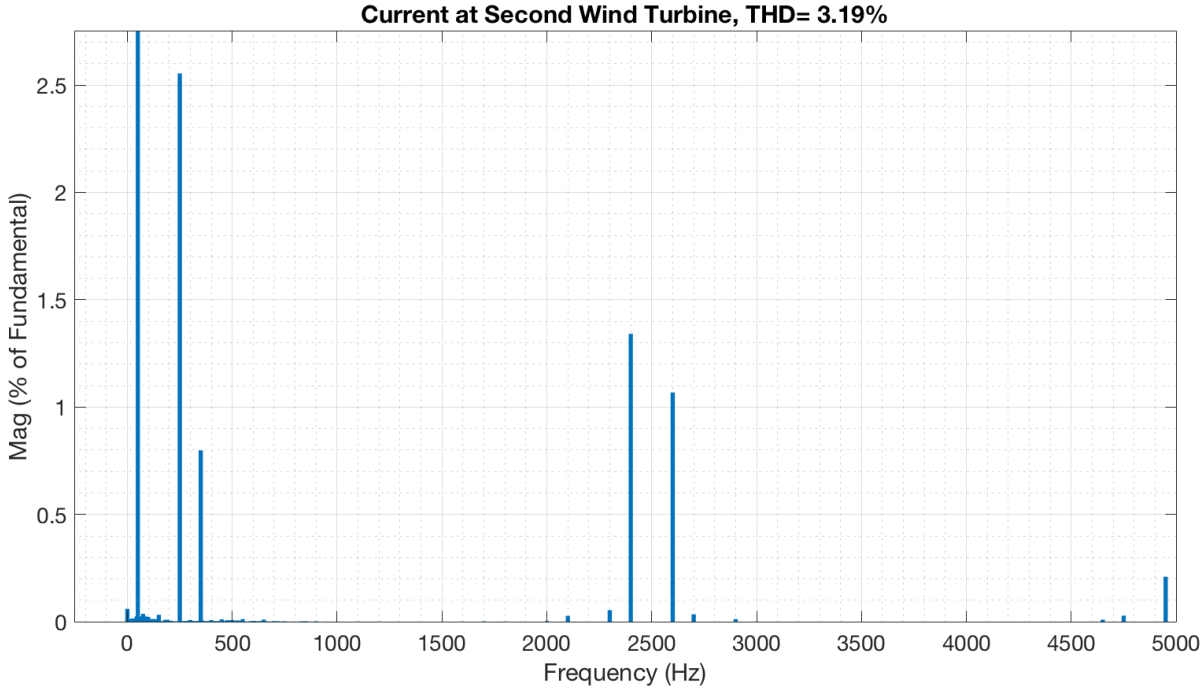

Figure 5.5: Current harmonics at the second turbine in *Scenario 1: base case*

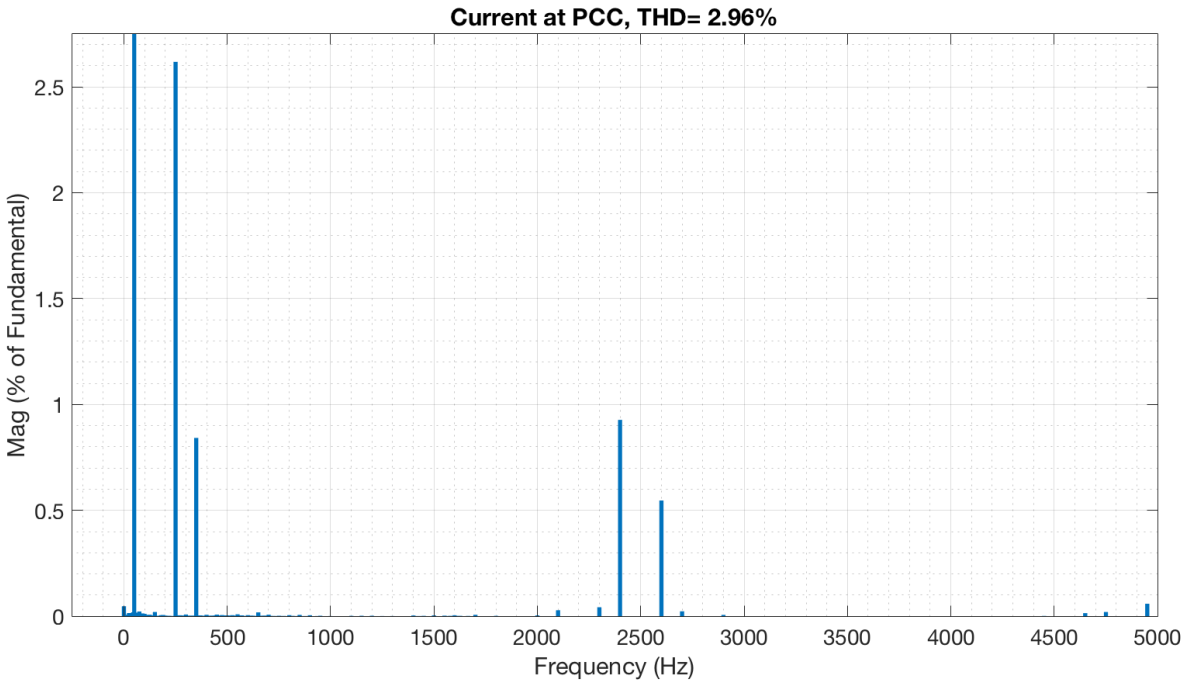

Figure 5.6: Current harmonics at the PCC in *Scenario 1: base case*

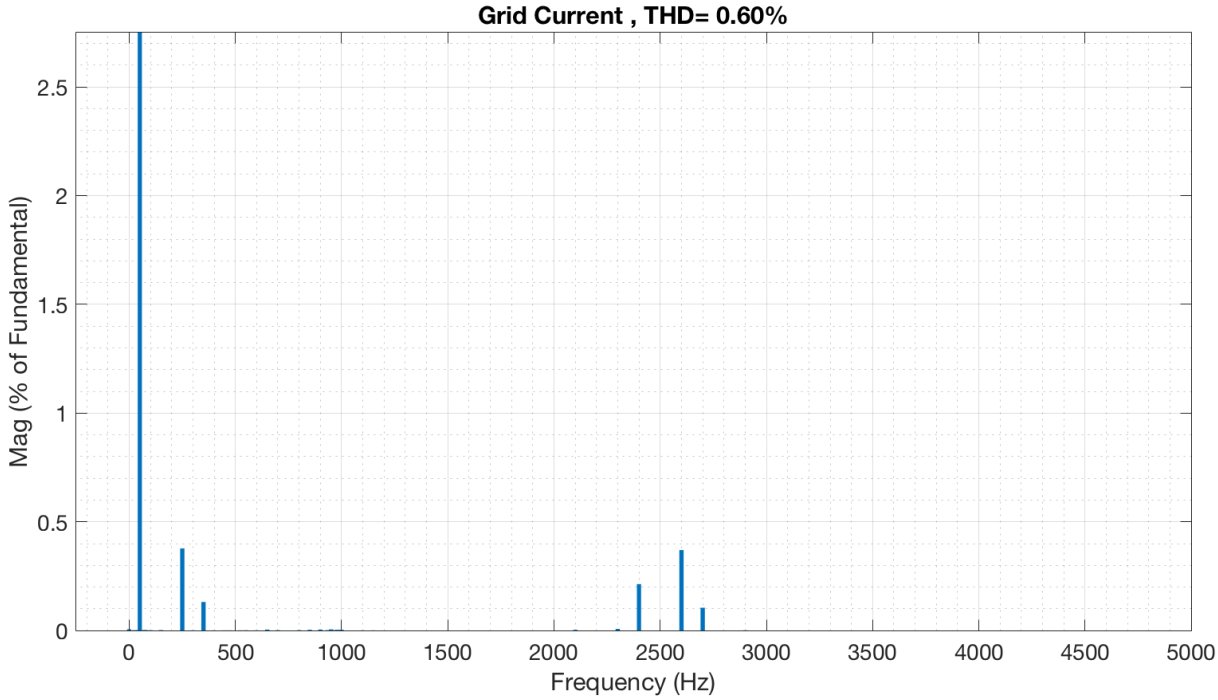

Figure 5.7: Current harmonics at the grid in *Scenario 1: base case*

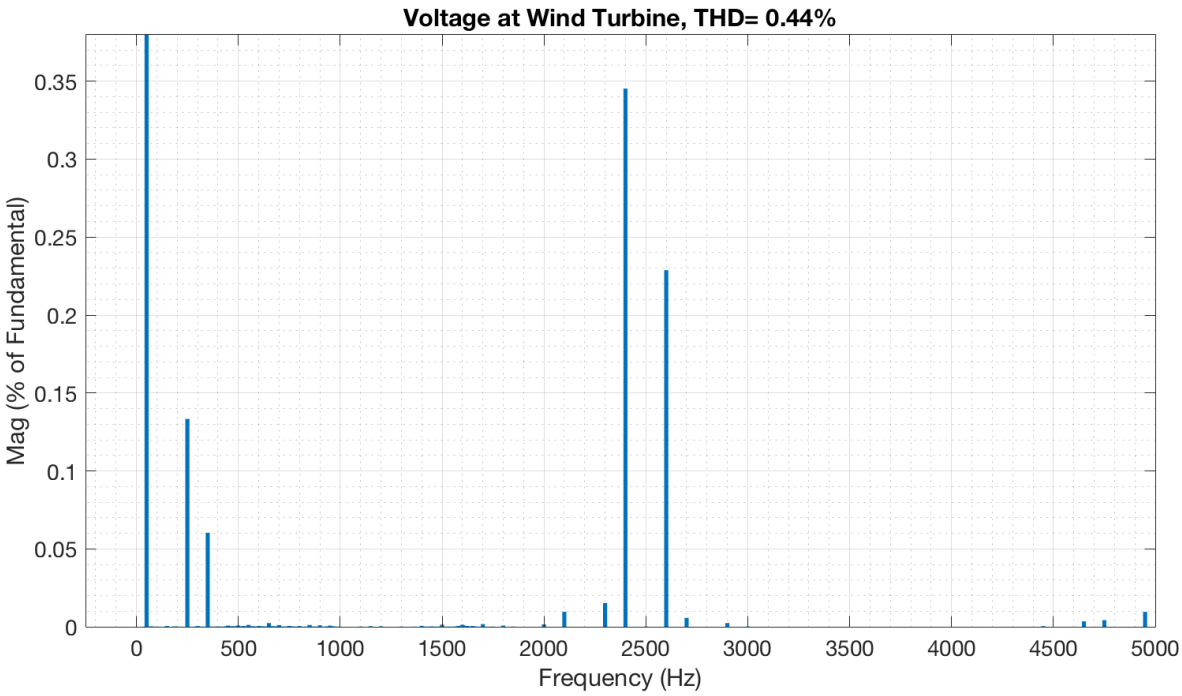

Figure 5.8: Voltage harmonics at the turbine in *Scenario 1: base case*

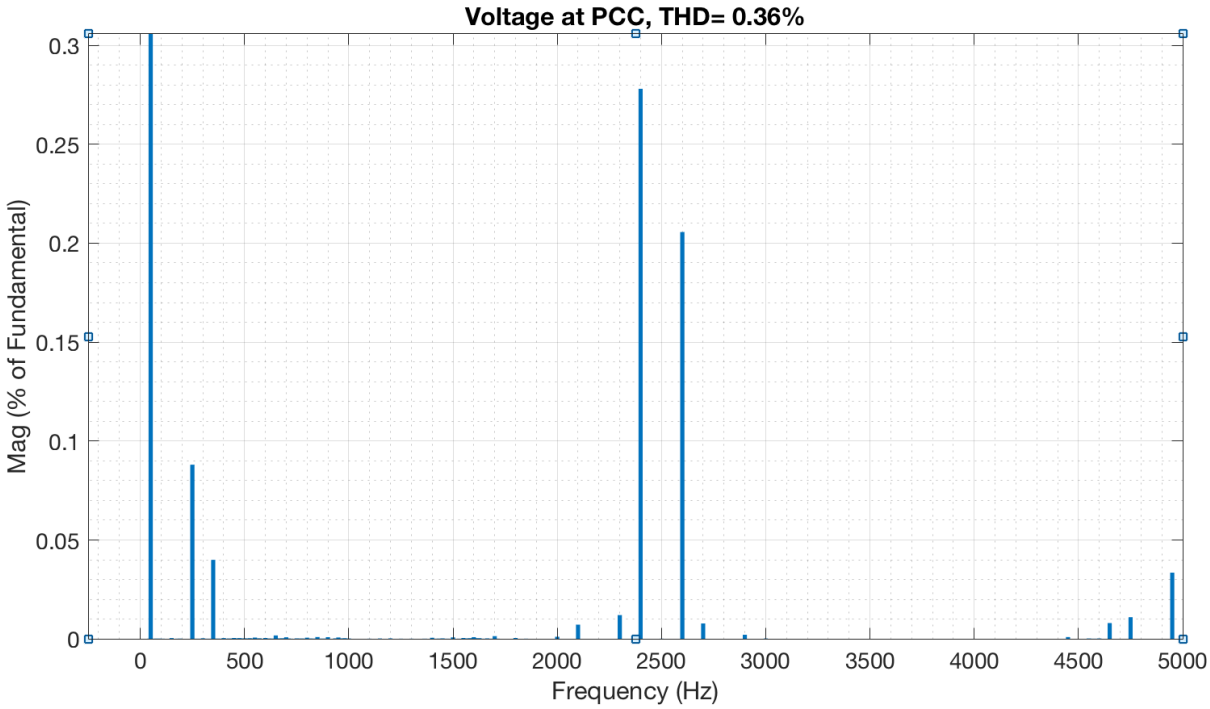

Figure 5.9: Voltage harmonics at the PCC in *Scenario 1: base case*

It should be noted that the current harmonics at the grid are extremely small, with a THD at only 0.60%. There is a transformer after the PCC measurement, which causes the current through the subsea cable to be very low. This cable is designed to hold the current of all 111 wind turbines, so running it with only two turbines might cause some undesired effects. Measurements were conducted between each π-section in the offshore cable and the results are shown in Figure 5.10. Indeed, it can be seen that the current is much smaller after the transformer than at the grid, and the grid is injecting a high current to excite the capacitors in the subsea cable. There is a 90° delay between the current at the PCC and the current at the grid, which means that the current is used to excite the capacitors in the cable. Since the grid is an ideal voltage source, this current will have no harmonic components. This explains why the current harmonics at the grid are so small compared to those at the PCC.

This will be explored further in scenario 8 and 9. For the first seven scenarios, the grid current harmonics will be ignored since they are so much smaller than the harmonics at PCC and the turbine.

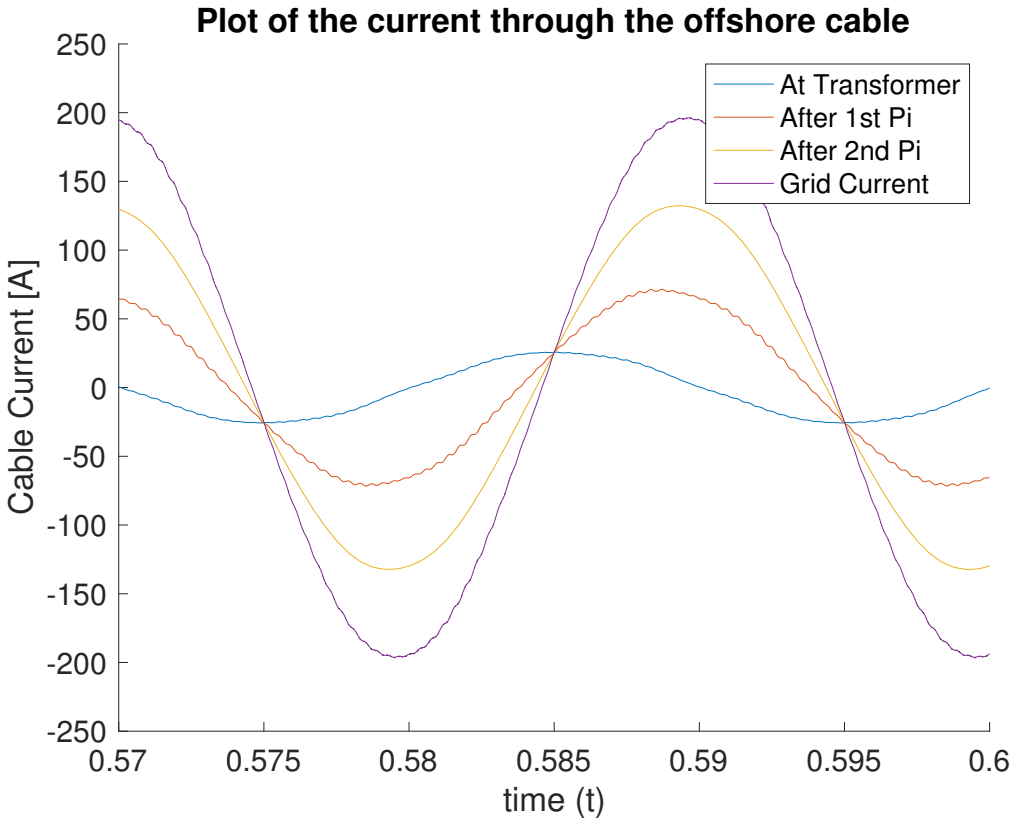

Figure 5.10: Current after each π-section of the subsea cable in *Scenario 1: base case*

5.3 Scenario 2 & 3: tuning the control system of the turbine

In this section, the same scenarios that were investigated without the offshore grid in the previous chapter will be investigated with the full grid connected. The results are expected to be very similar, proving that connecting the turbine to the offshore grid does not alter the control of the VSC.

Figure 5.11 shows the current harmonics at PCC with an ideal PLL. As expected, the current THD is much lower than in base case, decreased from 2.96% to 1.11%. The only harmonics higher than 0.5% are those around the switching frequency, which are the same results as from Section 3.4.2. The THD is actually lower than in the simulations with only the wind turbine, but this is caused by the π-section between the turbine and the PCC, which is filtering the higher harmonic orders. The THD at the wind turbine is 1.76%, which is slightly higher than the 1.59% from Section 3.4.2.

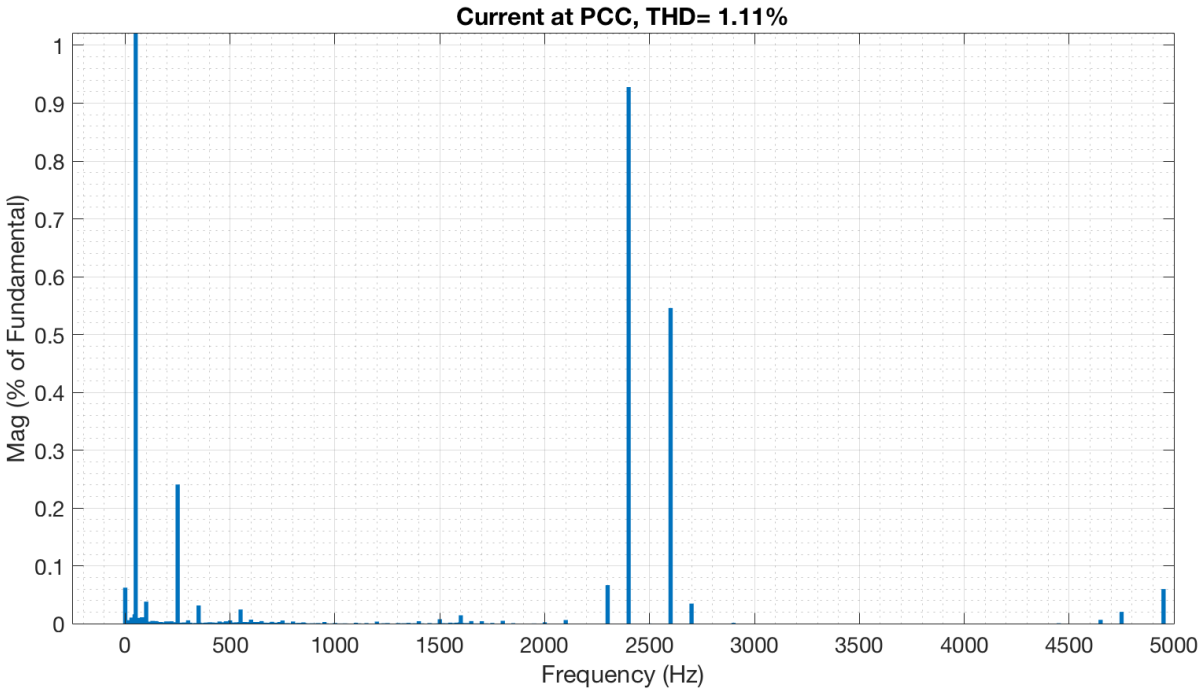

Figure 5.11: Current harmonics at the PCC in *Scenario 2: ideal PLL*

Figure 5.12 shows the current harmonics at the PCC when the PI-controller in the current control loop in the converter is de-tuned. The PI-controller is tuned the same way as in section 3.4.3. The current THD is 2.98%, which is slightly greater than the 2.96% in base case. The specific harmonics, however, are almost exactly the same as in base case. The small difference in THD is likely caused by the harmonic measurement being done slightly differently due to the longer stabilization time when the PI-controller is de-tuned.

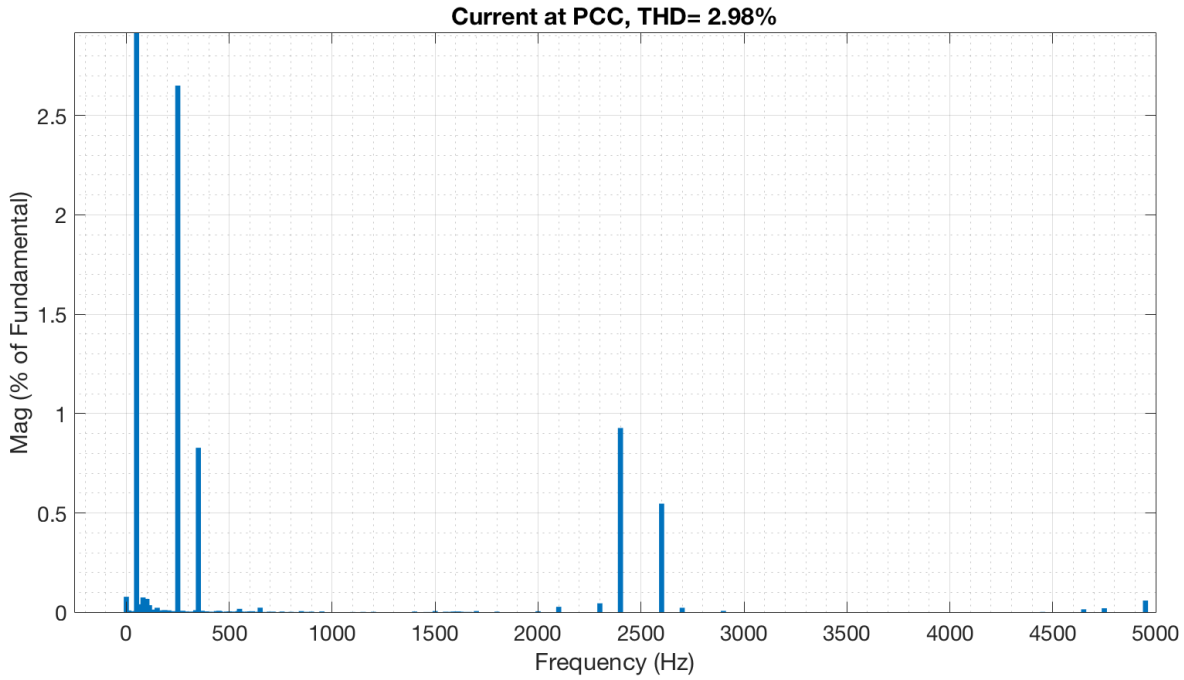

Figure 5.12: Current harmonics at the PCC in *Scenario 3: de-tuned PI-controller*

5.4 Scenario 4 & 5: running the turbines at not rated conditions

In this section, scenarios 4 and 5 will be investigated. These scenarios correspond to running the turbine at not perfect wind condition, or when the grid operator requires the wind farm to produce or consume reactive power. These two scenarios are tested by setting the reference current I_d^* and I_q^* to something other than 1 and 0, respectively. For *Scenario 5: half speed*, this is done by setting $I_d^* = 0.5$. For *Scenario 4: pf = 0.9*, this is done by fulfilling the following two equations:

$$pf = cos^{-1}(\frac{I_d^*}{I_q^*}) = 0.9 \qquad S = \sqrt{I_d^{*2} + I_q^{*2}} = 1 \tag{5.1}$$

$$i_d^* = 0.9 \qquad I_q^* = 0.436 \tag{5.2}$$

Figure 5.13 and 5.14 show the current harmonics at PCC for scenario 4 and 5, respectively. It is evident that the specific harmonic frequencies are not dependant on the output power of the converter. In all of the cases so far, there have been only the 5^{th} and 7^{th} harmonics present, in addition to the switching frequencies.

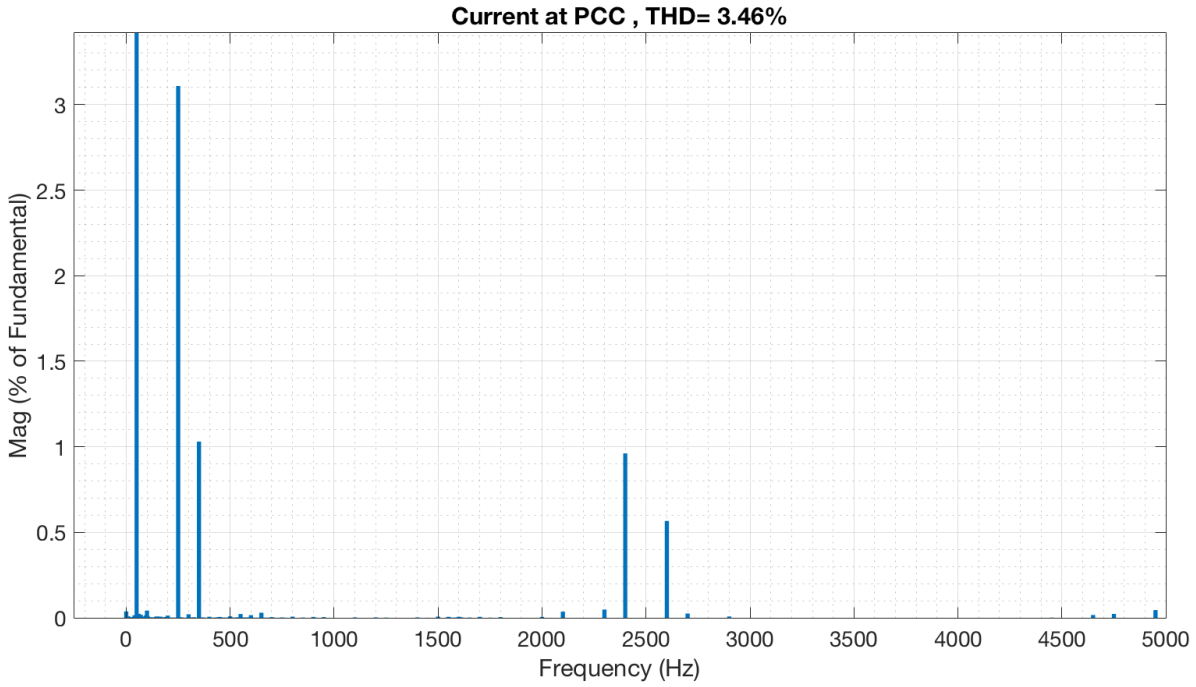

Figure 5.13: Current harmonics at the PCC in *Scenario 4: pf=0.9*

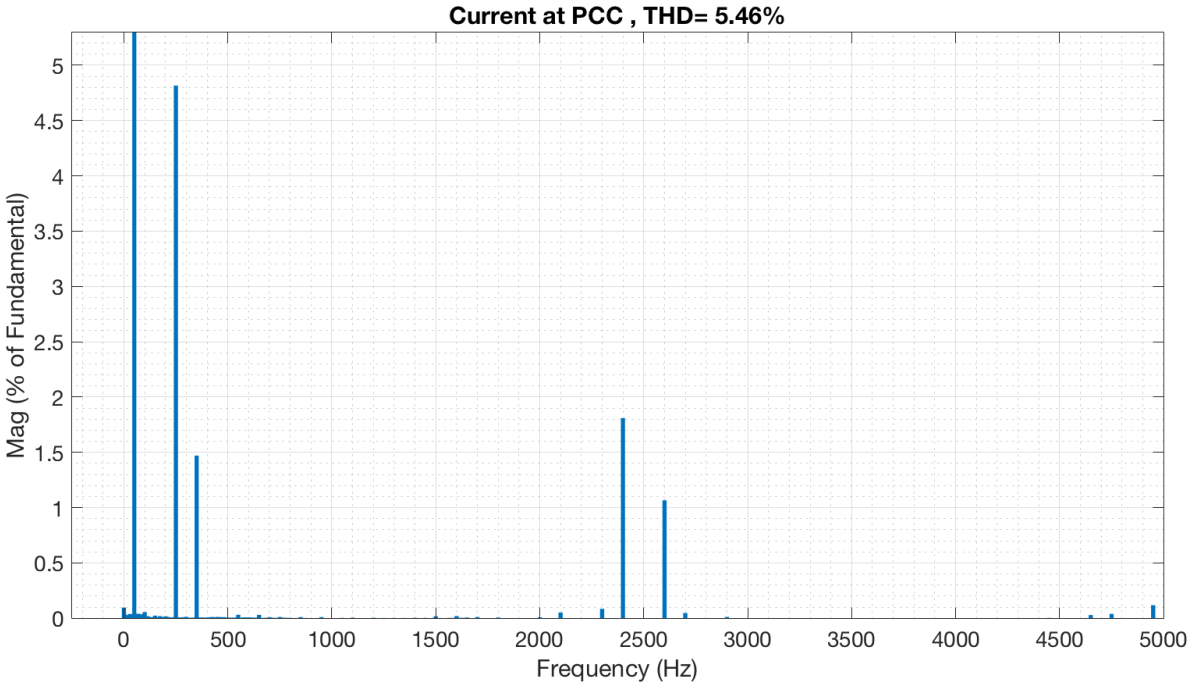

Figure 5.14: Current harmonics at the PCC in *Scenario 5: Half Power*

However, the THD is much greater in scenario 4 and 5 than in base case. When the turbine is running at a power factor of 0.9, there is a 17% increase in THD, from 2.96% to 3.46%. The harmonics around the switching frequency are the same, while there is an increase in the 5^{th} and 7^{th} harmonics. This is consistent with the experiments of B. Block et al [10].

Running the turbines at half speed produces even more harmonics than running with a lower power factor. While reducing the power factor to 0.9 only increased the 5^{th} and 7^{th} harmonics, running at half power increased all harmonics equally. At half power, the THD is increased from 2.96% to 5.46%, which is an increase of 84%.

By rearranging Eq. 3.1 from tuning the LCL-filter, the following can be shown:

$$\Delta i_{imax,p-p} = \frac{(V_{dc} - DV_{dc})D}{2L_1 f_{sw}} \tag{5.3}$$

Eq. 5.3 shows that running the turbine with a duty cycle of 0.5 will increase the current ripple at the switching frequency, compared to using a higher duty cycle. While this increased ripple explains the increased harmonics around the switching frequency, it does not explain the large increase in 5^{th} and 7^{th} harmonics. This will be discussed further in Chapter 7.

5.5 Scenario 6: switch-on delay

In this section, a switch-on delay will be added. In a similar experiment done by D. Dhua et Al, [15], this delay was fixed to 5 µs while the cable parameters were changed.

Figure 5.15 shows the harmonic plot at PCC with a switching delay of 5 µs. Contrary to the first five scenarios, adding a switching delay introduces harmonics at frequencies other than 5^{th}, 7^{th} and the switching frequency. The 11^{th} and 13^{th} harmonics are especially greater than in previous simulations. The 5^{th} harmonic is still the most dominant. The addition of more harmonic frequencies is aligned with what is found in the literature, as measurements of real offshore wind farms find harmonics in every single low order frequency [40] [10].

While there are more current harmonics when a switch-on delay is added, the value of the most dominant harmonic in the previous simulations, the 5^{th}, is reduced by 30% compared to base case. The 5^{th} harmonic is decreased so much compared to the base case that the current THD at PCC is actually lower with a switch-on delay (2.68%) than it is without (2.96%). While this is only a slight reduction, it is surprising that adding a non-ideality gives a smaller THD. It is only the 5^{th} harmonic that is reduced, while the 7^{th} harmonic is actually slightly increased, and the harmonics around the switching frequency are exactly the same.

$$\frac{1}{T_{delay}} = 2 * 10^5 = 800 * 250 = 800 * 5^{th} harmonic \tag{5.4}$$

Eq. 5.4 shows that adding a delay of 5 µs has a common multiple with the 5^{th} harmonic. A theory was proposed that this common multiple might cause the 5^{th} harmonic to shift into another order.

Since it has already been proven that the 5^{th} harmonic is generated in the PLL, another cause of the improvement in the THD could be that the PLL is tuned too fast, at least from a harmonic point of view. Three more simulations were run, one with a delay of 3 µs, one with a delay of 8 µs and one with a delay of 12 µs. The results can be seen in Table 5.2 and show that the ideal amount of delay is somewhere between 5 and 8 µs. This proves that the common multiple with the 5^{th} harmonic had nothing to do with the improvement, and strengthens the theory that the PLL was tuned too fast.

Table 5.2: THD at base case compared to different switch-on delays

Scenario	THD
Base case	2.96%
3 µs	2.76%
5 µs	2.68%
8 µs	2.68%
12 µs	4.04%

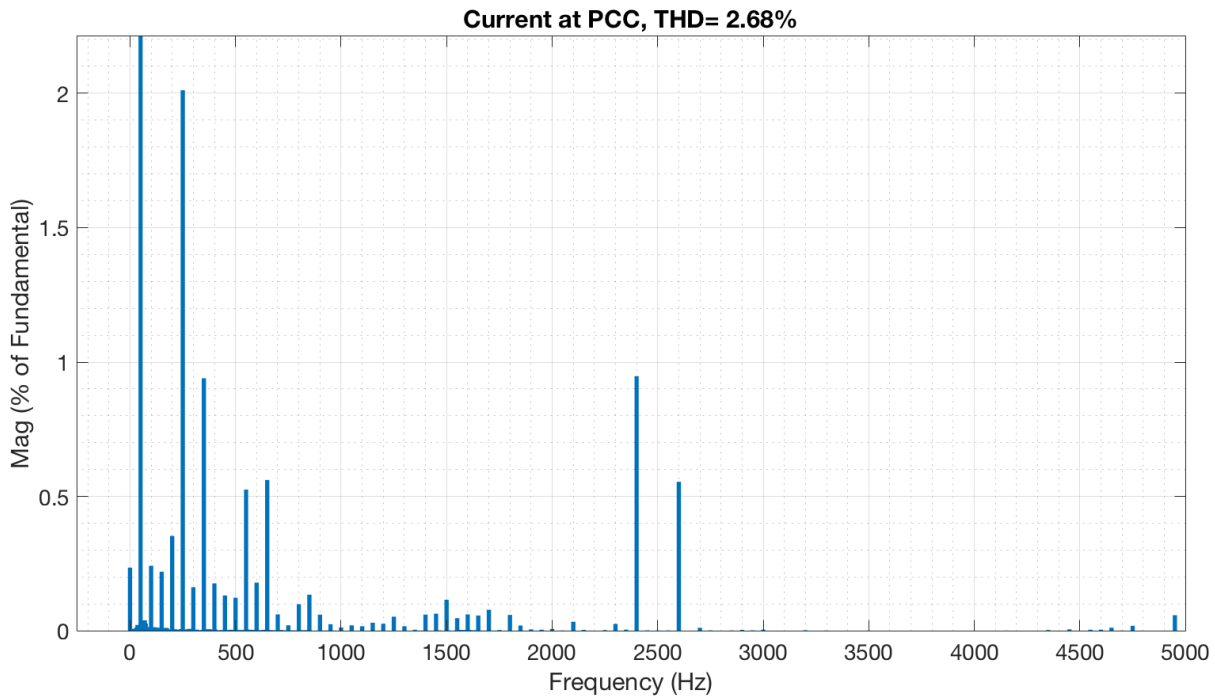

Figure 5.15: Current harmonics at the PCC in *Scenario 6: switch-on delay of 5 µs*

5.6 Scenario 7: non-ideal grid

In this section, the grid will be simulated as a non-ideal grid. The grid voltage will have two harmonic components, a 2% 7^{th} harmonic and a 1.5% 13^{th} harmonic. The 7^{th} was chosen to see what happens when the grid and the converter have the same harmonic component. The 13^{th} harmonic was chosen to see what happens when they have different harmonic components. These two harmonic components give the grid a voltage THD of 2.5%.

In all the scenarios that have been simulated so far, only the turbine has been changed. In this section, harmonics are coming both from the grid and from the turbine, and the propagation thorough the grid is therefore quite different from the other cases.

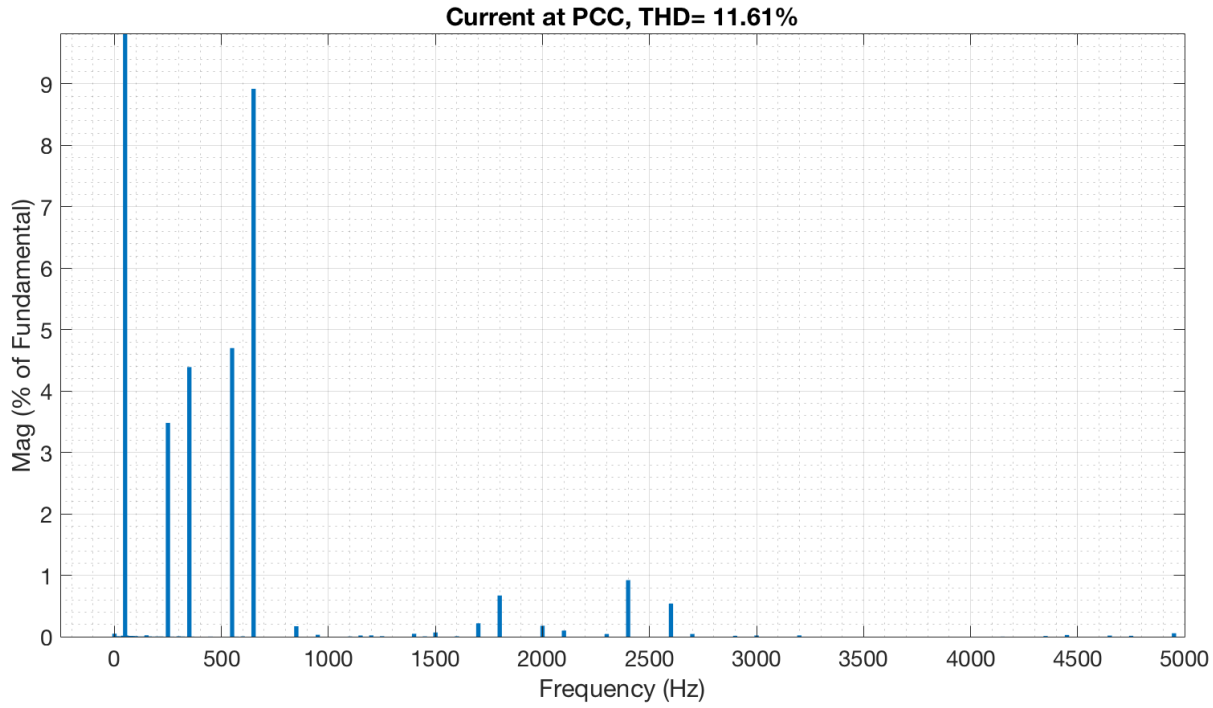

Figure 5.16: Current harmonics at the PCC in *Scenario 7: non-ideal grid*

Figure 5.16 shows the current harmonics at PCC. There are a couple of elements that distinguish this harmonic plot from the earlier harmonic plots. The first element is the THD of 11.61%, which is much higher than in the other scenarios. The second element is the specific harmonics. While the harmonics around the switching frequency are more or less the same as in the other scenarios, both the 5^{th} and 7^{th} are higher. In addition, there are significant 13^{th} and 11^{th} harmonics. In terms of the relationship between the specific harmonics, it is evident that the 7^{th} harmonic is greater than the 5^{th} this time, which is caused by both the grid and the converter producing the 7^{th} harmonic. The 13^{th} harmonic is also produced by the grid, but the 11^{th} harmonic can not be explained in the same way.

Figure 5.17 and Figure 5.18 show the plots of the current harmonics from the wind turbine and grid, respectively. It is clear that the current harmonics coming from the grid are only the 13^{th} and 7^{th}, which proves that the 11^{th} harmonic must be produced in the converter. In fact, a large 11^{th} component can be seen coming from the turbine in Figure 5.17. This is most likely caused by the PLL. In the previous chapter, it was shown that the PLL was very susceptible to voltage harmonics, and Figure 5.19 shows that there are in fact more than 4% voltage THD at the turbine, almost 10 times as much as in the base case. In the base case, it is almost exclusively voltage harmonics around the switching frequency, but with a non-ideal grid, there are a lot of voltage harmonics at the 7^{th} and 13^{th} harmonic order.

Figure 5.18 shows that the grid current has a THD of 34.99%. In base case, it was proven that the grid injects a large current to excite the capacitors in the subsea cable. When the grid is ideal, this will cause a current without any harmonics. Since the grid in this scenario has voltage harmonics, a large current with harmonics will result. The next scenarios will examine the relation between the amount of turbines and THD at the grid.

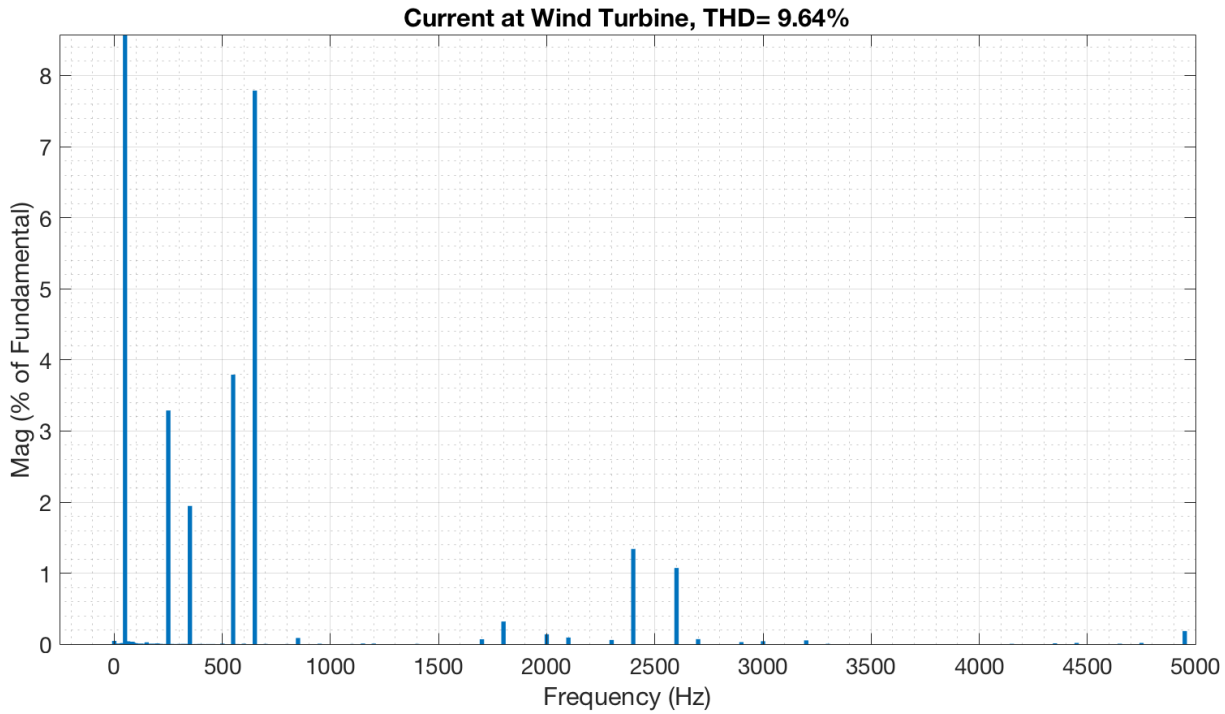

Figure 5.17: Current harmonics at the turbine in *Scenario 7: non-ideal grid*

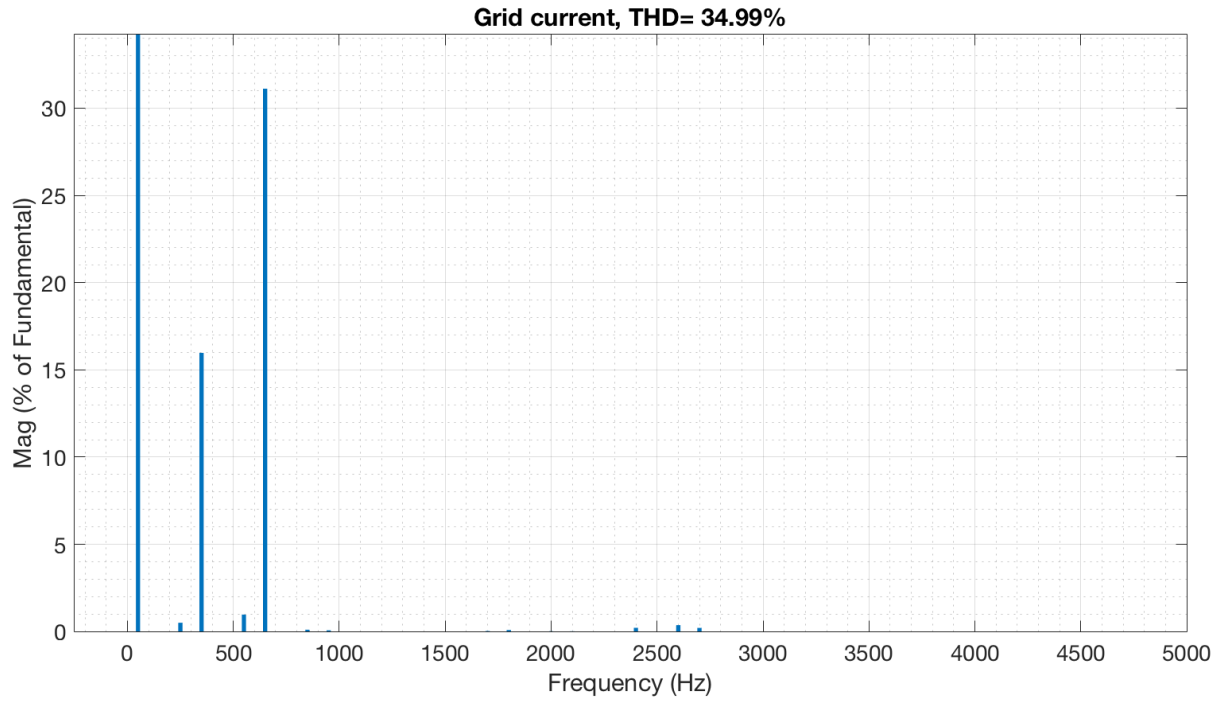

Figure 5.18: Current harmonics at the grid in *Scenario 7: non-ideal grid*

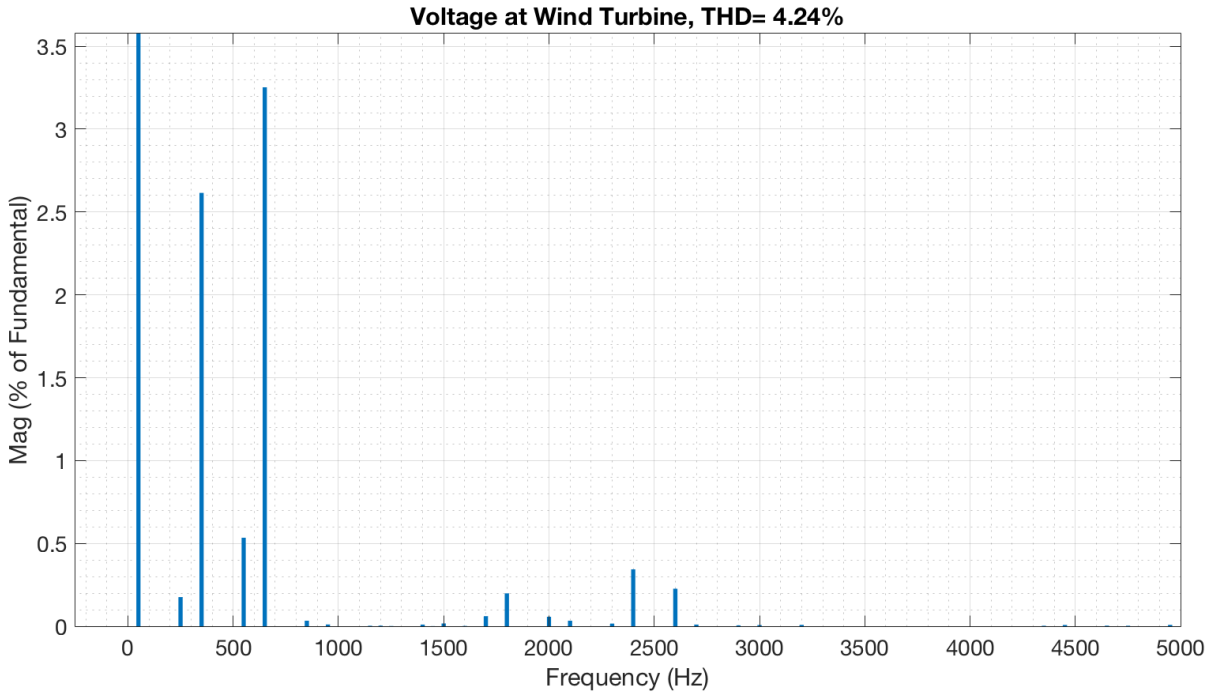

Figure 5.19: Voltage harmonics at the turbine in *Scenario 7: non-ideal grid*

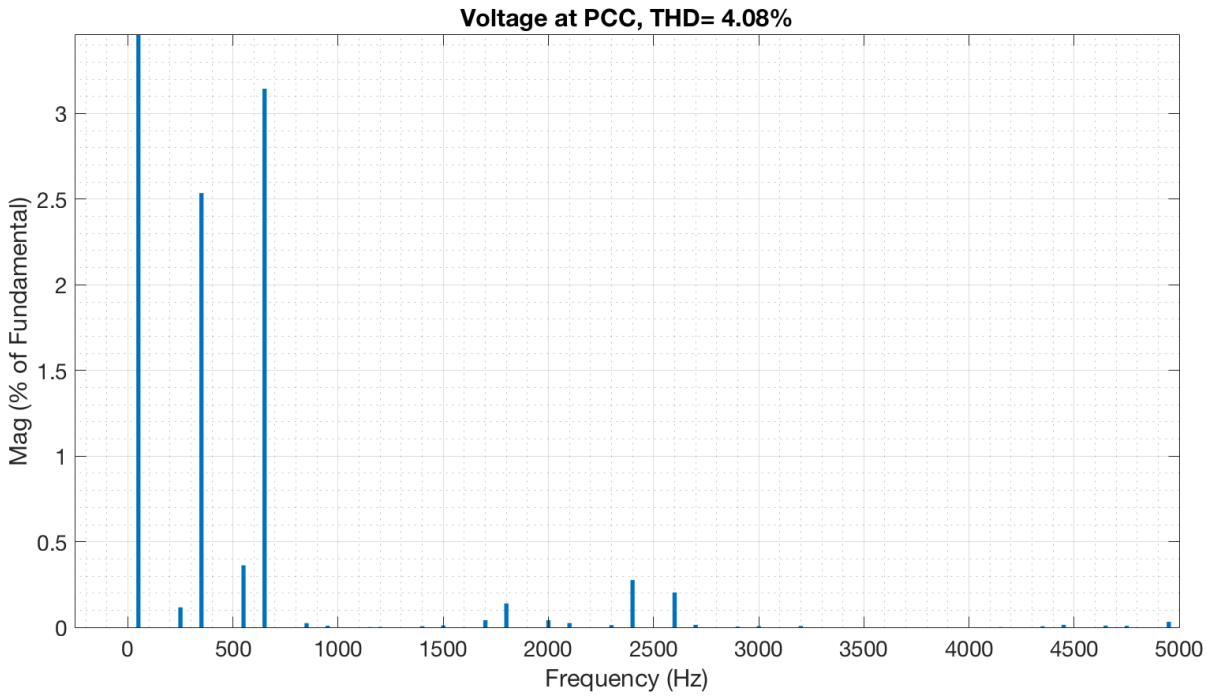

Figure 5.20: Voltage harmonics at the PCC in *Scenario 7: non-ideal grid*

5.7 Scenario 8: base case with 18 turbines

In this section, the scalability of the system will be investigated. There are two main reasons to investigate how the system reacts with more than two turbines: to see if simulating only two turbines is an acceptable simplification, and to investigate why the grid harmonics do not behave as expected. Two scenarios will be examined with 18 turbines; the base case and the non-ideal grid.

The reason for simulating only two turbines in the other scenarios is because of the complexity associated with simulating the turbines. To solve this, only one of the 18 turbines will be simulated as a converter, and the other 17 turbines will be simulated as current sources. The control signal for these current sources will be the output current measured from the one turbine that is simulated as a VSC (i_g from Figure 3.2). This means that all of the turbines will be controlled by the same control system. The 18 turbines will be simulated as two radials connected to the PCC, with π-sections between each turbine as seen in Figure 5.21. The big turbine in the figure is the VSC, while the smaller ones are current sources. The radials are made to be similar to the radials at Anholt Offshore Wind Farm, and the π-sections are simulated as the cable sections from Figure 4.1. More information on the 18 turbine model can be found in the Appendix.

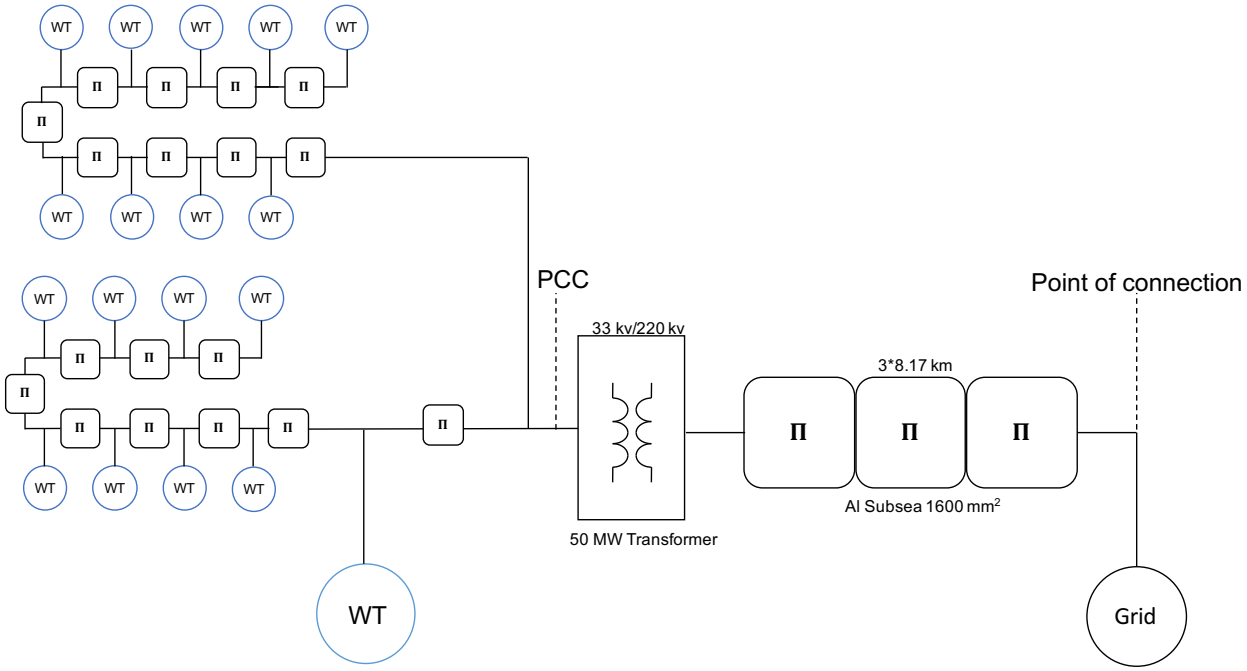

Figure 5.21: Single line diagram of wind farm with 18 turbines

First, the base case will be evaluated with one converter and 17 current sources to see if there are any major changes in the results when more current is going through the passive elements.

Figure 5.22 shows the current harmonics at PCC with 18 turbines simulated. It looks very similar to Figure 5.6, with the biggest difference being that the THD has increased to 3.68%, which is a 30% increase compared to base case with two turbines. This could be caused by the fact that the turbines are simulated as current sources, making their performance less ideal than if they were simulated as VSC. Since the voltage level and harmonics are different at all the turbines, this will make the performance worse compared to running it with 18 VSC.

Figure 5.23 shows the harmonic current plot at the grid. This is very different form Figure 5.7, and proves that the grid will in fact experience about the same amount of harmonics as at the PCC. The only reason that there were almost no current harmonics in the grid in the first six scenarios was because there was not enough current going through the subsea cable.

Figure 5.24 shows that the current harmonics produced at the wind turbine are also increased by about 30%. Since these are the harmonics produced at the converter, it can not be explained by the other turbines being simulated as current sources, but is likely explained by the increase in voltage harmonics seen in Figure 5.25. When the number of wind turbines are increased, there will be more current going through the cables, and more voltage harmonics will be generated. This will in turn impact the performance of the VSC as it has already been shown that a correlation exists between the voltage THD at the VSC and the produced current harmonics from the wind turbine.

Figure 5.26 shows that the same voltage harmonics can be found at PCC. This means that even with an ideal grid, the voltage at PCC will be distorted, as long as there is enough current going through the subsea cable. With only two turbines in operation, the grid was able to hold the same harmonic level at PCC and the grid, but with more current injected from the turbines, the ability of the grid to ensure a non-distorted voltage at PCC lessens.

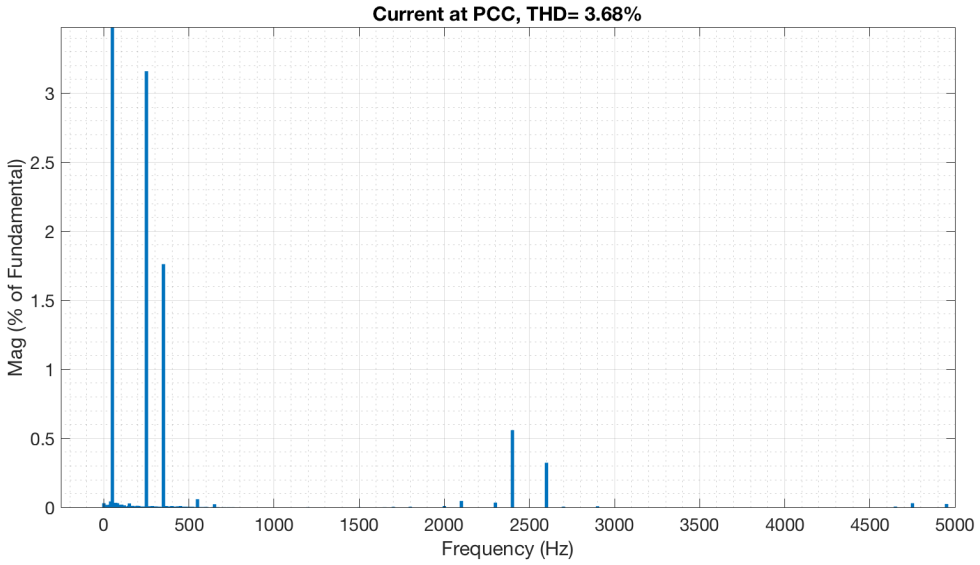

Figure 5.22: Current harmonics at the PCC in *Scenario 8: base case with 18 turbines*

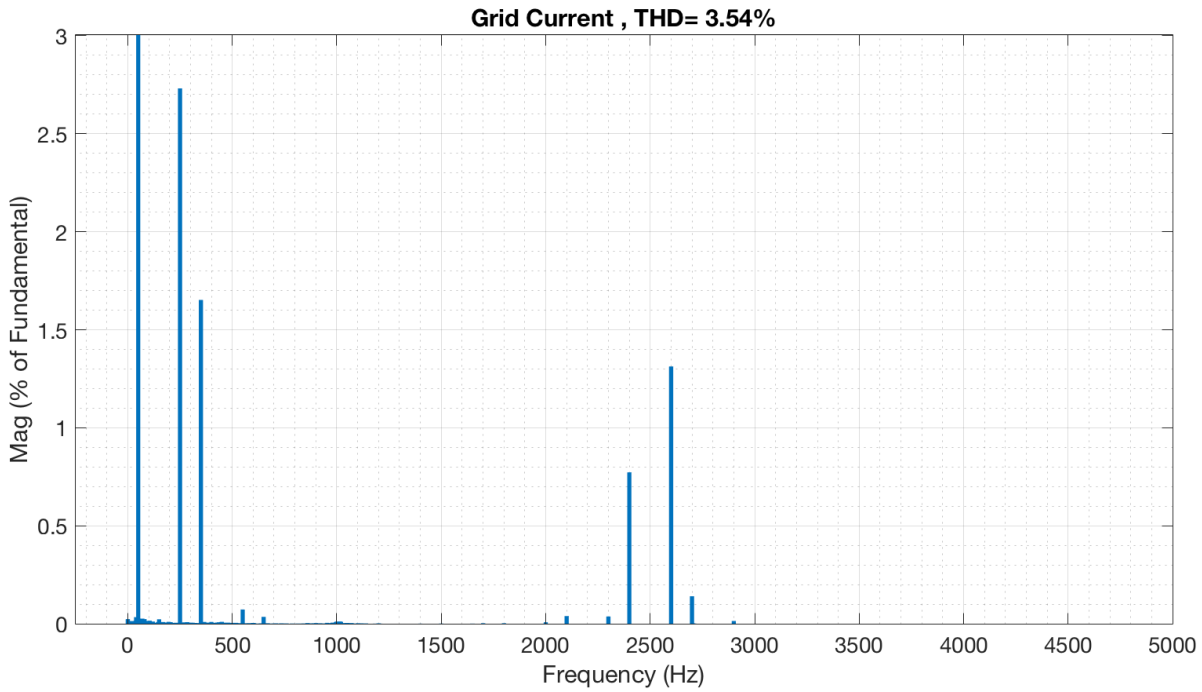

Figure 5.23: Current harmonics at the grid in *Scenario 8: base case with 18 turbines*

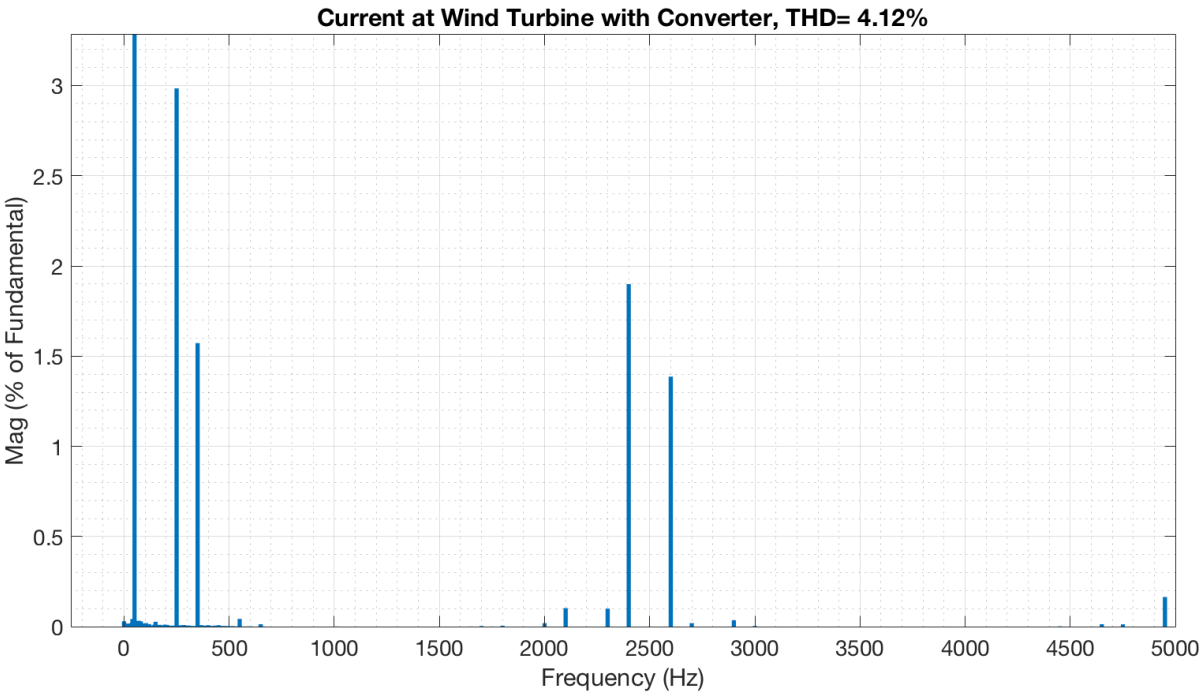

Figure 5.24: Current harmonics at the turbine in *Scenario 8: base case with 18 turbines*

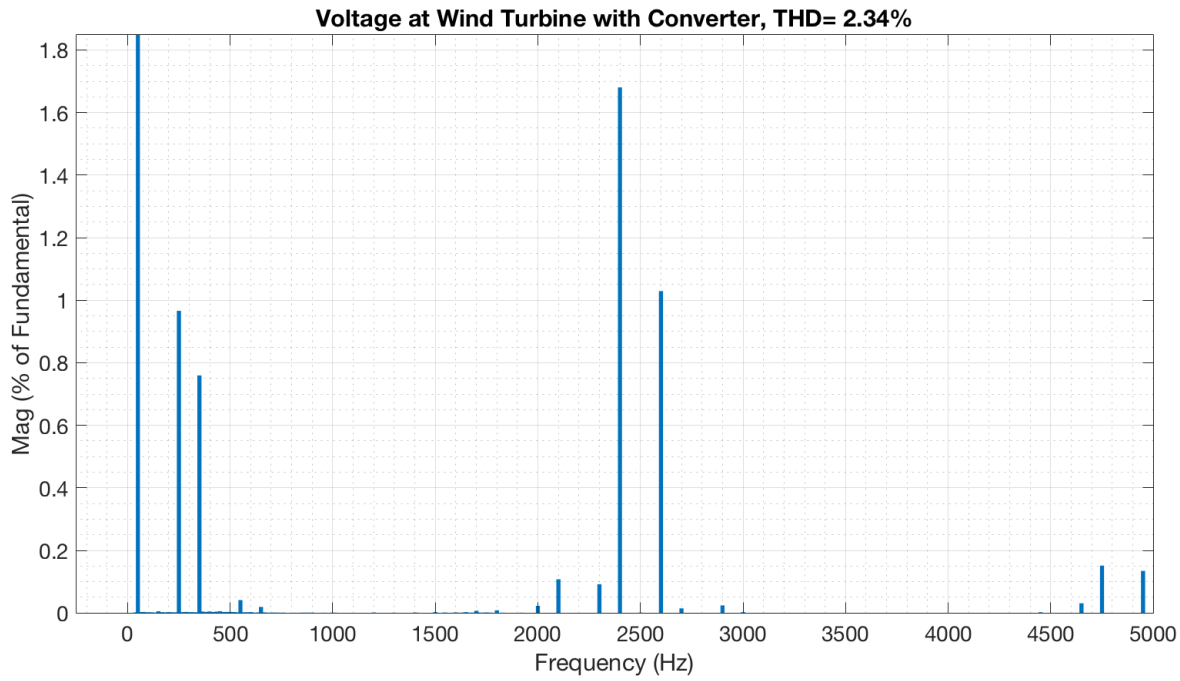

Figure 5.25: Voltage harmonics at the turbine in *Scenario 8: base case with 18 turbines*

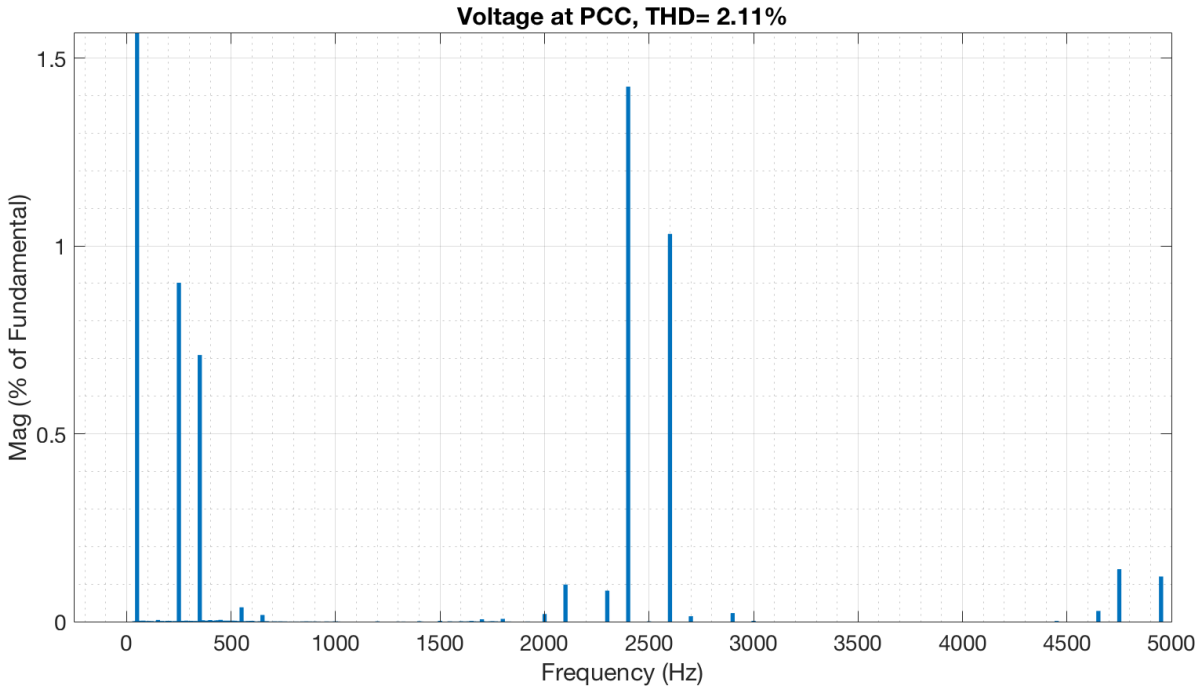

Figure 5.26: Voltage harmonics at the PCC in *Scenario 8: base case with 18 turbines*

Figure 5.27 shows the current going thorough the offshore cable. While the cable is still drawing some current from the grid to induce the capacitors, there is much less with 18 turbines than there is with two. With 111 turbines, there will likely be no injected current from the grid, even if the turbines are not running at full power.

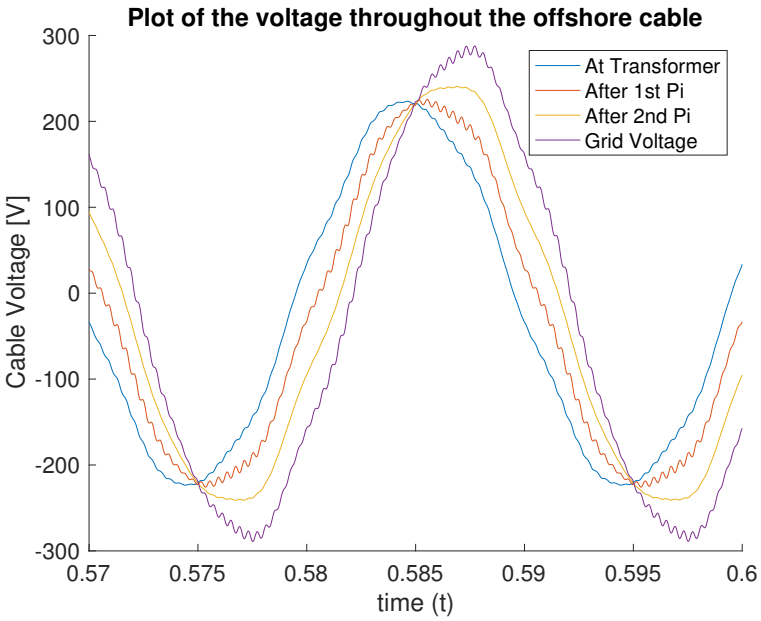

Figure 5.27: Current through the subsea cable with 18 turbines

5.8 Scenario 9: 18 turbines and non-ideal grid

The same 18 turbine scenario was run with the same non-ideal grid as in *Scenario 7: non-ideal grid*, with voltage harmonics at the 7^{th} and 13^{th} order. Figure 5.28 shows the current harmonics at PCC with 18 turbines and a non-ideal grid. It is evident that the same harmonics are present when there are 18 turbines as when there are only two. The relationship between the harmonics, however, has changed. With 18 turbines there are a higher share of 5^{th} and 7^{th} harmonics, and less of the 11^{th} and 13^{th} harmonics. The THD is also lower, which is caused by the fact that the turbines are pushing more current through the subsea cable, causing the grid to produce less current to excite the cables, and therefore also less harmonics. Figure 5.29 shows that the produced current THD is more or less the same as with two turbines, but the same shift towards more 5^{th} and 7^{th} and less 11^{th} and 13^{th} that was evident at the PCC can be seen at the wind turbine.

In *Scenario 8: base case with 18 turbines*, there was a relatively large increase in the voltage THD at both PCC and the wind turbine. With the non-ideal grid, there is no increase in THD, but Figure 5.30 and 5.31 show that the specific harmonics are shifting more towards the harmonics produced in the turbine and less towards the grid harmonics. This proves that with more turbines in operation, the harmonic impact from the grid is decreased, and the harmonic impact from the converter becomes more impactful, both on the current and the voltage harmonics.

Figure 5.32 shows the current harmonics at the grid with 18 turbines and a non-ideal grid. While the THD is still extremely high at the grid, it is reduced by 36% compared to the two turbine scenario. With 111 turbines in operation, it can be assumed that enough current will be pushed through the subsea cable to excite the capacitors in the cable without drawing current from the grid.

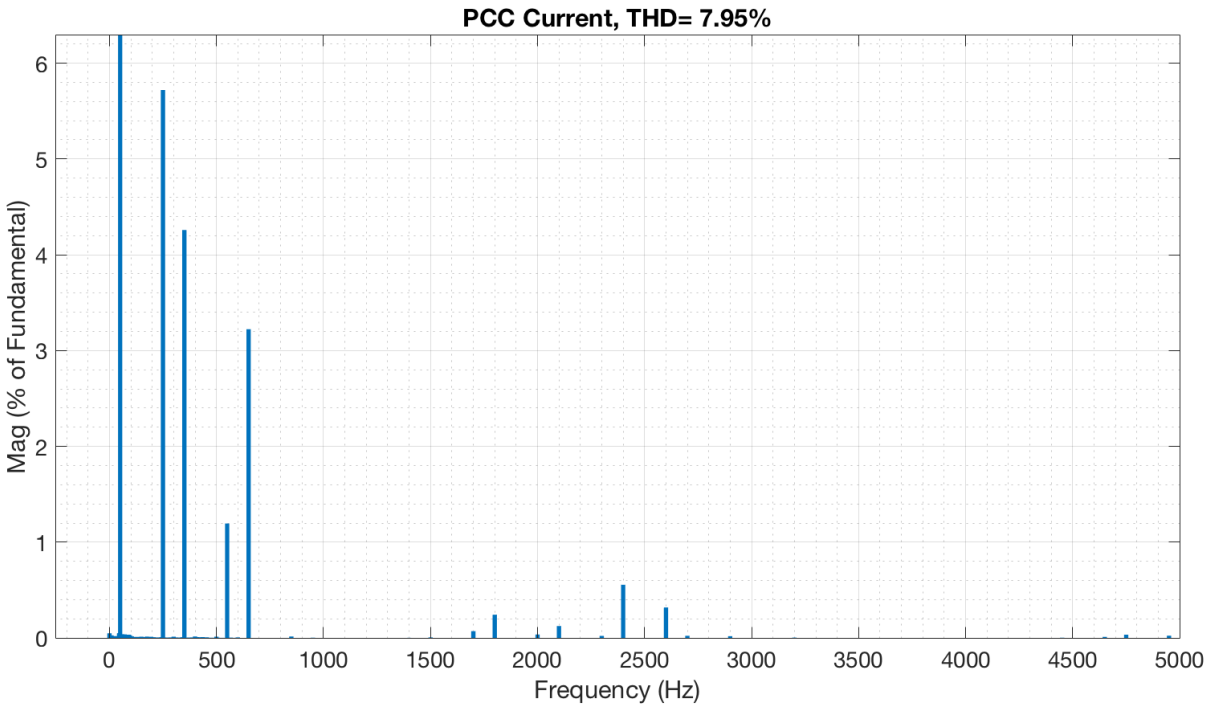

Figure 5.28: Current harmonics at the PCC with *Scenario 9: 18 turbines and non-ideal grid*

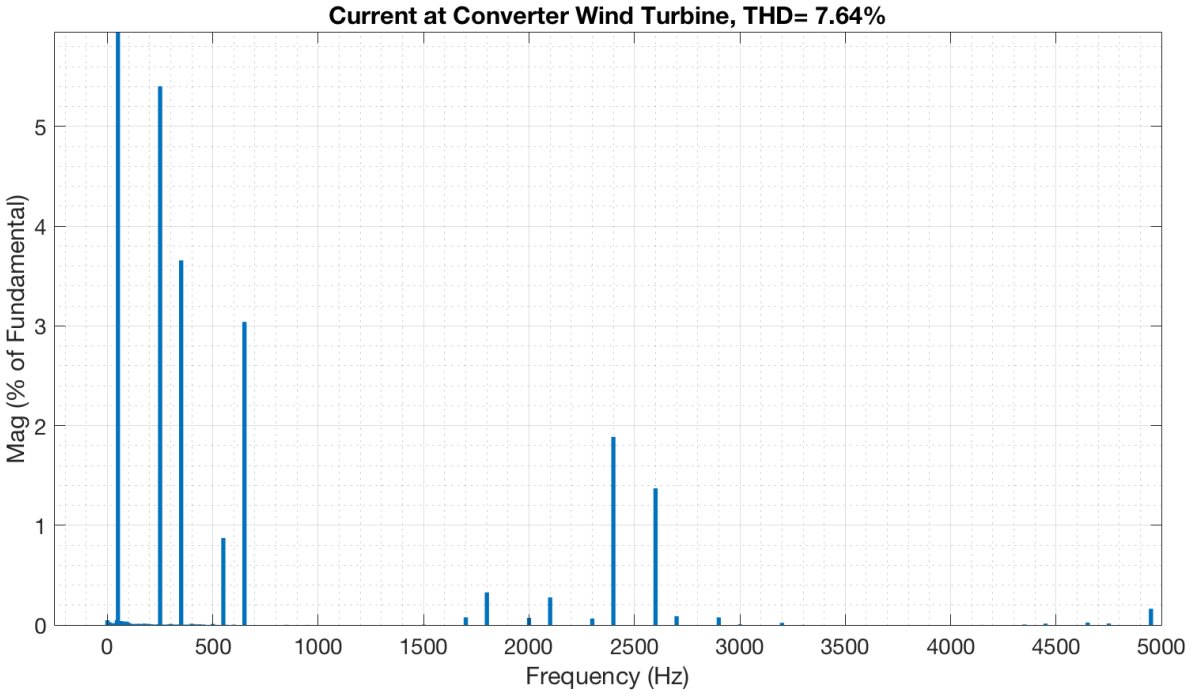

Figure 5.29: Current harmonics at the turbine with *Scenario 9: 18 turbines and non-ideal grid*

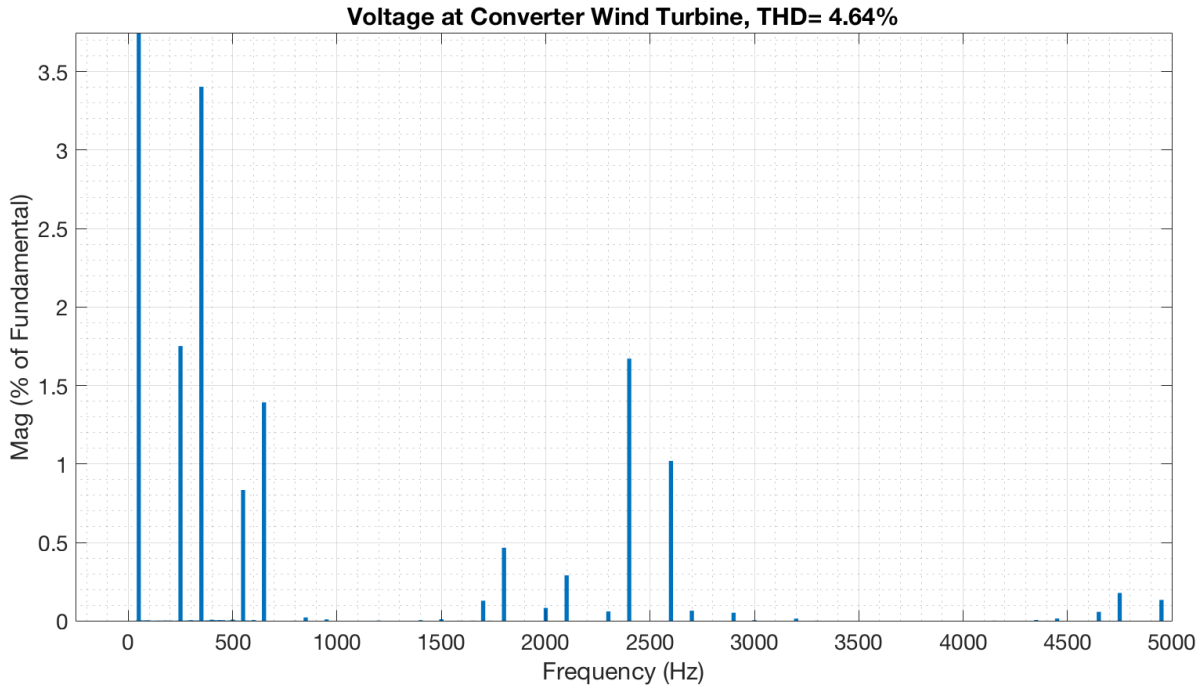

Figure 5.30: Voltage harmonics at the turbine with *Scenario 9: 18 turbines and non-ideal grid*

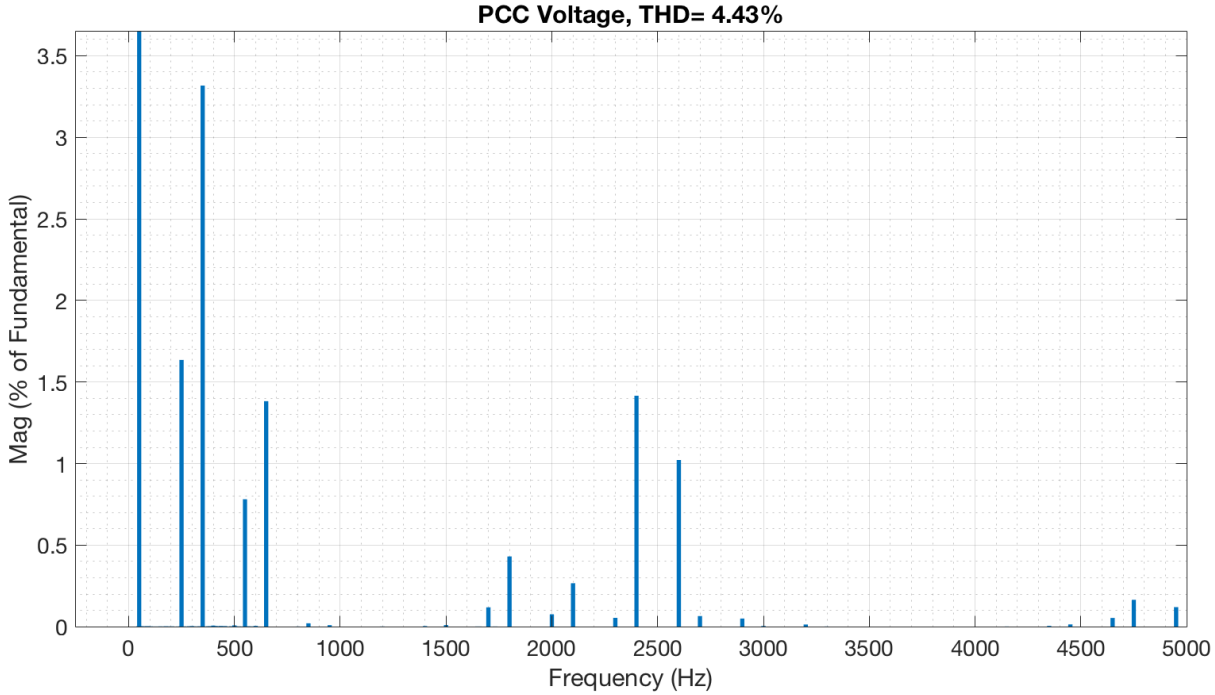

Figure 5.31: Voltage harmonics at the PCC with *Scenario 9: 18 turbines and non-ideal grid*

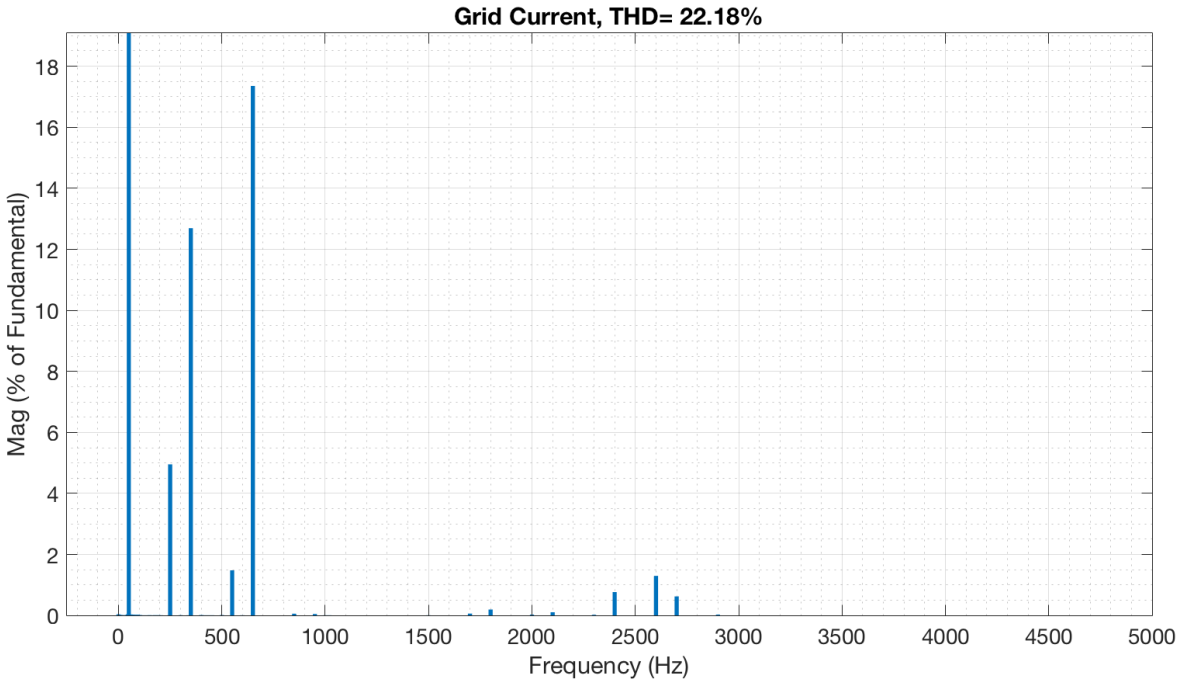

Figure 5.32: Current harmonics at the grid with *Scenario 9: 18 turbines and non-ideal grid*

Chapter 6: Active Filtering

This chapter will explore active filtering to reduce harmonics. When harmonics in the grid grow too large, measures must be taken to comply with the grid requirements. One option is to install a passive filter at the point of connection with the grid, as was done in Ormonde Offshore Wind Farm [41]. However, to remove the harmonics in the offshore grid and the turbines, it would be more suitable to place the filter offshore. Passive filters tuned for lower harmonic frequencies and a large amount of power will be exceedingly big and inconvenient as they require a large inductor and cooling system [21]. Additionally, passive filters are associated with high engineering costs, and have to be re-tuned when the grid changes.

Another option is to add a designated active filter at the PCC. With power electronic devices becoming cheaper and of higher quality, this option is increasingly more popular. While adding a designated active filter may solve the harmonics problems at the PCC, it does not necessarily solve the issue at other places in the grid.

With the amount of grid-connected converters already installed in offshore wind farms, a third option would be to apply active filtering techniques in the already existing VSC [12] [9]. This requires no extra equipment and solves the harmonic issue where it is created, instead of having to add additional components. The drawback with this solution is that the wind turbine converters often come as off-the-shelf products, where the control system is the intellectual property of the producer [42], thus making re-tuning the converter a sometimes unfeasible solution.

In this chapter, the third option will be applied to the system. A notch filter will be integrated in the control system to perform active filtering. This method was used by Ł Kocewiak when he analyzed the harmonic level of Anholt Offshore Wind Farm and found that the level of 17^{th} harmonics was higher than the permitted level according to the grid code. To shift and damp the level of 17^{th} harmonics, a notch filter was installed in the current measurements of the converter [12]. Figure 6.1 shows the control system with the addition of a notch filter in the current measurements.

Since the scenarios in Chapter 5 had similar results in terms of the specific harmonics, only *Scenario 1: base case*, *Scenario 4: half power* and *Scenario 7: non-ideal grid* will be re-run with active filtering. The 18 turbine scenarios only added current sources and not VSC, therefore

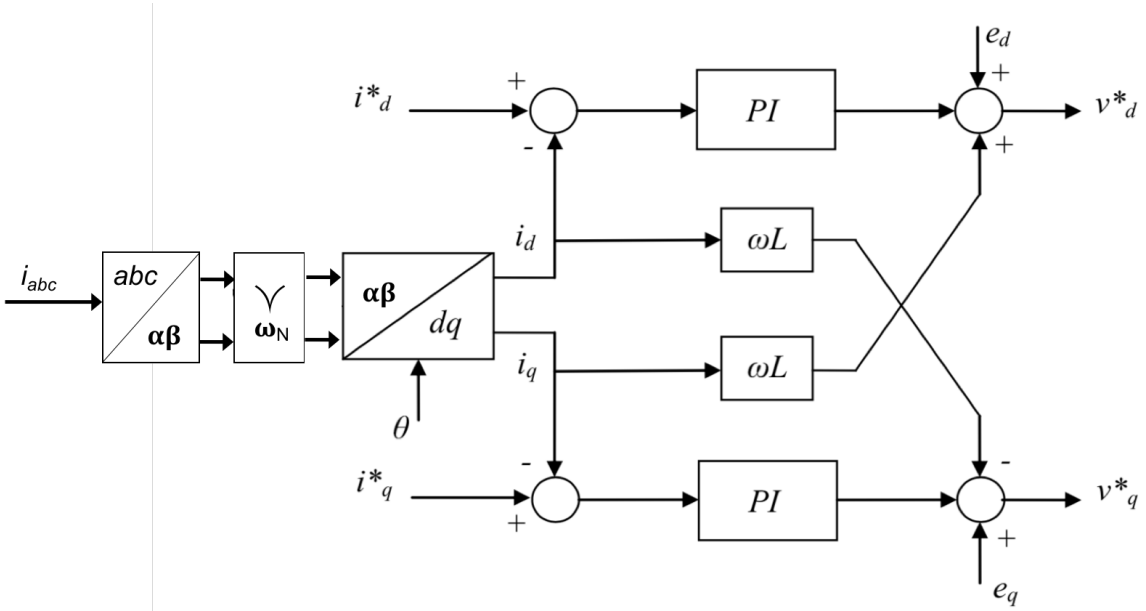

Figure 6.1: Control system of the converter with notch filter at the current measurements

none of these scenarios were run with a notch filter, which is added in the control system.

Figure 6.1 shows the control system with the addition of a notch filter in the current measurements. A notch filter, also known as a band stop filter, filters out only a given band of frequencies. Eq. 6.1 shows the transfer function of a notch filter, where ω_N is the central rejected frequency and ω_c is the width of the rejected band [43].

$$H(s) = \frac{s^2 + \omega_N^2}{s^2 + 2\omega_c s + \omega_N^2} \tag{6.1}$$

Chapter 5 found that the most dominant harmonic component was the 5^{th} harmonic. The notch filter will therefore have a central rejecting frequency $f_N = 5 * 50Hz = 250Hz$. The width of the rejected band will be set to 10% of the rejected frequency, $f_c = 25Hz$.

Figure 6.2 shows the bode plot of the installed notch filter. From the figure, it is evident that the gain is 0 for almost all frequencies, except for $\omega = 1571 \simeq 2\pi 250$, where the gain is -264.4. This is equivalent to removing the 5^{th} harmonic component from the measurements of the current, meaning that the control system will receive a signal without any 250 Hz oscillations.

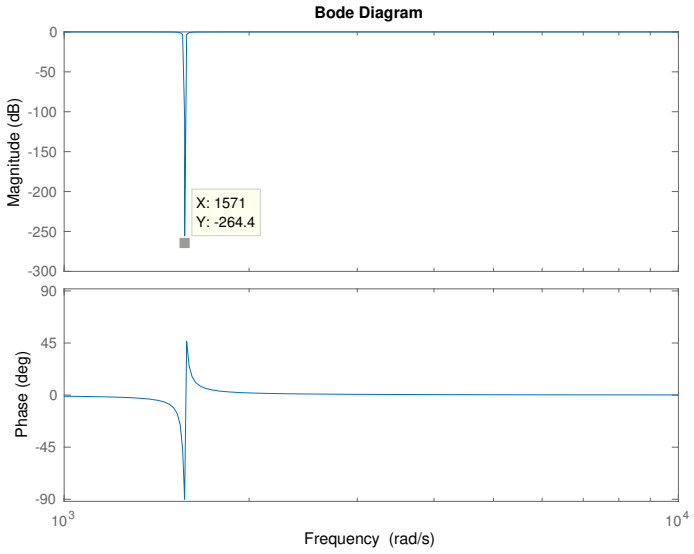

Figure 6.2: Bode plot of installed notch filter

6.1 Results

Figure 6.3 shows the current harmonics at PCC in base case with an installed notch filter. The plot shows that the range of harmonics are exactly the same as in Figure 5.6, which shows the current harmonics at PCC without the notch filter. However, both the THD and the 5^{th} harmonics are reduced in the simulations with a notch filter compared to the simulations without.

Table 6.1: Current harmonics and THD at PCC with and without a notch filter

Scenario	THD		5^{th} harmonics	
	w/o notch	with notch	w/o notch	with notch
Base case	2.96%	2.53%	2.61%	2.18%
Half power	5.46%	4.75%	4.81%	4.05%
Non-ideal grid	11.61 %	11.44%	3.43%	2.90%

Table 6.1 summarizes the results from the simulations with the notch filter. It is evident that the 5^{th} harmonic is reduced in every case where the notch filter is installed. In all three cases, the 5^{th} harmonic is reduced with about 16% (16.4% for base case, 15.8% for half power and 15.5% for non ideal grid), which proves that installing a notch filter is a suitable way to reduce the specific output of one specific harmonic.

The THD is also reduced, though not as much as the 5^{th} harmonic. The reduction in THD is only caused by the reduction in the 5^{th} harmonic, which is evident because the other harmonics all have the same value.

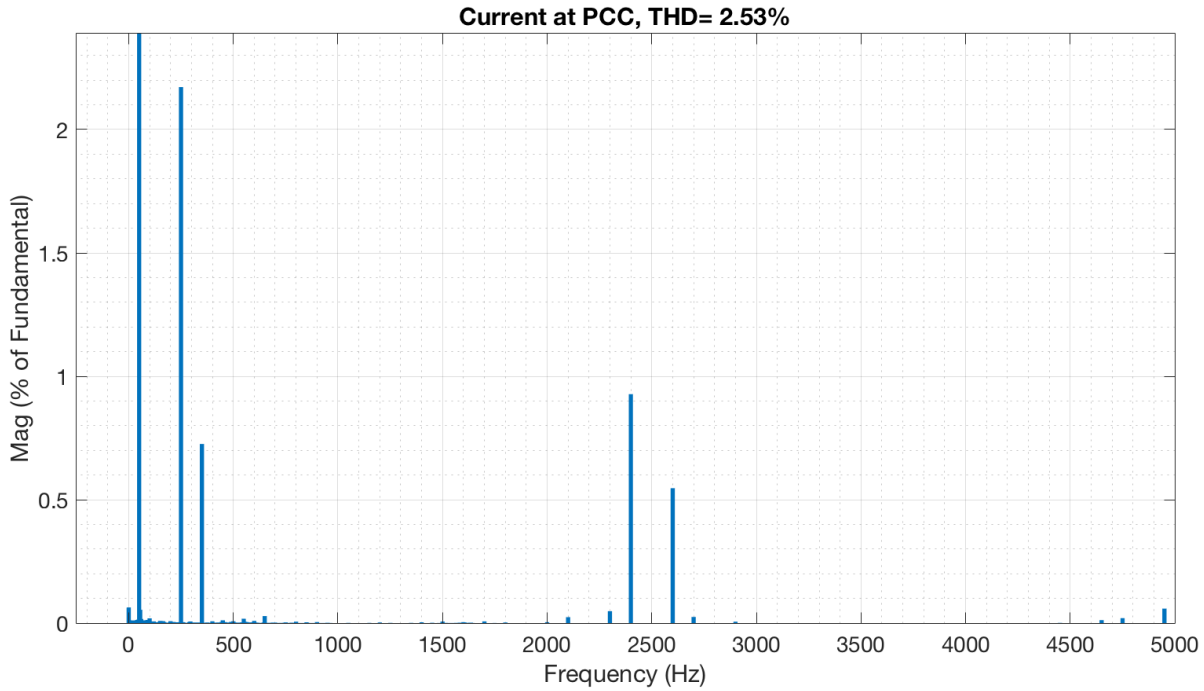

Figure 6.3: Current harmonics at PCC in *Scenario 1: base case* with installed notch filter

Chapter 7: Discussion

In this chapter, the results from all previous chapters will be examined and compared. Whether the results support the existing literature or represent new findings will be discussed. In the last section, the limitations of this project will be explained.

7.1 Current harmonics at PCC

Scenario	THD	5^{th}	7^{th}	48^{th}	52^{nd}
2: ideal PLL	1.11	0.22	0.01	0.92	0.55
6: switch-on delay	2.68	2.01	0.93	0.93	0.55
1: base case	2.96	2.61	0.83	0.92	0.55
3: de-tuned PI	2.98	2.63	0.83	0.92	0.55
4: pf=0.9	3.46	3.10	1.02	0.96	0.57
8: base case and 18 turbines	3.68	3.17	1.78	0.58	0.32
5: half power	5.46	4.81	1.48	1.80	1.08
9: 18 turbines and non-ideal grid	7.95	5.36	4.12	0.56	0.35
7: non-ideal grid	11.61	3.25	4.20	0.94	0.55

Table 7.1: Overview of current harmonics at PCC in the different scenarios

Table 7.1 shows an overview of the THD and the 5^{th}, 7^{th} 48^{th} and 52^{nd} harmonics from the 9 scenarios simulated in Chapter 5. The table is sorted by THD to more clearly showcase the differences in harmonic performance.

In every scenario except for *Scenario 7: non-ideal grid*, there is a clear correlation between the 5^{th} harmonic and the THD. This is caused by the way THD is calculated, making the more dominant harmonics count much more than the less dominant. The 5^{th} harmonic is also the harmonic that varies the most throughout the different scenarios. As already discussed, the 5^{th} harmonic is coming from the PLL, suggesting that the PLL is critical in regards to changes in the system. On the other hand, the switching harmonics (48^{th} and 52^{nd}) are more stable throughout the different cases. Almost every scenario with two turbines has approximately the same 48^{th}

and 52nd harmonics, showing that the PLL is much more exposed to changes in the grid and control system compared to the current controller and PWM.

There is, however, one exception, which is *Scenario 5: half power*. This scenario has a considerably worse performance not only in the THD, 5th and 7th order harmonics, but also in the harmonics around the switching frequency. While there is no research specifically for offshore wind farms confirming the connection between produced power and produced harmonics, P. M. Ivry et al. [44] found the same correlation in a similar experiment with VSC. Considering that Anholt offshore wind farm runs at less than half capacity 38% of the time [45], the harmonics produced when not running at rated conditions are something that must be taken into consideration when designing the offshore wind farm.

While the fact that both *Scenario 4: pf=0.9* and *Scenario 5: half power* increase the current THD coming from a VSC is documented, which components are affected by the two scenarios is not. [10] discusses how every low order harmonics is increased when the power factor is changed, but it does not discuss what causes these low order harmonics in the first place. In this thesis, it is confirmed that harmonics produced by the PLL will increase when the power factor is decreased, and that the harmonics around the switching frequency are independent of the power factor of the system. [44] concludes that there is a negative correlation between the output power of the converter and the current THD produced in the converter, but does not explain where these harmonics are coming from, or if only certain harmonics are increased. This thesis shows that while the switching harmonics were the same in every other scenario with two turbines, reducing the output power increased every single harmonic component.

When it comes to the two scenarios with 18 turbines, it is interesting to see that the harmonics around the switching frequency are actually decreased at PCC, even though the 5th harmonic and THD are increased compared to the same scenarios with only two turbines. This is caused by the fact that the impedance at the frequencies around the switching frequency is so much higher than the impedance at the 5th and 7th harmonic, making the cables work as filters for the higher order harmonics. Since the added turbines are placed with π-sections between them, there will be even more filtering of the higher order harmonics, and there will be a lower percentage of 48th and 52nd harmonics at PCC. These are the same results found by [44], namely that with a high impedance, the current harmonics will be reduced while the voltage harmonics will be increased.

Table 7.2 shows an overview of the allowed amount of current harmonics at PCC at 33kV. Since the wind farm is a 400 MW system, it is safe to assume that the short circuit current divided by the load current is no more than 20. The table shows that the THD can not be any higher than 5%, that the 5th and 7th harmonic can be no more than 4.0% and that the 48th and 52nd can be no more than 0.075%. While most of the scenarios satisfy the requirements for THD and 5th and 7th harmonics, there is not a single scenario that has 48th and 52nd harmonics lower than 0.075%.

Table 7.2: Maximum harmonic current distortion (in % of I_L) for a system rated 120 V < V < 69 kV [5]

I_sc/I_L	$3 \leq h < 11$	$11 \leq h < 17$	$17 \leq h < 23$	$23 \leq h < 35$	$35 \leq h \leq 50$	THD
< 20	4.0	2.0	1.5	0.6	0.3	5

The values given in this table are for odd harmonics. Even harmonics are limited to 25% of the values in this table.

To comply with the grid codes, additional measures must be taken to reduce the current harmonics. In every scenario, the 48^{th} and 52^{nd} harmonics have to be reduced, which could be done by installing a high-pass filter at the PCC or the wind turbine, by re-tuning the already existing filter at the wind turbine, or by installing an active filter.

7.2 Voltage harmonics at PCC

In this section, the voltage harmonics and how they comply with the grid codes will be discussed. The scenarios that have a voltage harmonic plot in Chapter 5 will be reviewed. Table 7.3 shows an overview of the voltage harmonics at PCC for the four scenarios with voltage harmonic plots. Since the most dominant voltage harmonic components are the harmonics around the switching frequency, and the switching harmonics had only small variations in most scenarios, only scenarios 1, 7, 8 and 9 are included.

While the different scenarios had a relatively large impact on the produced current harmonics from the converter, the voltage harmonics were kept relatively small throughout the first six simulation scenarios. The same harmonic frequencies can be found in the voltage as in the current, but the relationship between the different harmonics has changed. When it comes to voltage harmonics, the harmonics around the switching frequency are more prominent than the 5^{th} and 7^{th} harmonics.

Scenario	THD	5^{th}	7^{th}	11^{th}	13^{th}	48^{th}	52^{nd}
1: Base case	0.36	0.09	0.04	-	-	0.28	0.21
8: Base case and 18 turbines	2.34	0.96	0.76	-	-	1.68	1.03
7: Non-ideal grid	4.08	0.19	2.51	0.36	3.13	0.29	0.20
9: 18 turbines and non ideal grid	4.43	1.63	3.32	0.78	1.39	1.41	1.01

Table 7.3: Voltage harmonics at PCC

Table 7.4 shows the allowed voltage harmonics at PCC with a voltage of 33 kV. It is evident that the base case is well within the allowed limits of voltage harmonics, both with two turbines and with 18. However, there is a 600% increase in the 48^{th} harmonic when 16 turbines are added.

If the same trends continue, there will be too much voltage harmonics when all 111 turbines are simulated.

With a non-ideal grid, the voltage THD is a lot higher, but this is caused mainly by an increase in the 7^{th} and 13^{th} harmonic components, which are injected by the grid. Even with 3.32% 7^{th} harmonic and 3.13% 13^{th} harmonic, the THD is still within the allowed value of 5%, and only the 7^{th} and 13^{th} harmonics are not within the values recommended by IEEE. This shows that even though the non-ideal grid has a significant impact on the produced current harmonics, the voltage harmonics are not impacted in the same manner. In fact, with 18 turbines, the 13^{th} harmonic is greatly reduced, showing how the non-ideal grid is less impactful as more turbines are added.

Bus voltage V at PCC	Indivdual harmonic (%)	Total harmonic distortion THD (%)
$1kV < V \leq 69kV$	3.0	5.0

Table 7.4: Voltage distortion limits [5]

7.3 Propagation of harmonics in the offshore wind farm

P. Ivry et al. [44] found that while there was a negative correlation between the inductance in the grid and the produced current harmonics, there was a positive correlation between the inductance in the grid and the produced voltage harmonics from a VSC. Since the onshore grid is ideal in most of these simulations, the only source for voltage harmonics is the VSC and the voltage drop from the harmonic current going through the passive elements. If the current is constant, a higher inductance in the cable will lead to a higher voltage drop at the specific frequency.

Table 7.5 shows how the current and voltage harmonics propagate through the grid. Note that there are no voltage harmonics at the grid since the scenario presented in the table is *Scenario 8: base case with 18 turbines*. This case was chosen because it best shows the current harmonics at the grid.

Point	Current Harmonics				Voltage Harmonics			
	5^{th}	7^{th}	48^{th}	52^{nd}	5^{th}	7^{th}	48^{th}	52^{nd}
WT	2.98	1.58	1.89	1.38	0.97	0.76	1.68	1.03
PCC	3.15	1.78	0.57	0.32	0.90	0.71	1.42	1.04
Grid	2.72	1.66	0.78	1.31	-	-	-	-

Table 7.5: Voltage and current measurement at different points in the offshore grid in *Scenario 8: base case with 18 turbines*

From the frequency sweep in section 5.1, it is evident that the impedance at the 48^{th} and 52^{nd}

harmonic frequency is about ten times as high as the impedance at the 5^{th} and 7^{th} harmonic frequency. At the same time, the results in Table 7.5 show that the voltage harmonics around the switching frequency are much higher than the 5^{th} and 7^{th} voltage harmonics, both at the wind turbine and at PCC, while the opposite is true for the current harmonics. This correlates with the findings of P. Ivry et al [44]. However, while P. Ivry et al. proved that there was a correlation with the voltage and current THD and the impedance in the grid, this thesis find that this is also true for the specific harmonic frequencies.

The most curious observation is that the 48^{th} and 52^{nd} current harmonic components are actually growing from the PCC to the grid. This is caused by the capacitors in the cable drawing some current from the grid, as was explained in section 5.2. In *Scenario 1: base case*, the voltage drop in the offshore cable had a THD less than 0.5%. With 18 turbines simulated, the voltage drop is significantly higher at 1.42% for the 48^{th} harmonic component and 1.04% for the 52^{nd} harmonic component. This causes the capacitors to draw a distorted current, consequently increasing the current harmonics.

7.4 Filtering of harmonics

Earlier in this chapter, it was proven that some sort of filtering is required to comply with the grid codes especially for the current harmonics around the switching frequency. These harmonics can be easily filtered by installing a designated active or passive filter, or by re-tuning the passive filter connected to the wind-turbine.

In *Scenario 5: half power*, the 5^{th} harmonic was 4.81% and therefore not within the required current harmonic level. With the notch filter installed in Chapter 6, however, the 5^{th} harmonic is 4% and satisfies the grid requirements. This shows how installing the notch filter is a suitable way to reduce one specific harmonic component to comply with the grid code. While Ł Kocewiak proved this in [12], that paper does not discuss the origins of the harmonics. Since the PLL uses the voltage measurement as a reference to synchronize the converter to the grid, it is not obvious that installing a notch filter in the current measurement will limit the harmonics created in the PLL. However, this thesis has proven the technique successful in restraining the harmonics generated in the PLL. The 5^{th} current harmonic is limited by $\approx 16\%$ across three different scenarios, independent of the original value of the 5^{th} harmonic.

The results from Chapter 5 show that there are several possibilities for active filtering in the proposed system. Adding a switch-on delay and improving the PLL both reduce the 5^{th} harmonic compared to the base case. While the harmonic impact from the PLL and the importance of tuning it correctly to secure stability is rather well documented [46] [47], the impact of adding a switch-on delay is unique to this system. The improvement in the harmonics associated with the switch-on delay is, however, as discussed in Section 5.5, most likely connected to the PLL

being tuned too fast.

Another possible measure to improve the generated harmonics is to move the voltage measurement to the grid side of the wind turbine connected transformer. This thesis has proven that the voltage ripple impacts the production of 5^{th} and 7^{th} harmonics, and in chapter 3, the voltage plots show that there are more than 4% voltage THD at the point of measurement. By moving the point of measurement from the VSC side of the transformer to the grid side, the measured voltage harmonics would be reduced significantly, as would the current harmonics produced by the PLL.

[14] offers no explanation as to why the voltage at Anholt Offshore Wind Farm is measured at the VSC side of the transformer, but it is likely related to the voltage level and the rating of the measuring equipment.

7.5 Limitations

While the system simulated in this master project is suitable to discover the impact of different scenarios on the harmonic production in offshore wind farms, the scale of the simulation is too small to yield detailed results about the propagation of the harmonics. The harmonic propagation from the PCC to the grid is greatly impacted by the amount of turbines in the simulations, and the computational power required to simulate enough wind turbines is a limitation in this master thesis.

[7] discusses how the skin effect impacts the harmonic damping of the transformers and cables, and concludes that higher frequency harmonics will experience a higher damping than harmonics with lower frequency. Due to limitations in the simulation tools used in this thesis, this effect is ignored in simulations. This means that the specific high order harmonic values will be higher in the simulations than in a real world context. Since all simulations are done with the same assumptions, this does not impact the comparison between the different cases and only means that the values may be slightly too high.

Lastly, there were no sources on the specific control system used in Anholt Offshore Wind Farm, and it is therefore tuned with the parameters showed in section 3.3, using sources as described in the same chapter. The tuning of the PLL has a significant impact on the generated harmonics, and while this may cause the specific harmonic to be slightly off, it should not impact the relation between the different scenarios as they all use the same PLL.

Chapter 8: Conclusion

The harmonics produced in offshore wind farms are investigated in this master thesis. With them, a full guide on how to simulate the electrical components of an offshore wind farm and the harmonic impact of different electrical scenarios occurring in real offshore wind farms are shown. Simulations of the offshore wind farm show that current harmonics produced in the VSC vary greatly between the nine scenarios tested.

Investigations to identify which harmonics had the most impact and which components caused those harmonics were performed. In all scenarios using an ideal grid, the 5^{th} current harmonic was the most dominant. In the base case, the 5^{th} harmonic was 2.61%, but it varied significantly between the scenarios, with the greatest variation being 4.81% with turbines running at half power, compared to 2.01% when turbines had a switch-on delay of 5 µs. A scenario was also run with an ideal PLL in which the 5^{th} harmonic was only 0.22%, proving that the 5^{th} current harmonic was generated in the PLL, but amplified unequally in the different scenarios.

The correlation between voltage harmonics at the wind turbine and produced current harmonics was investigated. The base case was simulated three times. The first time involved only one turbine connected to a voltage source, and the other two scenarios used two and 18 turbines connected to an offshore grid. In each scenario, the voltage harmonics were different. It is evident that as more voltage harmonics are present at the wind turbine, more current harmonics are produced.

This was confirmed in the scenarios using a non-ideal grid, which were the scenarios that produced the most current harmonics. The scenarios with a non-ideal grid were also the only scenarios that had a considerable amount of 11^{th} current harmonics, even though the non-ideal grid only had 13^{th} and 7^{th} voltage harmonic components. These harmonics were created in the PLL, and showed how susceptible the PLL is to changes in the voltage harmonics.

When the specific current harmonic components were investigated across the different scenarios, it was evident that the low-order harmonic components created in the PLL behaved differently from the high-order switching harmonics. The switching harmonics remained constant across each scenario, except for when the turbines were running at half power, while the 5^{th} and 7^{th} harmonics varied with every different scenario.

To limit the required computational power, the first seven scenarios were simulated with

only two turbines. Two scenarios were simulated with 18 turbines to investigate the scalability of the system and the suitability of this simplification. The results showed that the same current harmonic components were present independent of the amount of turbines running. However, the THD was increased with 18 turbines. These results confirmed that the simplification did not have a significant impact on the relation between the specific current harmonics, nor did they alter the conclusions drawn from the two turbine simulations. Contrary to the two turbine system, simulating the system with more turbines showed that the current harmonics at the grid were similar to the current harmonics at the PCC.

To investigate the propagation of both current and voltage harmonics, harmonics were measured at three different points in the offshore grid. These measurements showed that the propagation and production of harmonics were dependant on the frequency-specific impedance; increased impedance lead to an increased voltage harmonic component and a decreased current harmonic component.

The produced harmonics were compared to the IEEE standards to determine whether harmonics in the offshore wind farm were within the recommended levels. The results showed that the switching harmonics in the current were the only harmonics consistently outside the recommended levels. However, low-order current harmonics produced in scenarios at half power and with grid harmonics were also out of range. Due to simplifications in the modeling and neglecting the skin-effect in cables, the specific peak value of the harmonics are not precise. Therefore, results from this thesis should be used primarily to compare the harmonic output in different scenarios.

Ł. Kocewiak [12] implemented an active filtering technique in Anholt Offshore Wind Farm, but did not specify if this technique would work for all kinds of harmonics, and more specifically, if it would work for harmonics created in the PLL of the current controller. Since the PLL uses the measured voltage as a reference, it is not obvious that filtering the current measurements will lead to an improvement in the harmonic output. The technique was implemented in this thesis to limit the 5^{th} harmonic. The active filtering strategy implemented a notch-filter to filter out the 5^{th} current harmonics in the current measurement for the VSC. The strategy proved successful in limiting the 5^{th} current harmonics, reducing it by approximately 16% across three different scenarios. This proved that Ł Kocewiak's method was successful even when the harmonics were generated in the PLL.

Chapter 9: Further Work

This master thesis established a basis for further simulations and investigated the harmonic impact of different scenarios. Building on the simulations of this master thesis, there are three different directions that should be explored further:

- Further exploration into active filtering. This thesis showed the successful application of adding a notch filter, but more active filtering techniques should be investigated. The addition of a designated active filter at the PCC, and experimentation with the cooperative control of a designated active filter and the already existing VSC should be investigated. In addition, further active filtering techniques in the control system of the VSC should be explored, such as *Local harmonic current compensation* [48].

- Expanding the simulations to include more wind turbines, cables and transformers to more accurately represent Anholt Offshore Wind Farm. Investigate the harmonic impact of expanding the wind farm. Look further into the resonance in the offshore grid and compare it with the results presented in this thesis. This would require significantly more computational power.

- Investigate the impact of the PLL. Try different tuning methods of the PI-controller and different algorithms to calculate the phase angle of the system. This project proved that while the different scenarios would amplify the low order harmonics, the PLL was the root of those harmonics.

As wind turbines and offshore wind farms grow larger, the importance of securing a good power quality becomes increasingly important. While this thesis addresses certain problems and pinpoints what causes and amplifies harmonics, further work is required to determine how to best deal with these harmonics.

Appendix A: Parameters

A.1 Offshore cables

There are four different cables used in the offshore wind farm. The data from these cables are from ABB data sheets [38] [39]. The data for the aluminum cable is from D. Dhua's wind farm experiments [15]

Cable	R $[m\Omega/km]$	L $[mH/km]$	C $[\mu F/km]$
500 mm^2 Cu cable	33.6	0.41	0.24
240 mm^2 Cu cable	70	0.41	0.21
150 mm^2 Cu cable	112	0.41	0.21
1600 mm^2 Al cable	40	0.74	0.14

Table A.1: Resistance, indcutance and capacitance of offshore cables

The zero sequence values are the same for all cables, and can be seen in table A.2

R_0	$1000\Omega/km$
L_0	$4.1264mH/km$
C_0	$7.7519nF/km$

Table A.2: Zero sequence value for all cables

A.2 Transformers

The data for the transformers can be seen in Table A.4 and A.3. The wind turbine transformer is the same for both wind turbines that are simulated.

Nominal power S	50 MW
Nominal frequency	50 Hz
V_1	$33kv$
V_2	$220kV$
Winding $L_1 = L_2$	$0.0415pu$
Winding $R_1 = R_2$	$0.004pu$
Magnetization R_m	$500pu$
Magnetization L_m	$500pu$

Table A.3: Offshore transformer connected to PCC

Nominal power S	5 MW
Nominal frequency	50 Hz
V_1	$33kv$
V_2	$690kV$
Winding $L_1 = L_2$	$0.0375pu$
Winding $R_1 = R_2$	$0.002675pu$
Magnetization R_m	$870pu$
Magnetization L_m	$50pu$

Table A.4: Wind turbine transformers

A.3 18 turbine simulation

In this section, all data needed to recreate the 18 turbine simulation will be presented. The π-sections used inbetween each transformer uses the data from Table A.1. The small wind turbines in Figure A.1 are simple current sources.

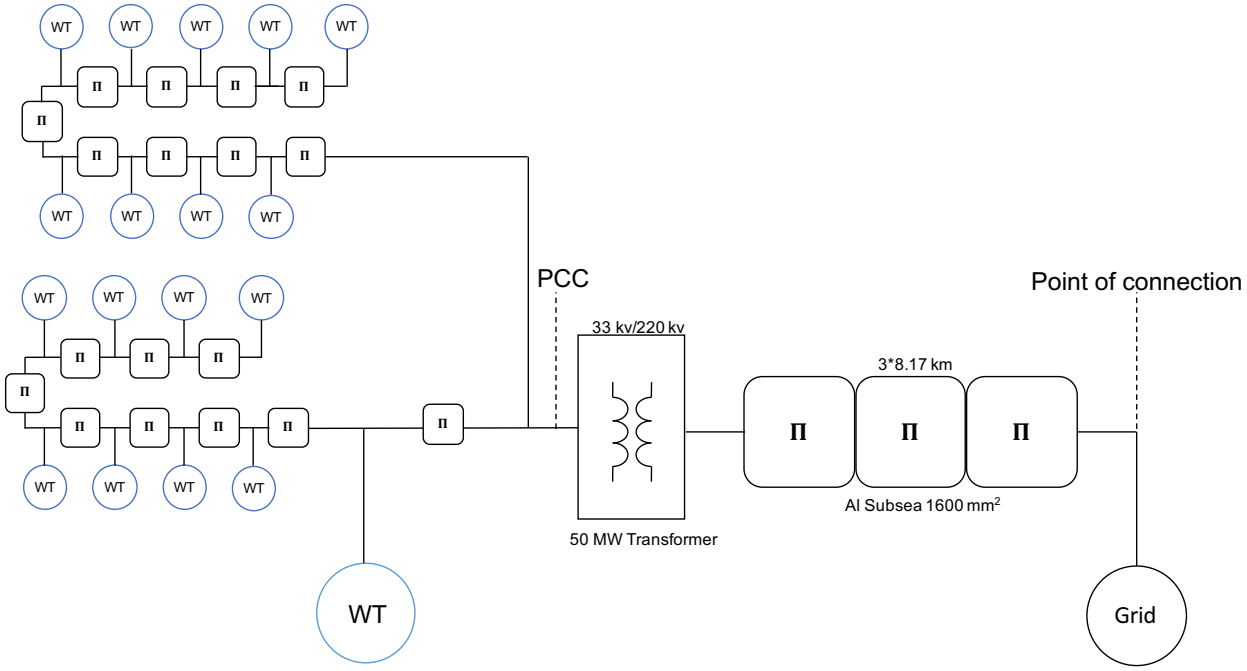

Figure A.1: Single line diagram of wind farm with 18 turbines

The length of each π-section is 1.33km, including the π-section between the VSC (the big WT) and the PCC. From the end to the PCC, there are nine π-sections. Starting from the end, there are: four $150mm^2$ cables, three $240mm^2$ cables and two $500mm^2$ cables. Both radials are exactly the same in terms of π-sections, but in the upper radial, there are only current sources and no VSC.

Appendix B: Simulink

In this section of the appendix, all screenshots from the Simulink models and the Matlab setup script are shown. Feel free to contact the author for the full model for further simulations.

Wind farm

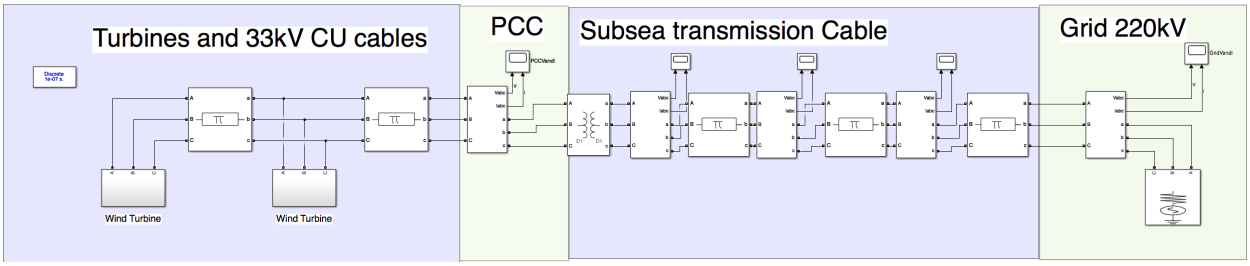

Figure B.1: Screenshot of the two turbine system

Wind turbine

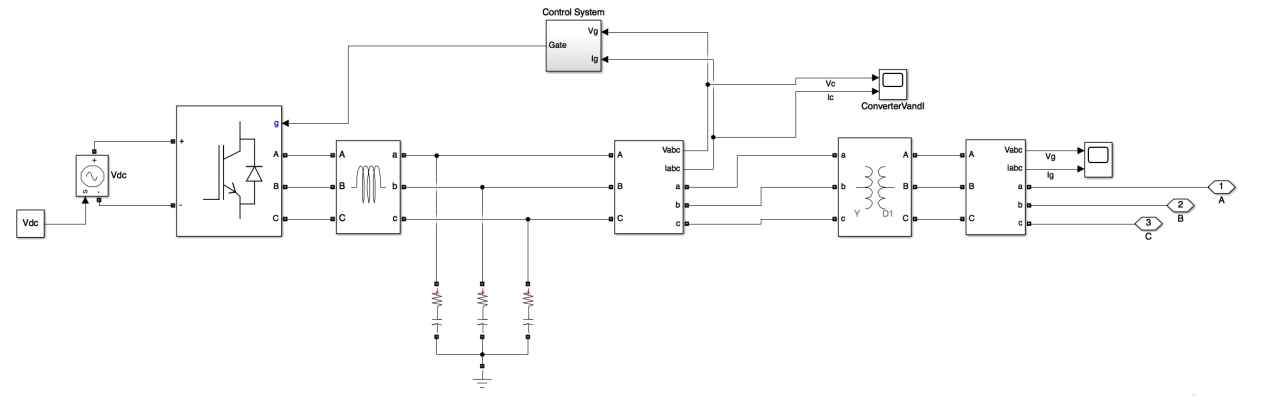

Figure B.2: Screenshot of the turbine

Control System

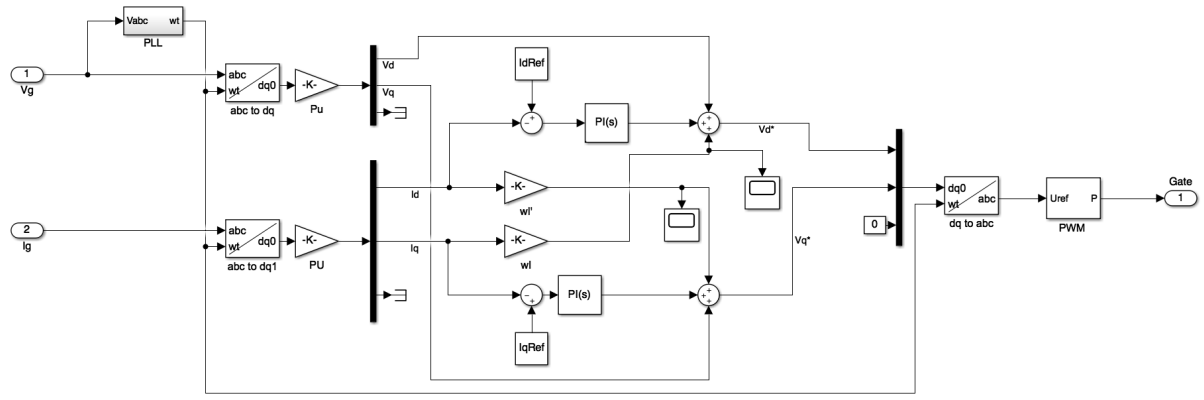

Figure B.3: Screenshot of the control system for the VSC

PLL

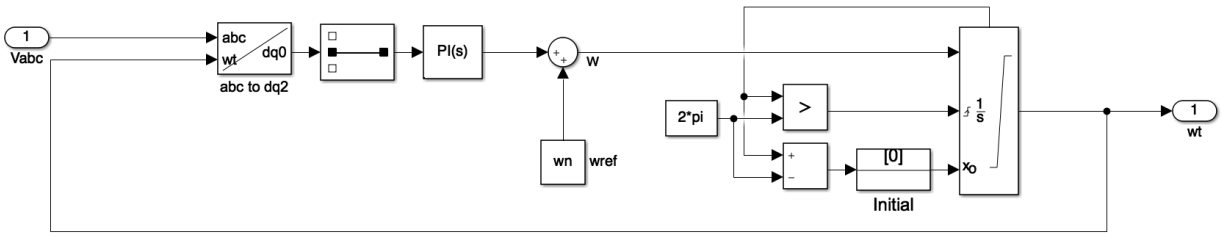

Figure B.4: Screenshot of the PLL in the turbines

18-Turbines

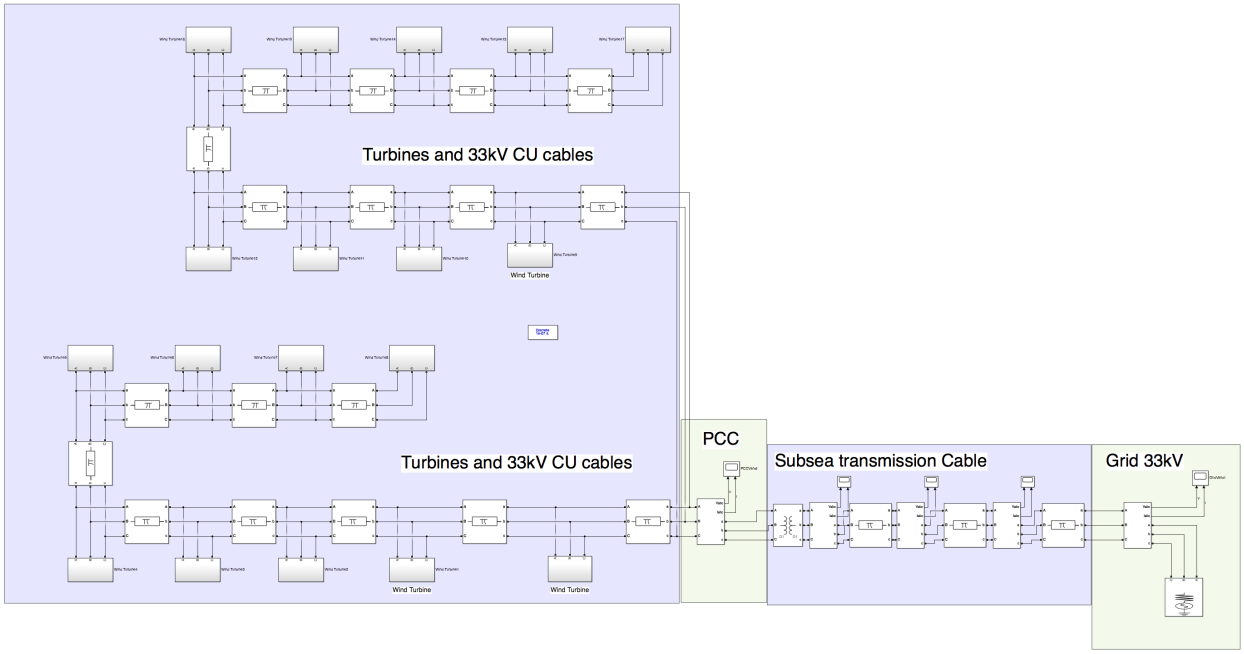

Figure B.5: Screenshot of the full 18 turbine system

Matlab code

Setup file:

```
%% Frequency constants
fn = 50; %Grid Frequency
fs = 2.5e3; %Switching frequency
wn = 2*pi*fn;

%% PU variables
Sbase = 5e6; %Sn
Vbase = 690; %V_LL_rms
Zbase=Vbase^2/Sbase; %Zn
Lbase=Zbase/wn; %Ln
Cbase=1/(wn*Zbase); %Cn
Ibase = Sbase/(sqrt(3)*Vbase); %In


```

```
%% Variables in the rest of the system
Vgrid = 33e3; %Offshore grid voltage at PCC
Vdc=1.2e3; %DC voltage at converter side

%LCL-Filter:
L1=0.10*Lbase;
Rc=0.2198*Zbase;
Cf=10.15*Lbase;
L2=0.075*Lbase;

L=L1; %For controlsystem


%% Variables in Control System:
IdRef = 1;
IqRef = 0;
Tsum=1/(2*fs);
%Scenario 4:
%IdRef = 0.9;
%IqRef = -0.436;

%Scenario 5:
%IdRef=0.5;
%IqRef=0;

%PI-values found using sisotool and LCLBodeplot.m Ziegler Nichols
Ki=58.558;
Kp=Ki*0.0011;

%Scenario 2: PI-values with a 100% change in values
%Ki=Ki*2;
%Kp=Kp/2;

%PI-values for the PLL, taken from Converters.m
wpll=10;    %frequency pll crossover
KpPLL=2*wpll;
KiPLL=wpll^2;
```

```
52
53
54 %% Math
55 fres=1/(2*pi)*sqrt((L1+L2)/(L1*L2*Cf));
56
57 %% Cobber Cables:
58
59 %R=rho*l/A
60 rho_cu=1.68e-8;
61
62 %500 mm cu Cable
63 A500=500e-6;
64 R500=rho_cu/A500*10^3; %Resistanc R/km
65 L500 = 0.34e-3; %Inductance, H/km
66 C500 = 0.32e-6; %Capacitance, F/km
67
68
69 %240 mm cu Cable
70 A240=240e-6;
71 R240=rho_cu/A240*10^3; %Resistance R/km
72 L240 = 0.38e-3; %Inductance H/km
73 C240 = 0.24e-6; %Capacitance F/km
74
75 %150 mm cu Cable
76 A150 = 150e-6;
77 R150 = rho_cu/A150*10^3; %Resistance R/km
78 L150 = 0.41e-3; %Inductance H/km
79 C150 = 0.21e-6; %Capacitance F/km
80
81 %Zero Sequence:
82 R0 = 1000; %Resistance
83 L0 = 4.1264e-3; %Inductance
84 C0 = 7.751e-9; %Capacitance
85
86 %CableSections
87 l1=10; %length
88
```

```
89 %% Aluminium cables
90
91 %R=rho*l/A
92 rho_Al= 2.65e-8;
93 AlVoltage = 220e3; % Voltage of Aluminium Cables
94
95 %Subsea Cable from Lukasz
96 AlSubR=0.04; %Resistance R/km
97 AlSubL=0.75e-3; %Inductance L/km
98 AlSubC=0.14e-6; %Capacitance F/km
99
100 %Subsea Cable
101 AlSubLength = 24.5; %Length of SubSeab cable from Brandts ter
102 AlSubArea = 1600e-6; %Cross section of sub sea cable
103 AlSubl = AlSubLength/3; %Length of each of the three PI-sections
104
105
106 %Offshore transmission transformer Lukasz
107 P_trans = 50e6; %Rated power
108 V1_trans = 33e3; %Rated primary voltage
109 V2_trans = 220e3; %Rated secondary voltage
110 R_trans = 0.004; %Resistance in windings
111 L_trans = 0.0415; %Inductance in windings
```

Bibliography

[1] K. M. Hovland, "Statoil om havvind: Kan bruke 12 mrd. per år," 2 2017, accessed 2018-05-21. [Online]. Available: https://e24.no/boers-og-finans/statoil/statoil-om-havvind-kan-bruke-12-mrd-per-aar/23918045

[2] PWC, "Unlocking Europe's offshore wind potential," PWC, Tech. Rep. May, 2017.

[3] G. V. Kuik, B. Ummels, and R. Hendriks, "Perspectives on Wind Energy," in *Sustainable Energy Technologies*. Springer, Dordrecht, 2008, p. 2.

[4] D. Weston, "Siemens teases a 10MW+ turbine," 6 2016, accessed 2018-06-04. [Online]. Available: https://www.windpowermonthly.com/article/1399841/siemens-teases-10mw+-turbine

[5] IEEE Power and Energy Society, "IEEE Recommended Practice and Requirements for Harmonic Control in Electric Power Systems IEEE Power and Energy Society," 2014.

[6] L. Kocewiak, "Harmonics in large offshore wind farms," Ph.D. dissertation, Aalborg University, 2012.

[7] L. H. Kocewiak, "Wind Power Plant Transmission System Modelling for Harmonic Propagation and Small-signal Stability Analysis," *16th Wind Integration Workshop*, pp. 1–6, 2017.

[8] L. H. Kocewiak, J. Hjerrild, and C. Bak, "Harmonic analysis of offshore wind farms with full converter wind turbines," in *Proceeding of the 8th International Conference on Large-Scale Integration of Wind Power into Power Systems*, Energynautics GmbH, 2009, pp. 539–544.

[9] C. Buchhagen, C. Rauscher, A. Menze, and J. Jung, "BorWin1 - First Experiences with harmonic interactions in converter dominated grids," in *International ETG Congress 2015; Die Energiewende - Blueprints for the new energy age*, Bonn, Germany, 2015, pp. 1–7.

[10] P. A. B. Block, F. S. Retorta, D. B. Dahlke, H. L. P. Salamanca, M. D. Teixeira, S. Paulo, and P. F. Ribeiro, "Harmonic Assessment of a Brazilian Wind Farm Regarding Reactive Power Requirements." in *2016 17th International Conference on Harmonics and Quality of Power (ICHQP)*, Belo Horizonte, 2016, pp. 867–872.

[11] Z. Emin, F. Fernandez, M. Poeller, and G. E. Williamson, "Harmonic Distortion Specification and Compliance of an Offshore Wind Generation," in *10th IET International Conference on AC and DC Power Transmission (ACDC 2012)*, Birmingham, 2012, pp. 1–6.

[12] L. H. Kocewiak, B. L. Kramer, O. Holmstrøm, K. H. Jensen, and L. Shuai, "Resonance damping in array cable systems by wind turbine active filtering in large offshore wind power plants," *IET Renewable Power Generation*, vol. 11, no. 7, pp. 1069–1077, 2017.

[13] H. A. Brantsæter, "Harmonic Resonance Mode Analysis and Application for Offshore Wind Power Plants," Master's thesis, NTNU, 2015.

[14] H. A. Brantsæter, Kocewiak, A. R. Årdal, and E. Tedeschi, "Passive filter design and offshore wind turbine modelling for system level harmonic studies," in *Energy Procedia*, vol. 80, 2015, pp. 401–410.

[15] D. Dhua, G. Yang, Z. Zhang, L. H. Kocewiak, and A. Timofejevs, "Harmonic Active Filtering and Impedance-based Stability Analysis in Offshore Wind Power Plants," in *Proceedings of 16th Wind Integration Workshop*. IEEE, 2017, pp. 1–8.

[16] N. Mohan, T. M. Undeland, and W. P. Robbins, *Power Electronics*, 3rd ed. John Wiley & Sons, INC, 2003.

[17] E. Tedeschi, "Specialization course: ELK-23 Power Electronics in Future Power Systems," 2017, accessed 2018-01-22. [Online]. Available: https://ntnu.blackboard.com/bbcswebdav/pid-222396-dt-content-rid-8181677_1/courses/Fordypningemner_IEL/Lecture_14_2017ns.pdf

[18] H. Akagi, "Modern active filters and traditional passive filters," *Bulletin of the Polish Academy of Sciences: Technical Sciences*, vol. 54, no. 3, pp. 255–269, 2006.

[19] S. H. E. Abdel Aleem, A. F. Zobaa, and M. M. Abdel Aziz, "Optimal C-type passive filter based on minimization of the voltage harmonic distortion for nonlinear loads," *IEEE Transactions on Industrial Electronics*, vol. 59, no. 1, pp. 281–289, 2012.

[20] R. Teodorescu, M. Liserre, and P. Rodriguez, *Grid Converters for Photovoltaic and Wind Power Systems*, 1st ed. Wiley-IEEE Press, 2010.

[21] L. Motta and N. Faúndes, "Active / passive harmonic filters: Applications, challenges & trends," in *2016 17th International Conference on Harmonics and Quality of Power (ICHQP)*, no. 1, Belo Horizonte, 2016, pp. 657–662.

[22] F. Medeiros, D. C. Brasil, C. A. Marques, C. A. Duque, and P. F. Ribeiro, "Considerations on the aggregation of harmonics produced by large wind farms," in *2012 IEEE 15th International Conference on Harmonics and Quality of Power*, Hong Kong, 2012, pp. 364–369.

[23] V. Yaramasu, B. Wu, P. C. Sen, S. Kouro, and M. Narimani, "High-Power Wind Energy Conversion Systems: State-of-the-Art and Emerging Technologies," *Proceedings of the IEEE*, vol. 103, no. 5, pp. 740–788, 2015.

[24] Wikipedia, "Doubly-fed generator for wind turbine," 2017, accessed 2017-11-22. [Online]. Available: https://en.wikipedia.org/wiki/Doubly-fed_electric_machine#/media/File:Doublyfed06.svg

[25] M. Asbarzadeh, H. M. Kojabadi, and L. Chang, "Power Electronics in Small Scale Wind Turbine Systems," in *Advances in Wind Power*. InTechOpen, 2012.

[26] M. B. Saïd-Romdhane, M. W. Naouar, I. S. Belkhodja, and E. Monmasson, "Simple and systematic LCL filter design for three-phase grid-connected power converters," *Mathematics and Computers in Simulation*, vol. 130, pp. 181–193, 2016.

[27] D. Schwanz, A. Bagheri, M. Bollen, and A. Larsson, "Active harmonic filters: Control techniques review," in *2016 17th International Conference on Harmonics and Quality of Power (ICHQP)*, Belo Horizonte, 2016, pp. 36–41.

[28] C. Xin, H. Minxiao, and Z. Chao, "Power Control Analysis for Variable Speed Pumped Storage with Full-Size Converter," in *IECON 2015 - 41st Annual Conference of the IEEE Industrial Electronics Society*, Yokohama, 2015, pp. 1327–1332.

[29] J. G. Balchen, T. Andresen, and B. A. Foss, *Reguleringsteknikk*, 5th ed. Department of Engineering Cybernetics, NTNU, 2003.

[30] T. Kalitjuka, "Control of Voltage Source Converters for Power System Applications," Master's thesis, NTNU, 2011.

[31] J. Machowski, J. W. Bialek, and J. R. Bumby, *Power System Dynamics Stability and Control*, 2nd ed. Chichester: Wiley, 2012.

[32] E. V. Liberado, "Design and Control of a Power Quality Interface and its Cooperation with Distributed Switching Power Interfaces," Ph.D. dissertation, University of Campinas, 2017.

[33] F. P. Marafao, S. M. Deckmann, J. A. Pomilio, and R. Q. Machado, "A software-based pll model: analysis and applications," in *Brazilian Automatic Conference (CBA)*. State University of Campinas, 2004.

[34] S. Sanchez, "Stability Investigation of Power Electronics Systems: A Microgrid Case," Ph.D. dissertation, Norwegian University og Science and Technology, 2015.

[35] J. G. Ziegler and N. B. Nichols, "Optimum Settings for Automatic Controllers," *Transactions of ASME*, pp. 759–768, 1995.

[36] E. B. Rosa, "The self and mutual-inductances of linear conductors," *Bulletin of the Bureau of Standards*, vol. 4, no. 2, p. 301, 1908.

[37] Matlab, "Three-Phase PI Section Line," 2018, accessed 2018-06-04. [Online]. Available: https://se.mathworks.com/help/physmod/sps/powersys/ref/threephasepisectionline.html

[38] ABB, "XLPE Land Cable Systems - User's Guide," vol. Rev 5, 2010.

[39] ——, "XLPE Submarine Cable Systems Attachment to XLPE Land Cable Systems - User 's Guide," vol. Rev 5, 2010.

[40] L. H. Kocewiak, J. Hjerrild, and C. L. Bak, "Harmonic models of a back-to-back converter in large offshore wind farms compared with measurement data," in *Proceedings of Nordic Wind Power Conference*, Lyngby, Denmark, 2009.

[41] R. Dimitrovski and M. Luther, "Investigation of Harmonic Interaction Between VSC-HVDC Systems and Offshore Wind Farms with DFIGs," in *2016 IEEE Power and Energy Society General Meeting (PESGM)*, Boston, MA, 2016, pp. 1–5.

[42] H. Liu and J. Sun, "Voltage Stability and Control of Offshore Wind Farms With AC Collection and HVDC Transmission," *IEEE Journal of Emerging and Selected Topics in Power Electronics*, vol. 2, no. 4, pp. 1181–1189, 2014.

[43] Wikipedia, "Band-stop filter," accessed 2018-05-21. [Online]. Available: https://en.wikipedia.org/wiki/Band-stop_filter

[44] P. M. Ivry, M. J. Rawa, D. W. P. Thomas, and M. Sumner, "Power Quality of a Voltage Source Converter in a Smart Grid," in *2013 IEEE Grenoble Conference*, Grenoble, 2013, pp. 1–6.

[45] Energy Numbers, "Capacity factors at Danish offshore wind farms," 2018, accessed 2018-07-08. [Online]. Available: http://energynumbers.info/capacity-factors-at-danish-offshore-wind-farms

[46] X. Zhang, D. Xia, Z. Fu, G. Wang, and D. Xu, "An Improved Feedforward Control Method Considering PLL Dynamics to Improve Weak Grid Stability of Grid-Connected Inverters," *IEEE Transactions on Industry Applications*, 2018.

[47] Y. Xu and Y. Cao, "Sub-synchronous oscillation in PMSGs based wind farms caused by amplification effect of GSC controller and PLL to harmonics," *IET Renewable Power Generation*, vol. 12, no. 7, pp. 844–850, 2018.

[48] L. Kozewiak, "Active Filtering Functionality in Wind Turbines Connected to Wind Power Plant Offhore Network," 2016, accessed 2018-06-18. [Online]. Available: http://lukasz.kocewiak.eu/blog/2016/08/21/active-filtering-functionality-in-wind-turbines-connected-to-wind-power-plant-offhore-network/